IMPROVEMENT OF HIGH TEMPERATURE OXIDATION RESISTANCE OF γ-TiAl ALLOYS BY SLURRY COATINGS.

BACHELOR THESIS IN AEROSPACE ENGINEERING

Madrid, Spring 2014.

Author:

Nicolás Fashho Musallam

Advisors: Elisa María Ruiz Navas & Sophia Alexandra Tsipas.

Department of Materials Science and Engineering and Chemical Engineering.

Universidad Carlos III de Madrid, Escuela Politécnica Superior.

Acknowledgments

Me gustaría dedicar mi 'Trabajo de Fin de Grado' a todos y cada uno de mis profesores con los que he aprendido, vivido y conmovido a lo largo de mi vida.

En especial, a mis tutoras Elisa y Sophia por esta magnífica oportunidad y a todos aquellos que han dejado una profunda huella en mí:

- Mi profesor y tutor de 3ºy 4ºde primaria: Pedro.
- Mi profesor de Kárate: David.
- Mi profesor de Mates, Física y Química: Nino.
- Mi profesora de Francés: Mayte.
- Mi profesora de Dibujo Técnico: Belén.
- Mi profesor de Filosofía: José Antonio.

También a María del Carmen, Isabel, Pepa, Raquel, Alicia, Asun y a María Jesús, y en general a los equipos docentes del colegio público Los Almendros y al del colegio Montpellier.

Agradecerles a mis compañeros de carrera por estar a mi lado, al pie del cañón, en todas y cada una de las batallas que hemos vivido juntos en estos cuatro años. En especial, a María que me ha acompañado y ayudado siempre fiel en todo este proceso.

Agredecrle a mi familia su incondicional e inquebrantable apoyo. I would also like to thank my aunt Sawsan for her kind support with my English.

Todos ellos han contribuido a mi formación y saber, y sin su ayuda y paciencia nada hubiera sido posible.

A todos, de corazón, GRACIAS.

Más allá de las nubes, el cielo siempre es azul.

Contents

Chapter 1

Abstract

This research document aims to deepen the understanding of slurry coatings as an effective barrier against the oxidation of promising Titanium-aluminide intermetallic alloys. For that purpose, the research is carried out with a Titanium-Aluminum alloy substrate –($Ti\ 45Al\ 2Nb\ 2Mn\ +\ 0.8\%vol\ TiB_2$)– which was manufactured by means of two different techniques: Hot Isostatic Pressing (HIP) and Centrifugal Casting (CC).

Additionally, two different slurry coatings have been applied and analyzed in order to understand the effects they produce. One of them was based on Aluminum powders and the other on a mixture of Aluminum-Boron powders. Both carry polyethylene glycol (PEG) as a binder.

A total of twenty four samples were used, from which twelve were manufactured by hot isostatic pressing and the remaining twelve by centrifugal casting. Each group of twelve pieces was divided in three subgroups, each made up of four samples. The first subgroup was subjected to oxidation without having any coating, the second was coated by the aluminum slurry and the third by the aluminum-boron slurry.

The samples were oxidized in static air for 300 hours at $800°C$ (1073 K) in an interrupted oxidation test.
Finally, the characterization of the samples was performed by means of mass-gain, X-Ray diffraction and Scanning Electron Microscope (SEM) analyses.

Keywords: Titanium aluminide, high temperature oxidation, diffusion and slurry coating.

Chapter 2

Titanium and its alloys

2.1 Titanium

Titanium is a chemical element with the symbol Ti and atomic number 22. It has a silvery dark color, and it is attractive since it has a high strength-to-density ratio and it is also a good resistant to corrosion [1, 2].

Titanium is a relatively new metal. The first documented discovery was made by the British mineralogist and chemist William Gregor in 1791 [3]. He isolated black sand known as 'Ilmenite' from a local river. He was able to remove the iron from the ilmeite with a magnet. The remaining substance was treated with hydrochloric acid yielding the oxide of this new metal [2]. Few years later, in 1795, the German Martin Heinrich Klaproth isolated titanium oxide from a mineral [4], now known as 'Rutile' (TiO_2).

However, a hundred years later, in 1910, Matthew Albert Hunter was the first man able to isolate the metal by heating titanium tetrachloride $TiCl_4$ with sodium. In 1932, the recognized father of the titanium industry, Wilhelm Justin Kroll (from Luxembourg), produced significant quantities of this metal by combining $TiCl_4$ with calcium as a reducing agent [5].

World War II boosted the industry of titanium substituting calcium by magnesium as the agent, making it more affordable and easy to obtain [6]. Hence, titanium-based alloys began to be considered as key materials for aircraft engines as well as for other industries, like chemical processing, medicine or power generation.

Titanium is expensive due to the difficulty of processing the metal to a pure state. It is not actually a rare substance since it is the fourth most abundant metal after iron, aluminum and magnesium. However, it is seldom found in high concentrations or pure state [6].

2.2 γ-TiAl alloys

2.2.1 Introduction

TiAl alloys are considered an intermetallic combination of Titanium and Aluminum. Specifically, γ-TiAl is the TiAl intermetallic that has an aluminum content ranging from 40-55 atomic percent (at.%) of the total intermetallic composition. Further details are introduced in subsection 2.2.2.

Intermetallic compounds are alloys formed by two or more metals combined in stoichiometric proportions. They form an ordered crystalline net where atoms are joined by ionic or covalent bonds. This property differentiates intermetallics from conventional metal alloys, since it provides intermediate properties between metals and ceramics.

Thus, there is a compromise between the different properties. For example, ceramics contribute to increase hardness and high temperature performance, while they sacrifice some toughness and ease of processing (ductility), typical of metals.

The intermetallic-based alloys for structural applications have been an active field of research around the world for the last 20 years [7]. These intermetallics include aluminides formed with either titanium, nickel, iron or silicides formed with transition metals [8].

Titanium aluminides are of great interest for several structural and high temperature applications, because of their remarkable low density (about 4 g/cm^3) and their excellent high temperature strength. They could replace the much heavier high temperature steels or nickel-base superalloys (up to 9 g/cm^3), which are usually in service. The implementation of this new group of intermetallic alloys in, for example, the aerospace [9] or automotive industry is, therefore, due to economical and ecological reasons [10]. Figure 2.1 compares the high temperature strength of TiAl with other in-service alloys.

Dimiduk [11] has assessed γ-TiAl alloys with other aerospace structural materials and has shown that new capabilities become available on account of its properties. The most important advantages involve [12]:

- High melting point.
- Low density.
- High specific strength and moduli.
- Low diffusivity.
- Good structural stability.
- Good resistance against oxidation and corrosion at low temperatures.

– High ignition resistance (when compared with conventional titanium alloys).

Nevertheless, the use of TiAl-based alloys is still limited to a temperature above 800°C [13, 14]. The problems of low ductility and toughness at room temperature, typical of intermetallics, have been partly alleviated by changing the chemistry and microstructure of the alloys [15]. However, there is an extensive research to improve their poor oxidation resistance at high temperature [10, 13, 15, 16, 17, 18, 19].

Some good results for the improvement of the oxidation resistance have indeed been achieved. However, simpler and less expensive protective methods are still sought [20].

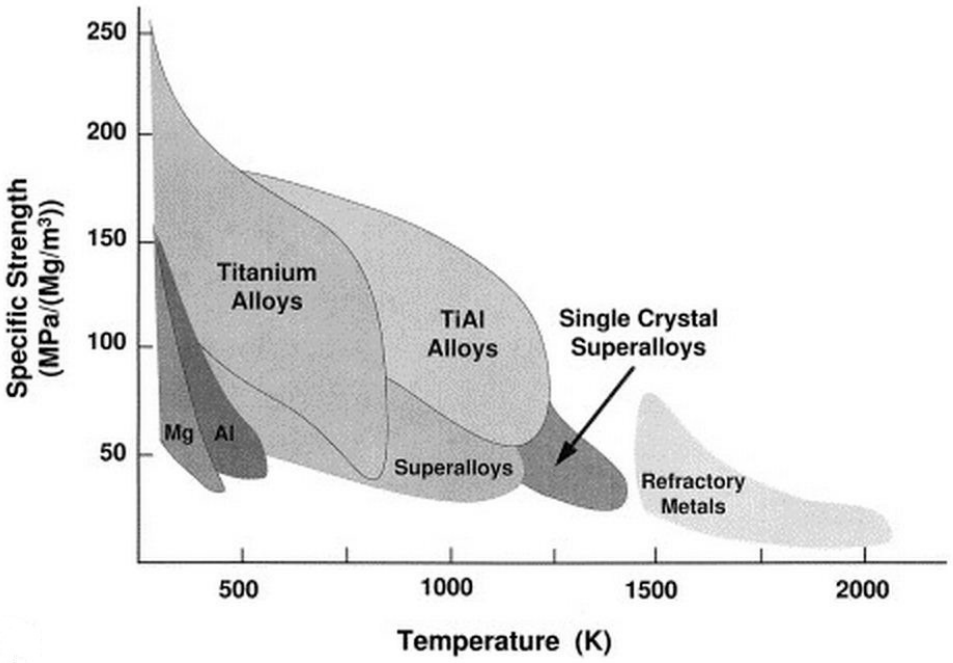

Figure 2.1: TiAl Specific strength vs. Temperature.

Source: DM. Dimiduk [11].

2.2.2 TiAl phase diagram

A binary (2-D) phase diagram is a representation that provides the variation of the phases of an alloy with respect to the change in temperature and in the content of one of the elements.

According to the Ti-Al binary phase diagram (Figure 2.2), there are four intermetallic phases of interest for high temperature applications. From lower to higher aluminum content, they are: α_2-Ti_3Al, γ-TiAl, $TiAl_2$ and $TiAl_3$ [11, 21, 22].

All of them are stable at room temperature.

The development of α_2-Ti_3Al alloy is due to the necessity of combining temperature capabilities between conventional near-α titanium alloys and nickel-base superalloys [6]. This results in an alloy with a good corrosion resistance [21], but with a high brittleness [14].
$TiAl_3$ alloy is of interest in the development of a new class of structural materials as well. It has the highest oxidation resistance properties due to the high content of aluminum, which will form stable superficial oxide layers. It also has a low density and a specific modulus and stress rupture resistance comparable to that of the superalloys. However, the complete absence of room temperature plasticity posed the primary challenge in using it as a structural material [17].

Finally, γ-TiAl and its alloys are mainly pursued, because they combine good properties among the four possible phases. There is an equilibrium between the properties of titanium and aluminum.
For instance, their crystalline structure remains ordered up to the melting point at about 1440°C. This is a contribution of titanium to pure aluminum, which increases the melting temperature of the latter. Another example is that they have high oxidation resistance properties due to the content of titanium and aluminum, which will form stable oxide layers. These properties make them attractive candidate materials for components in aeroengines [23].

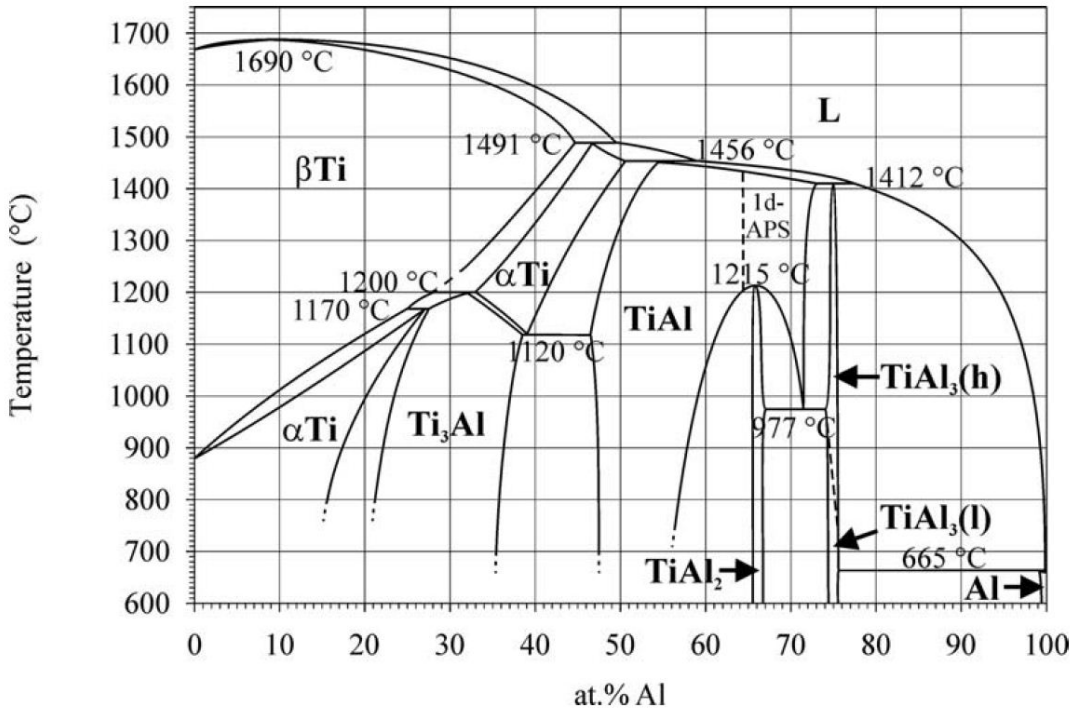

Figure 2.2: TiAl Phase Diagram.

Source: J.C. Schuster & M. Palm [24].

Influence of the alloying elements

The addition of alloying elements plays an important role in modifying the phase diagram up and down (temperature) and left or right (phases). In other words, alloying elements stabilize and consolidate the presence of a phase and its range, they can modify the transformation temperatures of the invariant reactions, and even the melting temperature of the alloy. For example, Al is an α-phase stabilizer (see Figure 2.2), Fe is the strongest β_2 stabilizer, Cr is the second, V is an intermediate stabilizer, and Nb is the weakest stabilizer for this last phase [25].

In the case of the *improvement of oxidation resistance*, it is found that according to the oxidation studies carried out by Shida and Anada [26] in a range of 800-1000°C for 100 hours of oxidation, the following elements have these specific effects:

- Detrimental: V (0.5-5.0 wt.%), Cr (0.5-5.0), Mn (1.5-5.0), Pd (2.0), Pt (2.0) and Cu (2.0).
- Neutral: Y (1.0 wt.%), Zr (2.0), Hf (2.0), Ta (2.0), Fe (2.0), Co (2.0), Ni (1.5), Ag (2.0), Au (2.0) and Sn (2.0)
- Beneficial: Nb (2.0 wt.%), Mo (1.5-6.0) , W (2.0-6.0), Si (1.0), Al (37.5/63), C and B

Additions of 4 at.% of W or Nb increased oxidation resistance, whereas the presence of a similar concentration of Ta, Cr or V had an adverse effect [17]. However, higher concentrations of Cr (>8 at.%) and alloying combinations of Cr+Ta, Cr+Nb, Mn+Ta, Mn+Nb, Mn+W added to TiAl yield very good oxidation resistant alloys [27, 28].

Boron also has a second beneficial effect; it refines the grain and stabilizes the microstructure [29, 30, 31, 32]. Moreover, ternary additions of Cr, V and Mn appeared to increase the ductility of the two phase Ti-48Al base alloys [6, 33, 34]. In general, Nb improves surface stability at high temperature exposure. The presence of Si increases strength and creep resistance. Al increases creep resistance and lowers weight. Low contents of Mo increase the creep resistance too.

Hence, the improvement of the oxidation resistance by the addition only of alloying elements is found to be not enough for practical applications. The alloying elements used to improve oxidation resistance may not have a fully desired effect on the mechanical properties of the material. Therefore, surface treatments are thought to be a good complement, enhancing the attractiveness of the final component against oxidation [14].

2.2.3 γ-TiAl microstructures

A microstrucure can be defined as the observable structure under a microscope of the different phases present in a prepared material surface. The microstructure strongly influences physical and mechanical properties of a material such as: strength, toughness, ductility, hardness, corrosion resistance, high temperature performance, wear resistance, etc. This, in turn, governs the applications of the material.

The microstructures may be generated and modified in a given alloy by thermal (heat) treatments, involving different temperatures and cooling rates [35, 36]. γ-TiAl alloys with Al concentrations between 35 and 49 at.% exhibit a wide range of two phase (α_2-Ti_3Al and γ-TiAl) microstructures, which are commonly classified as a function of the volume fraction of equiaxed grains and lamellar colonies [37]. These are:

1. **Fully Lamellar (FL):** Lamellar microstructures are composed of alternating layers of two or more phases (α_2 and γ) in the form of lamellae. They appear in cases where a phase transformation cooling front moves quick enough to leave behind it two solid products (i.e. forming lamellar colonies). Their formation requires treating at temperatures above the α-transus (Fig. 2.2). Low cooling rates ($\leq 10°C/s$) from eutectic or eutectoid systems promote the formation of lamellar microstructures.
   The lamellar spacing and the colony size will depend on the specific cooling rate. It is well documented that such a system could exhibit extraordinary mechanical properties when the layer thickness is small enough [12]. It increases creep resistance, but decreases ductility at room temperature.

2. **Nearly Lamellar (NM):** Contains a small fraction of γ equiaxed grains. Heat-treatment above the duplex microstructure temperature results in the coarsening of α grains and the formation of nearly-lamellar microstructure [35]. While, if it is heat treated at temperatures slightly above the eutectoid point, it results in the development of near-gamma microstructures.

3. **Duplex (D):** Comprise similar volume fractions of γ equiaxed grains and lamellar colonies. Both duplex and nearly lamellar structures will result from annealing heat treatment at increasingly high temperatures within the $\alpha + \gamma$ phase field.

4. **Near Gamma (NG):** Composed exclusively by equiaxed γ grains. The near-γ microstructure is formed when the material is heat-treated in the $\gamma + \alpha_2$-phase field at temperatures below the duplex microstructure temperature. Heat-treatment in this phase field results in the coarsening of the existing γ-grains [35] leading to the formation of near-γ microstructure.
   Higher cooling rates ($\geq 100°C/s$) will result in massive γ-phase transformation, i.e., the formation of bulk gamma grains [37].
   Duplex and near gamma decrease creep resistance by increasing alloy ductility at room temperature [38].

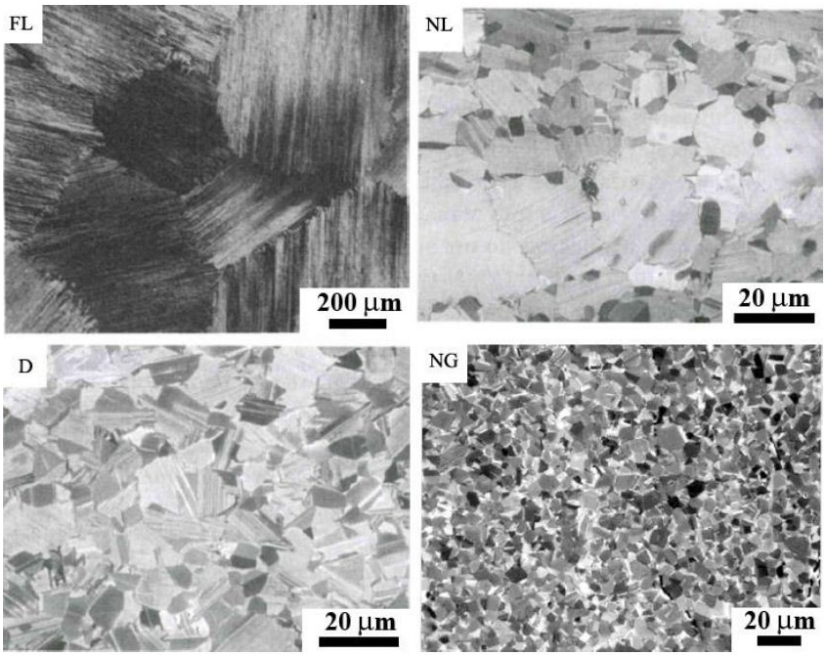

Figure 2.3: Typical γ-TiAl microstructures.

Fully lamellar (FL), nearly lamellar (NL), duplex (D) and near-γ (NG). [35, 39].

2.2.4 Ti45Al22-XD

This section introduces further details about the alloy used for the present research. Ti45Al22-XD makes reference to an intermetallic alloy composed of titanium with a 45 atomic % of Al, 2 at.% Nb, 2 at.% Mn and 0.8% in volume of TiB_2. The latter component works as reinforcing agent with a ceramic character. Its designation is abbreviated as 'XD' [40, 41].

The main application of this alloy is in aeroengines [42]. Two of the main aeroengine manufacturers, the American General Electric (GE) and the British Rolls Royce (RR), are implementing γ-TiAl alloys in their products.

GE has already found commercial uses for Ti-48Al-2Cr-2Mn alloy [43]. The last two stages of the seven-stage Low Pressure Turbine (LPT) blades of the GEnx turbofan engines are made of this alloy. This engine is currently used in the Boeing 787 Dreamliner and B747-8 [44].

On the other hand, Rolls-Royce (RR) in collaboration with ITP (Industria de Turbo Propulsores S.A.), the main company leading LPT manufacturing, are betting for the Ti 45Al 2Nb 2Mn+0.8% TiB2 alloy as the best candidate [45]. They are incorporating it on the RR Trent-1000 turbofan engines, which are also used in the B787.

2.2.5 Manufacturing processes

The properties of a material do not rely exclusively on the chemical composition and the proportions that form it, but also on the manufacturing method. This gives the desired phases, microstructure, grain size, etc. for the desired mechanical properties. If it is needed, there are mechanisms, like heat treatments, that exert further influence on the final properties of a material.
The studied samples were manufactured by applying *Hot Isostatic Pressing* and *Centrifugal Casting* techniques. Here are some details about these two methods.

Hot Isostatic Pressing (HIP)

Hot Isostatic Pressing is a type of 'Powder Metallurgy' technique. It plays an important role in the research and development of different materials, including metals and ceramics [46]. In the HIP technology, high temperature and high pressure can be simultaneously applied by a fluid to workpieces, resulting in fully isotropic material properties [47, 48]. Thus, it offers unique benefits for metal, ceramic and refractory applications.

The main advantage of HIP is its ability to produce compacts with effectively uniform grain structure and density (essentially 100%), good metallurgical bonding of powders, and very good mechanical properties with uniform strength and toughness [49]. However, the process is relatively expensive and is, therefore, used mainly for 'high-tech.' applications, like aerospace [42].

The major driving factor for HIP commercial development is its ability to form product shapes to precise tolerances (reducing costly machining) [50]. In other words, another advantage of this technique is that it produces net or near-net shapes, thus eliminating costly and time-consuming finishing operations [49] with a high level of mechanical properties.

The range of applications for hot isostatic pressing is expanding rapidly, producing dense components from powdered metals and ceramics [51].
HIP is used, for example, to optimize the properties of the latest generations of single crystal and directionally solidified investment cast blades (section 2.3.2), which are subjected to high in-service stresses. The removal of porosity is essential to maximize the properties and working life of the component by removing creep porosity developed during service [50].

Centrifugal Casting (CC)

Centrifugal casting consists of the solidification of the molten metal in a rotating mold, where the rotation speed and the metal pouring rate vary with the alloy characteristics, size and shape being cast [52]. γ-TiAl alloys manufactured by CC exhibit lower defect concentration than conventional ingot alloys, and their processing involves lower material loss. Additionally, they have good surface finish as well as good dimensional accuracy [49] and balanced mechanical properties

[34]. Parts like low-pressure turbine blades or automotive valves can be made of γ-TiAl alloys commonly processed by centrifugal casting [53].

2.2.6 Oxidation phenomena & mechanisms

Introduction

Oxidation can be defined as the chemical transfer of electrons between any metal that combines with an atom or molecular group. In this research, oxidation will refer to the formation of metal oxides. All metals and their subsequent alloys, with the exception of gold, form oxides [54].

As with all materials that are used at high temperatures in oxygen-containing atmospheres, oxidation is an ever-present issue [12]. During oxidation the base metal reacts with the surrounding atmosphere and hence various oxidation products are formed. The consequences of this reaction can result, for example, in the degradation of the material. In practical cases, it can lead to a reduction of the cross-sectional area of load-bearing material, thus increasing the present stresses. This may lead to a premature component failure over a long period of time.

Design of an oxidation-resistant alloy is usually aimed towards the establishment of a protective, slow-growing, stable oxide that is adherent to the surface and thus capable of shielding the underlying material [12].

Oxidation mechanism of γ-TiAl alloys

These are the qualitatively summarized steps leading to the formation of the oxide scale [54, 55]:

1. Oxygen molecules are adsorbed on the metal surface.
2. Molecular oxygen dissociates into atomic oxygen.
3. Oxygen atoms migrate to low-energy sites on the metal surface.
4. Atomic oxygen ionizes and forms bonds with the metal atoms of the surface.
5. Multiple adsorbed layers build up.
6. Oxide islands grow and overlap to form transient oxide film.
7. Oxygen/metal ions diffuse through the film to enable the formation and continued growth of stable oxide.

The kinetics at the initiation of oxidation are controlled by the availability of oxidation sites while the kinetics during the steady state oxidation are controlled by the rate of diffusion of the diffusing species through the oxide scale.
Depending on the oxygen pressure and metal activity, either Ti or Al may oxidize preferentially [15].

According to various authors [6, 15, 16, 17, 56, 57] the stable and protective oxides formed over the surface of γ-TiAl alloys are: Rutile (TiO_2) and Alumina (Al_2O_3). However, depending on the temperature of oxidation and titanium content, there may appear more oxides like: TiO or Ti_2O_3 (see Figures 8.4 and 8.5).

In general, to predict which oxide will stabilize more than the other, it is necessary to calculate the partial pressure of oxygen for the formation of the oxide. The smaller the more stable. The kinetics of formation of titanium oxides are typically greater than those of aluminum. This way, the metal surface is initially covered with a thin layer of Ti oxide. This leads to a local enrichment of the intermetallic in Al below the oxide surface. Hence, the formation of Al_2O_3 is subsequently favored [15].

Once the outer layer of TiO_2 and the inner layer of Al_2O_3 are sufficiently thick, the oxidation proceeds by diffusion of oxygen into the scale and the outward diffusion of Ti ions. This leads to 2 possibilities [15]:

- Formation of alternate channels of TiO_2 and a mixture of Al_2O_3 and TiO_2 oxides.
- Formation of a mixture of TiO_2 and Al_2O_3 in the interior.

These mechanisms are depicted in Figures 2.4 and 2.5. In general, the oxide layers close to the intermetallic surface are usually brittle and can develop cracks.

Oxide Scale Protectiveness

The oxide scale could be either protective against further oxidation or porous, allowing oxygen permeation and continuation of the oxidation process [55]. A general indicator of the protectiveness of the oxide scale is given by the *Pilling-Bedworth Ratio* (PBR) [58].

$$PBR = \frac{\text{Volume of formed oxide}}{\text{Volume of consumed metal}} \tag{2.1}$$

There are three possible situations to analyze this ratio:

- If **PBR<<1:** the volume of oxide formed is less than the volume of the metal consumed. The oxide is expected to be porous and hence, non protective.
- If **PBR$\sim$1:** the oxide is dense and fully covers the exposed surface. Then, it can be said that it is protective. Examples of these cases are alumina [58] and rutile [15].
- If **PBR>>1:** the oxide volume is greater than the volume of the metal replaced. The oxide scale is highly compressed, resulting in buckling and spall. Thus, it can have a pulverulent texture.

Therefore, for a protective oxide scale, PBR should be close to unity. This is strongly conditioned by geometry effects, volatility of oxides and chemical effects of alloying elements [55, 59].

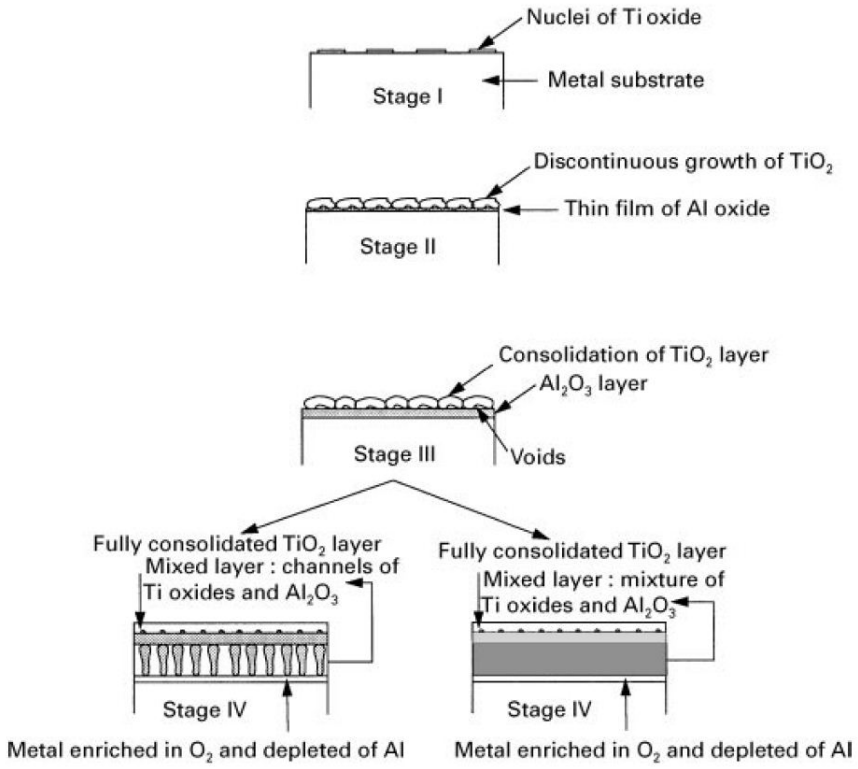

Figure 2.4: Stages of oxidation of TiAl based intermetallic alloys.

Source: S.A Kekare and P.B. Aswath [15].

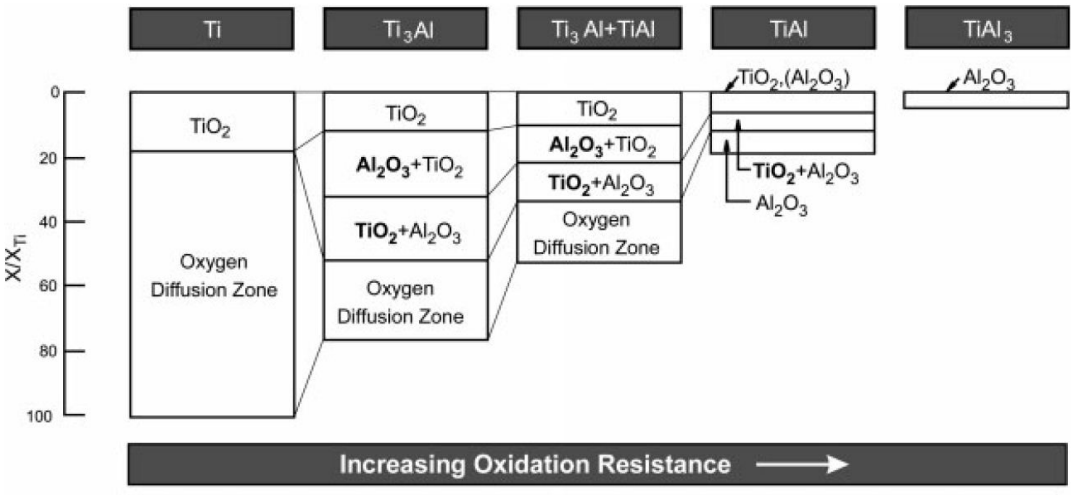

Figure 2.5: Representation of oxide scales and oxygen diffusion zones.

Source: C. Leyens and M. Peters [6].

Oxidation Kinetics

There are several factors which affect the oxidation of a material. In the case of an alloy, the main factors depend on: alloy composition, enthalpy of formation of relevant oxides, diffusion within the alloys, solubility and diffusion of oxygen in the metal (internal oxidation), etc. [6].

Oxidation Kinetics describe the growth of the oxide scales as a function of time. There is a total of four main oxidation rate laws for metals: Linear, Parabolic, Cubic and Logarithmic. A brief description of each one is provided below:

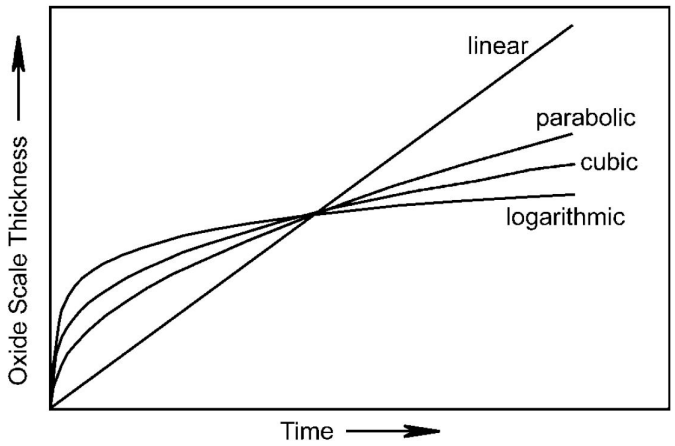

Figure 2.6: Representation of the oxidation rate laws.

Source: Leyens & Peters [6].

- **Linear:** It is characteristic of metals which form a porous or cracked scale, so that the scale does not represent a diffusion barrier between the two reactants [60].
- **Parabolic:** The rate of oxidation is controlled by the diffusion of ions through a compact oxide scale. Hence, parabolic nature is a thermally activated process. The thickness of the oxide layer increases with time [60, 61].
- **Cubic:** It is seldom encountered, but it may appear under certain conditions. Its behavior is in between parabolic and logarithmic curves [60].
- **Logarithmic:** It can be observed at low temperature oxidation (around 300-400°C). The mass-gain (oxide scale thickness) at the beginning has an abrupt increase. After this overshoot, it stabilizes and the curve gets nearly constant.

2.3 The state-of-the-art in Gas Turbines

2.3.1 Introduction

A gas turbine is a type of turbomachine which transforms internal energy of a fluid (gas) into useful work. The purpose of a gas turbine determines its design and so the most desirable energy output form. They are used to power trains, ships, electrical generators, tanks, automobiles, etc. In the case of aerospace applications, there are several adaptations for these devices, for example: to power rocket tank pressurization and airbreathing jet engines, which is the most important application.

Jet engines that produce thrust from the direct impulse of exhaust gases are often called turbojets, whereas those that generate thrust with the addition of a ducted fan are often called turbofans. There is a third type of aero-engine known as turboprop, which is similar to turbofans except that its fan is unducted, that is, the propeller blades are not contained in a casing.

Airbreathing engines have an upstream rotating compressor coupled by a shaft to a downstream turbine (both made up by numerous blades), and a combustion chamber in-between (Figure 2.7). Thus, they follow an ideal thermodynamic Brayton cycle, which is composed of three phases: isentropic compression, isobaric combustion and isentropic expansion (see Figure 8.1 in the appendix).

The higher the turbine inlet temperature (T_3), or equivalently the combustion temperature, the greater the available thrust and the higher the cycle efficiency.

For this reason, an optimization of the working temperatures of the combustion chamber and the turbine has to be carried out. The temperature range is limited by the properties of the materials that compose the engine, which could simply melt down. In the case of the turbines, there is a large effort put in developing complex blade cooling systems and materials able to withstand those temperatures.

Additionally, there is a source of fuel saving which is weight-reduction. This has become a big concern in the aerospace industry in the recent years, since it is a main factor for cost-effectiveness. Clearly, the reduction in weight is dependent on the materials composing the aeroengine.

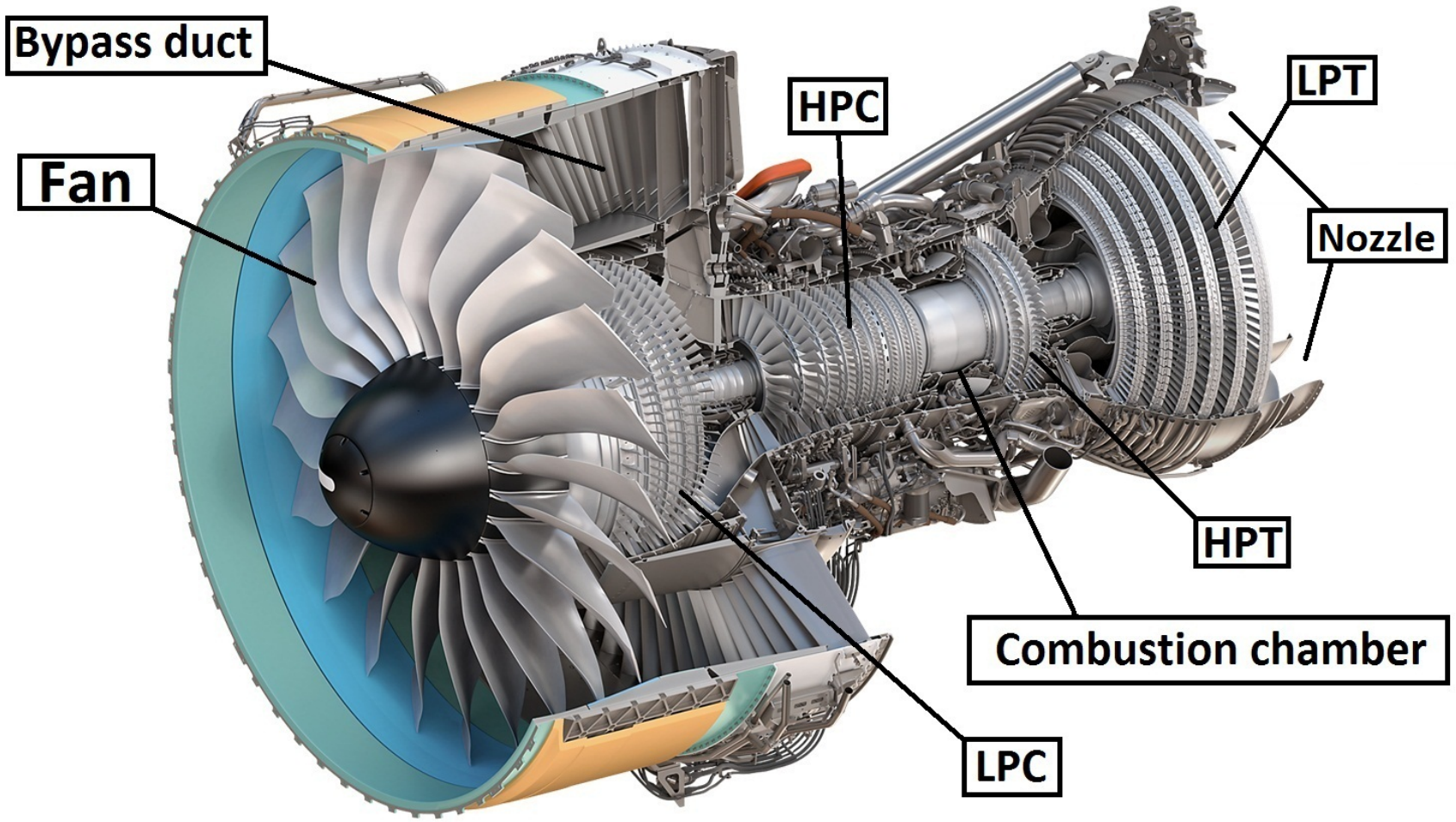

Figure 2.7: Turbofan engine layout. Pratt & Whitney GP7200 used in the A380.

Source: cielus.wordpress.com

2.3.2 Operative alloys

Structurally speaking, turbines are usually more complicated and sophisticated components than compressors. The alloys making up a turbine have to withstand a high-level of centrifugal stresses created by the rotating speed of the engine. They also have to resist fatigue, creep, oxidation and high temperatures as well as being light-weight [12].

A modern airbreathing turbine, which is installed in airliners and adds up to about 20% of the total engine weight [62], is usually divided in two main sections: a High-Pressure Turbine (HPT) and a Low-Pressure Turbine (LPT). The former has a cooling system, but not the latter.

The usual inlet temperature for a HPT ranges from 1100°C to 1400°C, due to the close presence of the combustion chamber. The cooling system allows to have a blade surface temperature of few hundred degrees lower. Therefore the thermal sensation for the blade alloy is lower than the actual machine working temperature (the one used for energy and performance computations).
A blade is cooled down by means of air coming from the latest stages of the High-Pressure Compressor (HPC). This air can be injected in the main flow, cooling the outer surface of the blade. It can also be present in a series of internal passages, cooling the inner surfaces [63, 64].
Just to mention, this heat transfer problem is quite complex, since there are many parameters involved, like: internal thermal stresses in the blade due to the difference in temperature between the outer and inner surfaces, mass flow rate of the injected air which will size the blowing holes, their number and the distance between them, the aerodynamic performance of the airfoils (boundary layer properties and stall conditions), etc. See Figure 2.8.

Conversely, LPT usually receives air at a temperature between 600°C and 800°C [12, 38, 65], which is still quite high. LPTs do not have have any cooling system. Hence, the alloy forming the blade is expected to resist this range of temperatures, since it has to be exposed directly to this environment. However, they employ a second protective mechanism, usually 'thermal barrier coatings'.

Nickel-base superalloys[1] are extensively used for components such as blades and vanes in industrial gas turbines. Modern superalloys are chemically and microstructurally optimized to have an excellent creep resistance, but are not sufficiently resistant to long-term oxidation and corrosion. Thus, the surface of the components has to be modified to enable proper operation [66].

For this reason and for a greater weight reduction, TiAl alloys are now being introduced in LPTs, substituting Ni-base ones [9, 38, 42, 67, 68, 69].

[1] A superalloy is a metallic alloy which can be used at unusual high temperatures, often above $0.8T_m$ (melting temperature).

Manufacturing optimization

When designing an alloy, there are a lot of parameters that have to be taken into account: from the chemical elements composing the alloys to the microstructure and properties. All these conditions form a set that has to be meticulously optimized.

A practical example regarding the manufacturing technique is that cast nickel-base alloys give better creep and fatigue properties. Moreover, improved in-service life can be obtained by aligning the crystals to form columns along the blade length, produced by a method known as 'Directional Solidification', which controls planar solidification temperature gradient fronts. A further advance of this technique is to make the blade out of a single crystal [70]. Each method extends the useful creep life of the blade. In the case of the single crystal blade, the operating temperature can be substantially increased as well as the low-cycle fatigue life [62, 71]. This method is more expensive than usual casting methods. However, it is commonly applied in turbomachinery.

Thermal Barrier Coatings (TBCs)

Heavy-duty gas turbines are generally subjected to an excessive contamination and to an accelerated attack known as *'Hot Corrosion'*, which reduces the turbine blade operating-life. Hence, these blades have to be protected somehow by a coating. The function of all coatings is to provide a surface reservoir of elements that will form very protective and adherent oxide layers, which will protect the underlying base material from oxidation, corrosion attack, cracking and degradation [62, 72, 73, 74, 75].

In todays advanced machines, oxidation is a concern not only for external blade surfaces, but also for internal passages and cooling holes. This is due to the high temperature of the cooling air, which contains oxygen, coming from the compressor.

Another degradation phenomenon associated with temperature is *'Thermal fatigue'*. This is a secondary failure mechanism. Temperature differentials developed during the start and stop of the turbine produce thermal stress. The cycling of these thermal stresses is the so-called 'thermal fatigue'. Thermal fatigue is a low-cycle fatigue (i.e. above plastic limit) and has an outcome similar to a creep-rupture failure. The analysis of thermal fatigue is essentially a problem in heat transfer and material properties, such as modulus of elasticity, coefficient of thermal expansion, and thermal conductivity [62, 76].

Components located in certain sections of gas turbine engines, such as the turbine, combustor and augmentor, often require some form of thermal protection in addition to an environmental coating. One approach is to deposit a ceramic thermal barrier coating on the external surfaces of the component [77, 78].

As above mentioned, the coefficient of thermal expansion of the TBC should be similar to that of the protected alloy, in order to avoid thermal stresses that could create and propagate undesired cracks. Additionally, TBCs should have the lowest possible thermal conductivity.

Ceramic coatings can enhance the heat resisting properties and, for the same set of conditions, reduce the amount of cooling air required, thus improving engine efficiency [71, 79, 80], since less air is bled from the compressor.

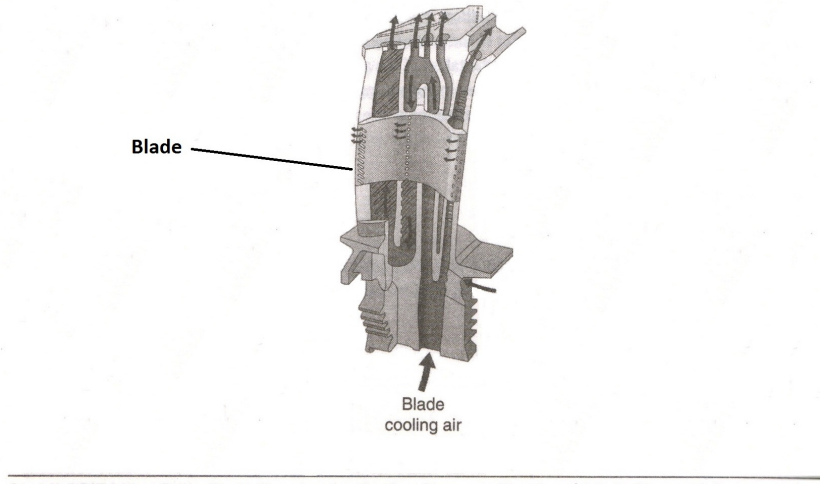

Cooled HP Turbine Rotor Blade Showing the Cooling Passages (Courtesy of Rolls-Royce plc)

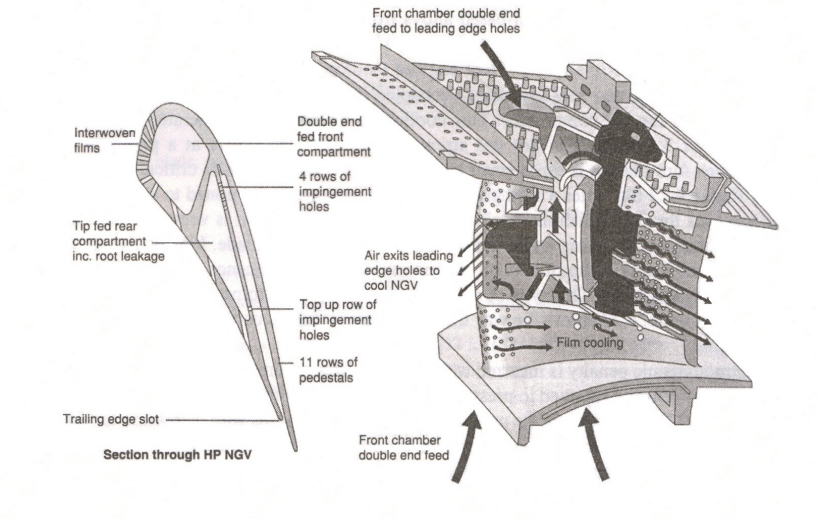

Cooling Arrangement for a Nozzle Guide Vane in a HP Turbine of a Modern Turbofan

Figure 2.8: Turbine cooling scheme.

Source: Dixon & Hall [65]. Rolls-Royce.

Chapter 3

Surface protection: Slurry coatings

3.1 Introduction

The in-service temperature of existing materials is limited by, for example: erosion and wear, creep, fatigue, chemical phenomena like oxidation, etc. These limitations can be somehow overcome by using high temperature resistant coatings.

Extensive research has been made by the metallurgical industry towards the development of new alloys for high temperature applications. However, relatively little attention was given to 'high temperature coatings' until 1970 [81].

The basic requirements of these kinds of coatings involve a wide range of characteristics. First, they should withstand high temperature environments, that is, being able to maintain their mechanical properties despite extremely high heat and contact with corrosive gases like air. Second, they have to be non-reactive (chemically inert) with the substrate to be protected. Third, they should have a low coefficient of thermal expansion (CTE) in order to better resist creep and fatigue: deformation and cracking. Finally, it is desirable to have a low-density coating; making it more attractive to 'high-tech.' and 'light-weight' applications.

In general, two types of coatings can be distinguished: 'overlay coatings' and 'diffusion coatings'. Overlay coatings are applied by techniques such as thermal spraying, cladding, or physical vapor deposition. Diffusion coatings, on the other hand, are deposited by techniques such as chemical vapor deposition (CVD) or the well-established method of pack cementation, as well as slurry-aluminizing processes [66], discussed in this document.

Slurry coatings are compounds used for oxidation protection of metallic materials at high temperatures. Slurries contain a high volume of metallic substances used to protect the substrate. In other words, protection is achieved by using sacrificial materials (i.e. metallic compounds) that will react with oxygen, getting

oxidized, and so preventing the substrate from suffering this phenomenon.
The reason, why the material that compose the substrate has to be protected, is because it carries the mechanical properties of the structure that will perform the desired tasks of the user.

Generally, a slurry coating is applied via dipping, brushing or spray, followed by a thermal treatment in a protective atmosphere. Coating protection is achieved by interdiffusion of the sacrificial material with the substrate. Thus, it is an irreversible mechanism. That is, a slurry coating cannot be used as temporary oxidation protector, since once it diffuses, it remains in the substrate permanently.

Specifically, this protector has been widely used for the formation of high-temperature coatings for refractory metals and superalloys [82]. Nowadays, it is also implemented in additional applications [80, 83, 84, 85]. It started to be used for different substrates like intermetallic alloys and with different coatings composition, for instance, ceramic substances. Industries like: aerospace, automotive, military and electronics require and demand these type of protectors.

Slurries present some advantages with respect to classic coatings such as paintings and chemical deposition baths, or even modern techniques like pulsed laser deposition, cathodic arc, ion bombardment, plasma spray, vapor phase deposition, etc.
In general, the main advantages are the following:

- Slurries can be considered green coatings, since they are environmentally friendly due to their simple composition (usually water-based) and easy production [86].
- They are non-toxic.
- They are economically affordable. The expensive part comes from the application process, which is mainly the energy required to diffuse the coating into the substrate.
- They can be stored at room temperature.
- Their properties remain stable during storage.
- They are easy to manipulate; they do not require any special deposition technique or device (except for the diffusion step).

To close, it is worthy to mention that this research document intends to discover new valid applications of slurry coatings to promising light-weight alloys like those based on TiAl intermetallics.

3.2 Description of the composition of a slurry

Slurry coatings are relatively simple mixtures, similar to paints. They are usually based on an aqueous solution and are basically made of: distilled water, desired protective metal powder, a water soluble binder and a dispersant. In addition to that, activators and additives could be used to get additional properties. Subsections 3.2.5 and 3.2.6 present more details about these components.

When a slurry is ready to be used, its appearance is like a paint and its ideal texture is that of a homogeneous sludge. The adhesion of the fresh mixture to the substrate is essential for the final effectiveness of the diffused coating. Here, the type of binder and the metallic protector particle size play an important role, since they control crucial driving factors like: viscosity and homogeneity.

For example, in Figure 4.7, it can be clearly seen that the slurry mixture appearance is similar to that of a shining viscous soap bubble. The binder, in this case PEG (Polyethylene glycol), provides this characteristic.

3.2.1 Carrier fluid

The carrier fluid is normally a liquid such as organic solvent or water. It enables the coating material to flow and be applied, for example by immersion. Solvents play a major role in how well the coating will perform. This component evaporates after application allowing solid materials (metal powders) to immobilize and form a thin protective film.

Organic solvents like: volatile alcohols, ketones, and hydrocarbons evaporate easily creating environmental concern. For instance, they contribute to a detriment of the ozone layer, some of them are toxic to human health, etc. Therefore, using water as a carrier fluid is advantageous in that sense. Industries and scientific groups are currently moving and conducting research towards the use of non-pollutant solvents [66, 87, 88].

Distilled water: Treated water by distillation has to be used in order to decrease the chances of some possible alteration of the chemical nature of the slurry coating.

Distillation involves boiling the water and then condensing the steam into a clean container, hence removing impurities such as chemicals, inorganic minerals, metals, etc. The process of distillation is one of the technologies used to purify water.

3.2.2 Metal powder

The metal compound is the most important element of a slurry coating. Its role can be understood as acting like a shield against corrosion. In other words, this substance is the one reacting with oxygen and the one that degrades over time. Thus, the substrate is protected while it preserves the physical, chemical and mechanical properties of the structure where it is placed.

As previously mentioned, the slurry coating has to diffuse into the substrate and remain in the grain boundaries, interstitial voids and vacancies, and in the crystal lattice of the material. Thus, diffusion creates a shield in the upper-most part of the work-piece surface.

Once the metal coating has diffused, the expected shield layout would be composed of 3 main layers: a diffusion part, an interdiffusion zone where both coating and substrate compounds are found mixed, and the unmodified substrate. See Figure 3.1.

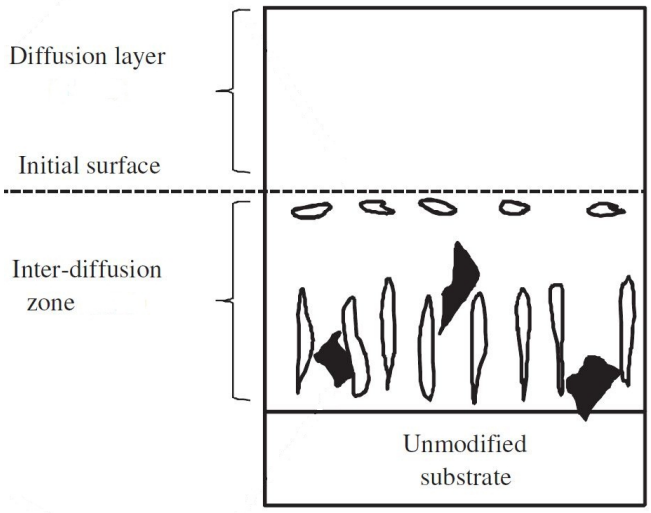

Figure 3.1: Diffused coating layout.

Source: X. Montero, M.C. Galetz, M. Schütze [66].

The microstructure of the coating is essential for the effectiveness against corrosion. It contributes to an improvement of the protective properties against oxidation and corrosion and avoid early spallation of the oxide scale [15, 16, 66].

Section 3.4 explains in more detail the application techniques to achieve a correct slurry deposition.

Rich in Aluminum

Slurry aluminide coatings have been well-known for a number of years and are widely used to protect metallic surfaces from oxidation, corrosion, erosion, and thermal shock which form part of the normal operating conditions. The life-time of these aluminum-based diffusion coatings depends not only on their thickness, but also on the 'resistance to rupture of the protective oxide layer' which forms on the surface [78].

A variety of commercial slurries is available to aluminide, for example, the surfaces of nickel-base superalloys. However, commercial slurries have several disadvantages: they contain environmentally harmful substances such as cadmium, chromates or halides which are used as binders or to activate the diffusion species [83]. They were combined to form CoCrAlY, NiCrAlY or YCrAl [85, 89, 90] which were more protective than isolated aluminum. Figure 3.2 provides a scheme of the effectiveness of different aluminum-containing coatings.

Aluminide slurry coatings can be classified in two groups: coatings with low-activity and coatings with high-activity. This has to do with the reaction interface and with which element diffuses and which one controls the diffusion process. Therefore, the aluminum activity plays a critical role in determining the predominant diffusing species [55].
The coating is considered to have a low-activity if the growing mechanism is predominated by an outward diffusion of the elements of the substrate. On the other hand, high-activity coatings grow by inward diffusion of aluminum. For this to happen, a high content of the Al is required [90, 91].

Additionally, slurry coatings, up to now, were only used to produce precipitate-rich coatings with a microstructure comparable to high-activity precipitate coatings produced by chemical vapor deposition and pack cementation [66].

One of the most important applications of aluminide coatings is turbomachinery protection. Temperatures inside the internal cooling passages of a turbine blade can be sufficiently high to require a coating for oxidation protection. A good candidate to perform this task is a diffusion aluminide coating, which is generally formed by depositing and diffusing aluminum into the surface of a component at temperatures at or above about 760°C [92]. This figure is within the usual working temperature range of an airliner aircraft gas turbine. However, the protection of turbine blades has become more and more critical with the continuing tendency to increase the operating temperature [78].

For all these reasons, in this research project, an aluminum-based slurry is going to be applied, since in certain applications, superalloys like those based on nickel are being replaced by intermetallics such as TiAl alloys. The behavior of the aluminum coating on TiAl is still under research. Moreover, this slurry coating is chromium and activator free, becoming a 'green' coating.

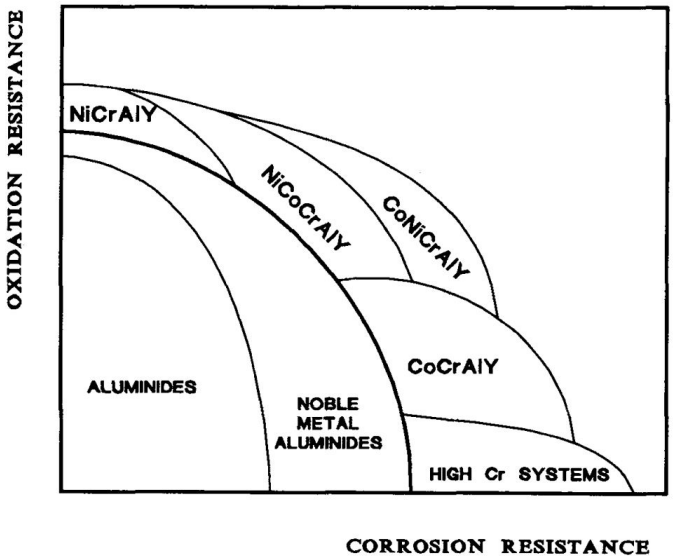

Figure 3.2: Effect of composition of overlay and diffusion aluminide coatings.

Source: A.J.A. Mom [90].

Rich in Aluminum-Boron

In order to carry on with the experiment described further on this document, a second slurry composition is going to be tested and analyzed. In this case, it was decided to use aluminum and boron powders at the same time.
The reason to do that is to investigate the performance of boron against oxidation and to see if it enhances the behavior of aluminum or not. The results of the experiment will be treated in Chapter 5.

Boron is classified as a metalloid, that is, a chemical element whose properties are in between those of metals and nonmetals. It presents certain peculiar mechanical characteristics apart from those regarding oxidation resistance.
A common process of applying boron into a metallic surface is known as 'Boriding', that is a diffusion process at elevated temperatures.

With respect to oxidization resistance, boron layer performs differently depending on the type of substrate to be protected. For example, the boride layer in nickel and cemented carbide base materials has a very consistent interface between the boride coating and the base material. However, the boron layer in iron-base materials, such as low alloy steels, tends to have a greater thickness [93].

The main application of boriding process is to obtain a hard, low-friction and wear-resistant surface. The hardness achieved is many times higher than any other surface hardening process.
The combination of high hardness and low coefficient of friction enhance wear, abrasion and surface fatigue properties. Other benefits associated with boriding are retention of hardness at elevated temperatures, corrosion resistance in acidic

environment (H_2S) and reduction in use of lubricants [94].

Pack Cementation is commonly used as a boriding technique. Components to be diffusion coated are embedded in a powder mixture, referred to as the pack or compound [95]. This powder mixture consists of a boron source, an activator (read subsection 3.2.5 for more details) and a filler.

When heating to the coating temperature, the activator reacts with the source element which is transferred to the component substrate surface by gradient of activity (i.e. partial pressure). The gas decomposes at the substrate surface depositing the coating element and releasing the halogen activator. The activator returns to the pack and reacts with the source element again. The process is maintained for the desired time [96].

3.2.3 Binder

Binders are polymer resin compounds with varying molecular weight and properties. Their primary function is to work as an adhesive between metal powders and substrate as well as a slurry homogenizer. After their application, they must convert into a dense, solid and adherent membrane providing coherence to the coating system.

Hence, binders are crucial in the slurry creation and optimization processes. In other words, developing an appropriate binder having good compatibility with water and attaining desired properties of intermediate and final products are the major factors of slurry-based processes [97].

Taking a look at the molecular level, the long polymeric chains will be in charge of trapping and sustaining the metal powders within the solution. Therefore, it is highly recommendable to use those binders with the highest molecular weights, since they will form high-quality films, once the carrier fluid evaporates.

Common binders are epoxies, acrylics and polyesters. Specifically, the typical water-based binder systems are, for example: polyvinyl alcohol (PVA) and cross-linked PVA, polyethylene glycol (PEG), carboxymethyl cellulose (CMC), hydroxyethyl cellulose (HEC), hydroxypropylmethyl cellulose (HPMC) [87], thermoplastic starch, acrylic latexes, etc. So far, they have been mostly used for ceramic slurries and not for metallic ones.

By controlling the rheological properties –those that affect the flow of matter, primarily in liquid state– of the suspensions, prepared with the aforementioned aqueous-compatible binders and through careful adjustments of dispersant content, the use of these binders was found feasible for applications like tape casting [88]. Section 5.1 deals with slurry and binder optimization processes performed for the experiment presented in Chapter 4.

Here are further examples and applications of water-soluble binders:

- *Thermoplastic starch:* Starch is an environmentally friendly, biodegradable, and readily available biopolymer consisting of condensed glucose units.Due to its gelling properties [88], the material has been used as a binder for gel-casting processes and as a binder and pore former for the fabrication of porous ceramics [87, 97].

- *Latex:* A latex is a stable colloidal dispersion of a polymeric sub-micron particles in water [98].The polymer particles are usually spherical and in the size range of 30 to 500 nm [87]. During the evaporation of the solvent, these particles coalesce and form a polymeric network, providing green strength to the dried product [88]. See Figure 3.3.

- *Polyvinyl alcohol*: It is a thermoplastic polymer that is water-soluble, and that exhibits good flexibility, and dries quickly [98]. Commercial polyvinyl alcohol is often a mixture of polyvinyl alcohol and polyvinyl acetate of which the alcohol is the hydrolyzed form. Both the chemical and the physical properties of PVA largely depend on the degree of hydrolysation and the molecular weight [87].

  The solubility in water increases with the number of acetate groups as a result of a weakening of the intermolecular and intra-molecular hydrogen bonding. Other properties influenced by the degree of hydrolysis are the viscosity and the surface tension which are lowered in partially hydrolyzed grades. Solutions of PVA generally have lower viscosity than solutions of cellulose ethers at comparable molecular weights [81, 87, 88, 99].

- *Cellulose ethers:* The cellulose polymer is insoluble in water. However, its chemical composition can be modified. The α-glucose units that make up the backbone of the polymer are changed by substituting attached hydroxyl groups (-OH) with ethers like: hydroxyethyl, carboxymethyl (CMC) or side groups of hydroxypropyl [87]. It is then, when the polymer becomes soluble in water (more hydrophilic).

  Figures 3.4 and 3.5 give an illustration of the above mentioned compounds. In general, due to the chemical inflexibility of these molecules the binder solution has rather high viscosity characteristics.

- *Polyethylene Glycol:* It is a synthetic polyether which is available in a range of molecular weights. It is soluble in water as well as in many organic solvents: methylene chloride, ethanol, toluene, acetone, and chloroform.

  Low molecular weight ($M_w < 1,000 \frac{g}{mol}$) PEGs are viscous and colorless liquids, while higher molecular weight PEGs (also known as polyethylene oxide – PEO) are waxy, white solids with melting points proportional to their molecular weights with an upper limit of about 67°C [100].

Further properties for glycol ethers include according to *'The Dow Chemical Company'*:

- Powerful coalescing ability.
- Superior coupling ability.
- Wide range of evaporation rates for the best possible film formation.
- Low surface tension for improved wetting of the substrate.
- Penetrating ability to promote adhesion to porous substrates like ceramics.

PEGs are obtained by polymerization of ethylene oxide and are commercially available over a wide range of molecular weights from 300 g/mol to 10,000,000 g/mol. PEG and PEO with different molecular weights find use in different applications, and have different physical properties (e.g. viscosity, due to chain length effects). Their chemical properties are nearly identical.

Finally, this polymer has a wide variety of applications in areas such as: medicine, biology, chemical industry, etc. More specifically, PEG is the basis of many skin creams, toothpastes (binding water with xanthan gum keeping it uniformly distributed). It acts as a binder in the preparation of technical ceramics and has been used as the gate insulator in an electric double-layer transistor to induce superconductivity in an insulator [101], etc.

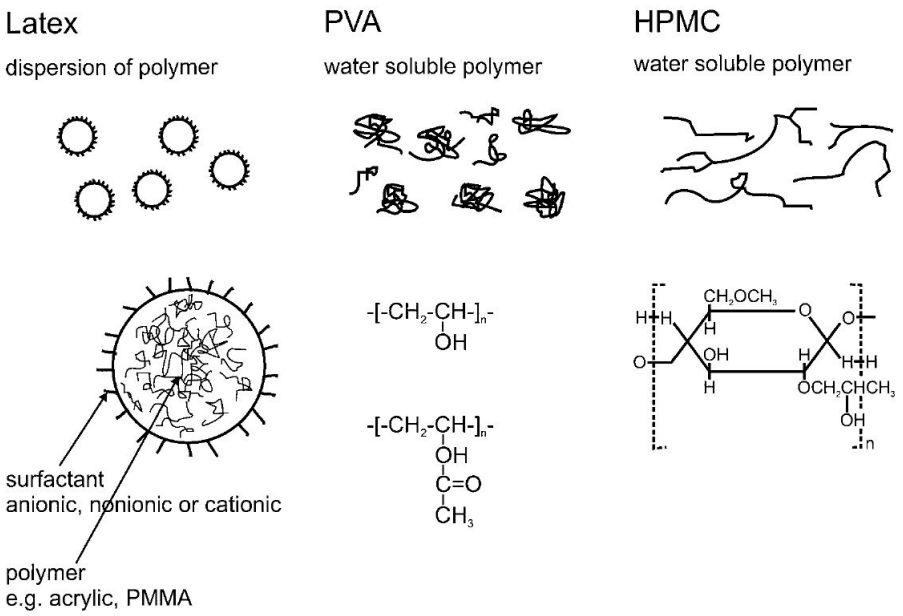

Figure 3.3: Representation of latexes, PVA and HPMC.

Source: A. Kristoersson, E. Roncari and C. Galassi. [87]

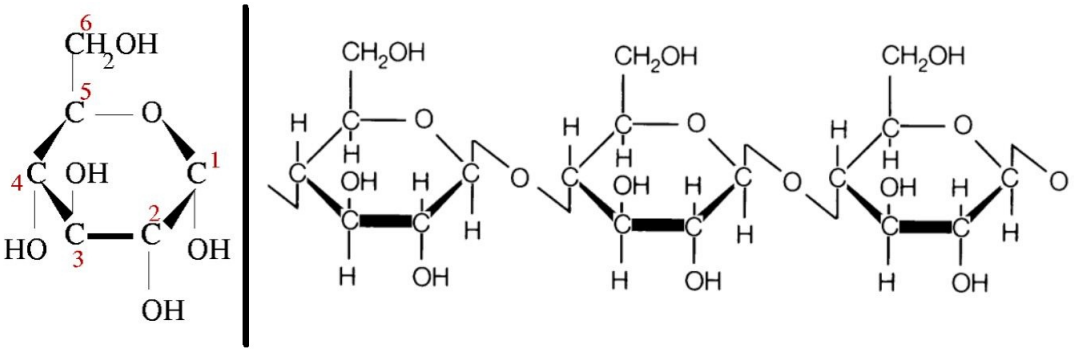

Figure 3.4: Left: α-group. Right: Unmodified cellulose chain.

Source: technologyinscience.blogspot.com

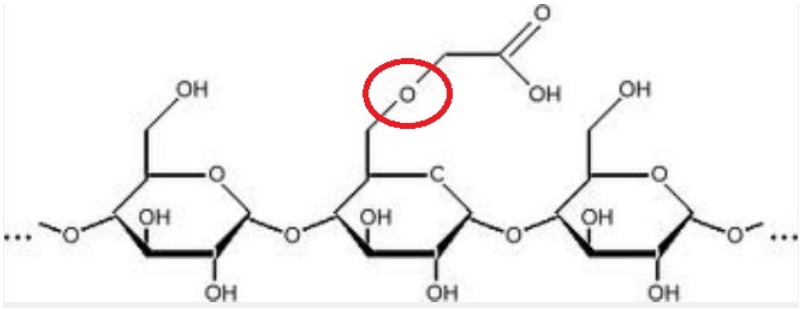

Figure 3.5: Modified cellulose. Ether group is marked in red.

Source: sci-toys.com

3.2.4 Dispersant

Wetting and dispersant agents are chemical compounds of low molecular mass, which reduce the interfacial tension between the binder solution and the powder particle surface.

These kinds of substances are also known as 'deflocculants'. Deflocculants are substances which prevent agglomeration (flocculation) by increasing the repulsive forces between particles [102]. When added to scattered particles in suspension, they cause a reduction in apparent viscosity.

After the agglomerates have been broken down into smaller particles by impact and shear forces (grinding, milling), the particle dispersion must be stabilized to avoid reformation of larger clusters by flocculation [103]. See Figure 3.6.

The use of a specific dispersant depends on the composition of the slurry: carrier fluid, binder and powder. Practical examples include organic compounds like: Polyacrylic acid, Polyethylenimine and *Carboxylic Acid*. The latter is going to be used later in the experimental procedure and it is characterized by possessing a carboxylic group:

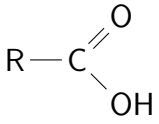

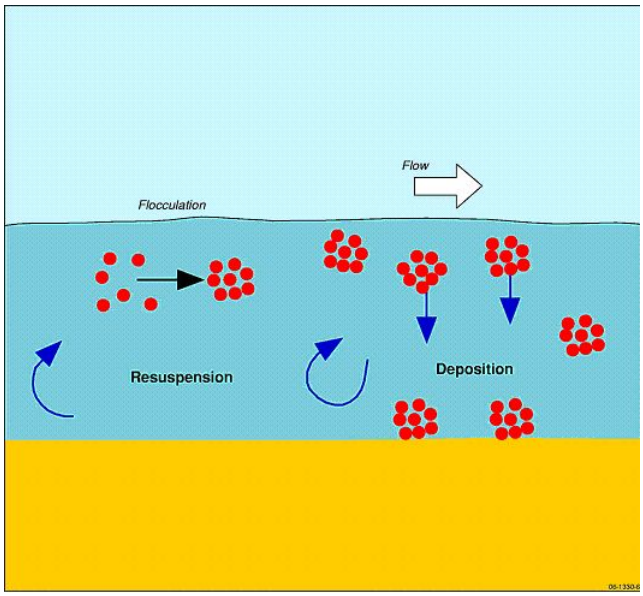

Figure 3.6: Flocculation formation process.

Source: ozcoasts.gov.au

3.2.5 Activator

An activator is a chemical substance (usually a halide salt) that is able to enhance the initiation and development of a reaction process by reacting with the metallic component of the salt pack, to form metal halides having high vapor pressures [55]. They are usually applied to diffusion coating for Ni-base superalloys.

Donchev et al.[10] report that the oxidation resistance of TiAl-alloys can be improved by a treatment with fluorine (a halide) up to temperatures of at least 900°C. The fluorine effect works under enhanced oxidation conditions such as wet environments and thermocycling where untreated components would fail quite quickly at this temperature.

However, for this research project, the slurry coating does not contain any activator in order to avoid any possible chemical reactions between this substance and the TiAl work-piece, degrading the latter.

Another practical example can be found in two common Chemical Vapor Deposition (CVD) coating techniques: Pack cementation and Vapor Phase Aluminide. These processes generally involve the use of an activator to transport aluminum from an aluminum source to the surface of the component being coated.

For instance, a halide activator (typically ammonium halide or an alkali metal halide) can be reacted with an aluminum-containing source material (donor) to form an aluminum halide gas (such as aluminum fluoride (AlF_3) or aluminum chloride ($AlCl_3$)) that travels to the surface of the component, where it reacts to form and deposit aluminum [55, 104, 105].

In contrast, aluminum deposited by slurry coating is typically diffused without any activator, relying instead on the melting and subsequent diffusion of the aluminum deposited over the surface [92]. Section 3.4 gives further details about the application process of a slurry.

3.2.6 Other Additives

They are usually low-molecular weight compounds that enable coatings to perform specific functions. Hence, they can be added in order to obtain improved properties.

Their chemical composition varies depending on the application and they include: stabilizers that, for instance, block the attacks of ultraviolet light and heat, curing agents that accelerate the crosslink-polymeric reaction, plasticizers to improve uniform coverage, flow agents and co-solvents that control viscosity, surfactants (like calcium alkylbenzene sulfonate) that they produce porous/dense structures, anti-foaming compounds, diluents, pigments to provide colored slurries, etc. [97, 103]

3.3 Slurry creation

The production process begins by choosing the appropriate slurry components and their proportions. For this reason, each application may have its own composition and, in some cases, an optimization step has to be previously taken (section 5.1).

The preparation usually starts by preparing the liquid mixture: carrier fluid to which binder, dispersant and other additives are added and dissolved. Then, the metal powders are incorporated.
If a case seeks specific slurry characteristics, then the order of preparation can vary. For example: Depending on the physical and chemical properties of some additives, these might be added once the metallic powders are poured into the solution [97].

The method presented in this section shows the basic 'computational' part of a slurry coating preparation. In this case, the compounds that are included in the scheme are: carrier fluid, binder and metal powder. If any further compound is required, its contribution can be directly included in the main equations: 3.3 and 3.4. Since the equations are linear (mathematically speaking) the terms of the additional components can be directly added to the rest. However, the system of equations to be solved becomes more cumbersome, since more terms imply more equations (i.e. these including the requirements of the new substances).

Normally, the available data to solve the problem are: total volume of the solution, density of each substance and mass ratios of the solid compounds. Conversely, the aim of the computations is to find the required amount of mass of each element, and the total mass and density of the slurry. The following scheme summarizes the different parameters of the problem.

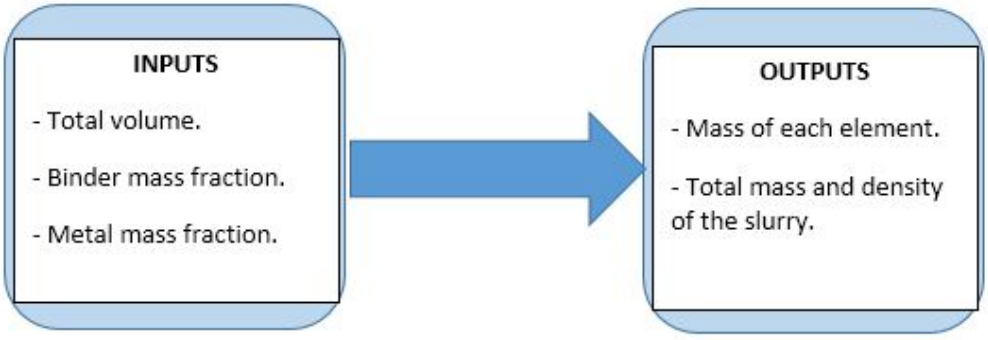

Finally, the equations governing these variables can be stated as follows:

First, the mass ratios are defined in terms of *weight-percentage* (wt.%).

- Mass fractions:

$$\alpha = \frac{m_{binder}}{m_{metal}} \tag{3.1}$$

$$\beta = \frac{m_{metal}}{m_{tot}} \tag{3.2}$$

Both parameters α and β, which represent the wt.%, are picked by the designer.
The proportion of the wt.% of binder (α) is taken with respect to the total amount of metal in the slurry (eq. 3.1). Hence, the real contribution of the binder to the solution represents less than the chosen wt.% figure.

The total mass of the mixture is the addition of the individual masses of the species.

- Total mass:

$$m_{tot} = m_{H_2O} + m_{metal} + m_{binder} \tag{3.3}$$

The total volume, which is also set by the designer, is also equal to the addition of the partial volumes. The densities are known data.

- Total volume:

$$V_{tot} = \frac{m_{H_2O}}{\rho_{H_2O}} + \frac{m_{metal}}{\rho_{metal}} + \frac{m_{binder}}{\rho_{binder}} \tag{3.4}$$

Now with these equations, the aim is to obtain the mass of each element so that the slurry can be prepared at the laboratory. The algebraic process reads as follows:

First of all, Eq. 3.3 is substituted in Eq. 3.2. The resulting equation is divided by m_{metal}, which goes down in the denominator, and then, one of the resulting terms can be substituted by Eq. 3.1, yielding a relation between the masses of water and metal as a function of known constants:

$$\frac{m_{H_2O}}{m_{metal}} = \frac{1 - \beta - \alpha\beta}{\beta} \tag{3.5}$$

After that, we need again to divide Eq. 3.4 by m_{metal} and substitute Eq. 3.1 and Eq. 3.5 in order to get an expression for m_{metal} as a function of known data.

$$m_{metal} = \frac{V_{tot}}{\frac{1-\beta-\alpha\beta}{\beta\rho_{H_2O}} + \frac{1}{\rho_{metal}} + \frac{\alpha}{\rho_{binder}}} \tag{3.6}$$

With m_{metal} known, the next step to be performed is to substitute the result back in Eq. 3.5, getting m_{H_2O}, and in Eq. 3.1, getting m_{binder}.

Finally, to close the problem, one can compute the total mass of the slurry by applying Eq. 3.3 and the total density by dividing m_{tot}/V_{tot}. Then, the problem is solved.

Sometimes, the designer may require more elements to prepare a desired slurry. As above mentioned, the procedure to compute these contributions becomes longer, but not more difficult.

On one hand, if an additional metallic substance is required, its computations can be enclosed and performed, as in the presented procedure, under the term 'm_{metal}'. However, an additional definition is required for the proportion between the two metals or between the new element with respect to the total metal mass, in case there are more than 2 metal species.
For example, suppose that 2 different metals are needed, then the new expressions would be:

$$m_{metal} = m_1 + m_2 \tag{3.7}$$

and

$$\gamma = \frac{m_1}{m_2} \tag{3.8}$$

On the other hand, if an additive (dispersant, activator, etc.) is required, then its contribution enters directly in equations 3.3 and 3.4, altering the proportions of the different elements in the slurry: carrier fluid, metal(s) and binder.

Section 4.3 gives the details about the slurry prepared for this research document.

3.4 Application techniques

The material to be protected has to be completely covered with fresh slurry. For that purpose, the covering process can be performed by immersing the work-piece in a container filled with slurry, or by means of a brush, or any other technique. In any case, the preferred process has to ensure complete coating.

Once the samples are covered, they have to be left for drying. In other words, the carrier fluid has to evaporate leaving on the surface a compact powder layer. If the coating is applied incorrectly or does not have a good appearance, for whatever reason, before and after drying, then the slurry can be removed by gently cleaning the element with water.

The time it takes for the slurry to dry depends on the nature of the carrier fluid. Nevertheless, the process can be accelerated by putting the element in a stove. Note that the temperature of this step should not be very high.
In general, the stove temperature (if needed) has to be as high as being able to ensure evaporation, but as low as possible, so that the substrate does not have enough activation energy to start oxidizing.
Similarly, special care has to be taken into account with the binder and the additives. Elevated temperatures may change their properties or even make them react either with the substrate or with the environment.
After drying, a visual inspection may be necessary in order to detect possible areas with lack of coating. In that case, a second layer can be applied locally on the affected zones.

Now, the crucial and the most expensive step of the 'slurry coating application' process is that of the diffusion. The effectiveness of the coating is essentially related to its capacity to diffuse inwards in the substrate.

When diffusing, any oxidation or pollutant interaction shall be avoided. Hence, a protective atmosphere such as those rich in argon or nitrogen, or even vacuum are suitable for this step of the process. These environments are free of moisture and oxygen, which is present in the atmosphere that surrounds the work-piece to be protected.

In the experiment described in Chapter 4, a vacuum furnace is used. Within this device, heat is transmitted by conduction and radiation allowing the coating to enter the substrate and ensuring no chemical interaction of the substrate with the ambient.
The time and temperature required for the vacuum furnace are set according to the characteristics of the metal powder and the substrate. For the former: particle size, atomic weight, chemical and physical behavior, etc. and for the latter: composition, microstructural features, temperature of the possible invariant reactions like the eutectoid and the peritectic points, etc.

Finally, once it gets out from the vacuum furnace, the work-piece is cleaned with a brush and water in order to remove the powder particles remaining on the surface. That said, the element is ready for further treatments beyond the scope of oxidation protection or directly ready to be used.

3.5 Solid diffusion

It is the phenomenon associated with the mass (atoms) transport within a solid matter. To allow this movement some energy is needed, that is, thermal activation is required in order to excite the atoms, thus creating vibrations. The movement is performed through the vacancies and interstitials arising within the crystalline structure of the material [6, 106].

Materials with lower melting temperatures tend to have faster diffusion than those with higher ones, since the activation energy required to excite the atoms is smaller. Moreover, diffusion is slower in materials having covalent bonds and compact crystalline structure like intermetallics [107, 108, 109, 110].

Generally, there are three major mechanisms for diffusion in solids. The first is known as volume diffusion. Atoms diffuse by migrating from atomic sites through vacancies. The second mechanism is a modification of the first in which atoms migrate through defect sites such as dislocations, surfaces, and grain boundaries. The third mechanism involves movement through interstitial atomic sites [55].

The main factors influencing the diffusivity are: the type of diffusion mechanism, type of crystalline structure of the matrix lattice (i.e. the solvent, in this case, the substrate), type and amount of defects in the crystal, concentration of the species that diffuse, temperature at which the process takes place and the allotted time for this phenomenon.

Controlling these parameters is crucial for achieving the desired results. Slurry coatings as well as oxidation mechanisms behave in this manner, both interchange and even react with atoms of the solvent.

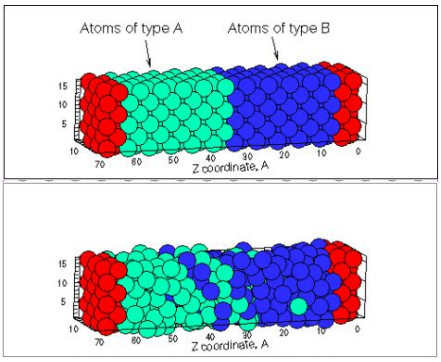

Figure 3.7: Diffusion phenomena [111].

Chapter 4

Experimental procedure

This chapter aims to describe the procedure followed from scratch to obtain the oxidized samples. This will permit to study the behavior of the raw material and the coatings against oxidation.
The specific composition of the alloy that is going to be analyzed is *Ti 45Al 2Nb 2Mn + 0.8% Vol.* TiB_2, which is introduced in subsection 2.2.4.

For this research, 24 samples were prepared, from which 18 were oxidized. That is, 3 from each surface treatment type (aluminum, aluminum-boron and without slurry) and multiplied times the 2 types of substrates: centrifugal casting and hot isostatic pressing. The remaining 6 pieces were characterized in the as-deposited or non-treated state.

The 18 samples were subjected to oxidation in static air for 300h at 800°C. After that, they were characterized by X-Ray diffraction and by the Scanning Electron Microscope (section 4.5) analysis. A relatively large number of samples was used in order to obtain points that conform the oxidation graphs presented in section 5.3.

Conversely, the first 6 pieces, the ones that were not oxidized, will give important results regarding the characteristics of the material and the slurry diffusion before the oxidation process takes place. These samples were also analyzed by both X-Ray diffraction and SEM.

4.1 Description of the raw material processing

The material provided to perform this experiment was manufactured by Hot Isostatic Pressing, which is a type of technique of powder metallurgy, and by Centrifugal Casting.

The Ti4522-XD intermetallic prealloyed powders were consolidated by hot isostatic pressing at 1200°C and 200 MPa during 4 hours at the Forschungszentrum Jülich (Jülich, Germany) [37]. The samples used for this experiment and

manufactured by this technique presented a *near-gamma* microstructure.

The samples manufactured by centrifugal casting presented a *fully-lamellar* microstructure, which can be appreciated in section 5.4. The studied alloy was centrifugally cast at ACCESS e.V. TechCenter (Aachen, Germany) in a Linn Supercast equipment with the following conditions: Mould rotation velocity = 250 rpm; mould preheating temperature: 1200°C; superheat: 20-100°C; ceramic moulds coated with Yttria (Y_2O_3). The cast specimens were subsequently hot isostatically pressed at 1185°C and 170 MPa for 4 hours in order to remove any remnant porosity. The dimensions of the castings were 44 mm x 20 mm x 2.5 mm. Cuts were made from this bar in order to obtain a desired sample size [37].

4.2 Sample preparation

4.2.1 Cutting

The first step was to give the appropriate size to the samples that were studied. The provided material came from cuts performed to bigger specimens, from these cuts the samples were obtained. The required dimensions have to be the following ones:

◦ The surface size of a sample has to be approximately that of a human thumb nail, that is, 1 cm^2.

◦ The thickness has to fulfill the requirement of being high enough so that it can bear the grinding and the slurry diffusion steps. In the case of the samples manufactured by HIP, the thickness is about 2 mm and those made by CC measured around 5 mm.

The metallic samples were cut in a standard semimanual cutting machine, which can be seen in Fig. 4.1. The used cutting disk was that suitable for titanium, which has a diamond protection film around its contour in order to create a high quality cut. Special care has to be taken with the cutting speed: The disk was rotating at 1500 rpm. This speed is neither very low –so that it would not cut the metal–, nor very high –so that it would not create a lot of residual shear stresses in the sample surface–.

Additionally, the advancement speed of the plate that holds the sample must be low enough for the disk to have enough time for making a clean cut to the material. In this case: $25\frac{mm}{min}$.

Clearly, a lubricant must be used in the cutting process, since titanium-aluminum alloys are hard to slice. Lubricant helps in many aspects: it lowers the cutting temperature, preventing, for example, local heat treatment, it increases the tool life-time (lower wear), it decreases the cutting force as well as the re-

quired power, it gives a better surface finish and quality, etc.

Furthermore, the lubricant has to be filtered from scrap particles, in order to prevent particle deposition in the pump and pipes of the machine.

Interestingly, the alloy manufactured by means of centrifugal casting technique was harder than that made through pulvimetallurgy. One could even see sparks and vapor oozing from the sample when cutting it.

(a) This is the used cutting machine. **Source:** Presi.

(b) Interior view. **Source:** Presi.

Figure 4.1: Cutting machines.

4.2.2 Surface preparation

Once the samples had the required size, the next step was to create the appropriate surface finish (plain and smooth), in order to have a correct adhesion of the slurry to the surface. For this purpose, one of the main faces of the sample has to be sanded down. The process consists of grinding the sample to the desired characteristics.

Grinding paper (similar to sandpaper) with several grain sizes or particle densities was used (i.e. the smaller the grain size per unit area, the higher the amount of particles for the same unit area). These are numbered from larger to smaller grain size or, equivalently, from lower to higher particle density. The grain is made of Silicon Carbide (SiC), which is a ceramic substance able to scratch this alloy.

Due to the different particle sizes, the depth and thickness of the scratches produced on the surface become smaller, every time the sandpaper number is changed. Thus, acquiring the desired surface finish.

The sandpaper is placed and attached to a disc which rotates at different velocities; for this case 250 rpm. The sample is then placed onto that rotating sandpaper. By applying light pressure, the sample gets grinded. Once a uniform surface is obtained, the abrasive paper has to be changed to a higher number. In other words, each phase will end, once all the stripes from the previous paper disapppear.

It is recommended to rotate the sample 90 °, in order to get an easier visual control of the grinding process and to ensure a correct finish.
Water was used as a coolant during the whole process.

In this experiment, the used grinding paper numbers were: 180, 320, 400, 600 and 1000 particles per unit area.
Additionally, the base material had a protective coating layer. So first, this film had to be removed with the largest grain size in order to clearly expose the substrate to the ambient.

When the samples were ready, they were immersed in ethanol (acetone can also be used) and washed in an ultrasonic cleaner.
The purpose of these organic compounds is to remove the remaining undesired particles from the samples. The presence of these compounds does not alter any further step in the experiment, since their evaporation temperature is well below those used in the following steps; like the one for the slurry diffusion.

4.3 Slurry preparation and deposition

This section describes the steps to create a slurry coating following the theoretical background, descriptions and indications provided in sections 3.3, 3.4 and 5.1.

For this experiment, two slurries were chosen to be produced: one containing aluminum and the other a mixture of aluminum-boron. In both cases, distilled water is the carrier fluid, PEG the binder and Dolapix the dispersant. Neither activators, nor other additives were added. Hence, this slurry can be considered as a simplified model that may achieve good oxidization-resistance performance.

After making an experimental optimization process (described in section 5.1), it was decided to have in both coatings a proportion of metal powder of 60 % in weight of solids with respect to the total percentage of mass in the mixture. However, the percentage of binder differs from one slurry mixture to another. As it is described in section 5.1, one of the main driving factors for the amount of binder to be added in the coating depends on the particle size of the metal powder. In both cases, PEG, manufactured by *Sigma-Aldrich*, with molecular weight of 20,000 g/mol was used; according to section 3.2.3 high molecular weights provide better adhesion performance.

Finally, the dispersant Dolapix CE 64 was used adding by a volume 10 μl per 5 ml of solution.

Dolapix CE 64 is a commercial Carboxylic acid preparation. Dolapix is free from alkali and it does not foam [112]. This product produces slip between solid particles. Therefore, it is particularly suitable to create deflocculation.

The product is in liquid state and is completely dissociated. Hence, the deflocculant effect commences immediately after addition.

According to the manufacturer ('Ceramics Keramik') DOLAPIX CE 64 can be employed in combination with the conventional temporary binders, such as polyvinyl alcohols, polymer dispersions, polysaccharides, cellulose derivatives and others. Table 4.1 contains its characteristics.

Appearance:	yellowish liquid
Active matter:	approx. 65%
Solubility:	water-miscible
Density ($20°C$):	approx. $1.20 g/cm^3$
pH (original):	approx. 7

Table 4.1: DOLAPIX CE 64 characteristics.

4.3.1 Preliminary computations

Applying directly the equations and conditions described in section 3.3, the required mass of each component forming the slurry coating can be obtained. The inputs of the problem were:

- Total volume of the slurry: 20 ml.
- Available densities: aluminum, boron, PEG and water.
- The proportion in weight of aluminum with respect to boron was 1 to 3 (i.e. 3 parts of B per 1 of Al). See equations 3.7 and 3.8 in page 34.
- Metal and binder weight percentages.

Note that the amount of dispersant (Dolapix) was not included in the calculations for two reasons: first its volume, around 0.2%, is usually negligible compared to the total one, and second to simplify the computations.

Aluminum coating

The components of this slurry are: Aluminum powder with a particle size of *45* μm, PEG-20,000, 40 μl of Dolapix and distilled water. Since the particle size of the powder is large, the amount of binder added was a 10% of that of the metal.

The following table summarizes the output results after solving the equations presented in section 3.3.

Compound	**Density** $[\frac{g}{ml}]$	**Weight percentage of solids**	**Partial mass** $[g]$
H_2O	1	34 %	10.957
Aluminum	2.6984	60 %	19.336
PEG	1.03	6 %	1.934

Table 4.2: Aluminum Slurry Coating Composition.

Aluminum-Boron coating

The components of this slurry are: Aluminum powder with a particle size of *45* μm, Boron powder with a particle size of *5* μm, PEG-20,000, 40 μl of Dolapix and distilled water.

In this case, the amount of binder was selected to be at 3 wt.%, according to the work performed by M. Amirjan and H. Khorsand [97] and thanks to two additional facts found when optimizing the slurries. First, the small particle size of boron, and second, the aluminum adherence. Although aluminum is present in the slurry mixture, its particles did not drop down as in the case when it was alone. The proportion of this metal has to be included and is reflected in equations 3.7 and 3.8.

The following table summarizes the output results after solving equations of section 3.3.

Compound	**Density** $[\frac{g}{ml}]$	**Weight percentage of solids**	**Partial mass** $[g]$
H_2O	1	38.2 %	11.819
Aluminum	2.6984	15 %	4.641
Boron	2.34	45 %	13.923
PEG	1.03	1.8 %	0.557

Table 4.3: Aluminum-Boron Slurry Coating Composition.

4.3.2 Slurry preparation

A description of the steps is the following:

1. The different components were weighed taking the values from tables 4.2 and 4.3. Then, mixing started by adding the binder to the moving water. If the binder is not easy to dissolve, then, applying heat to the breaker would be required. In this case, it took few minutes to dissolve PEG at room temperature.
   Note that temperatures approximately above $70\,^{\circ}C$ risk to create undesired water vapor, hence, altering water proportion in the slurry.
   To avoid any additional difficulties when dissolving, it is important to add the binder little by little and wait until it is completely absorbed by the solution. Figures 4.2 and 4.3 display the components of the prepared Al-B slurry.

2. After complete dissolution of the binder, Dolapix was added, creating a liquid with high viscosity, similar to a glue. Figure 4.4 gives a visual representation. One can see that there are no bubbles, even though the liquid is rotating. This is due to the fact that PEG increases liquid viscosity considerably.

3. Once the aqueous solution was ready, the next step was to add the metal powder. Again, this addition shall be done little by little, so that the slurry is evenly mixed and gets a good appearance.

4. The mixture was subjected to ultrasonic vibration at an amplitude selection of 20 mA for 30 seconds. The aim of this step is to destroy any possible powder agglomerations, enhancing dispersant effect, and helping binder to sustain these new free metal particles. Figures 4.5 and 4.6 show the slurries once finished.

5. Finally, the samples were immersed in the slurry and left over a 'drying bed'. A small brush can be used to add coating to the uncovered parts. This is suitable for large particle size powder. The aluminum coating had to be applied up to 3 times until getting full coverage (see Fig. 8.2 in the appendix).

Figure 4.2: Preliminary layout of laboratory equipment for slurry preparation.

Figure 4.3: Preliminary layout for preparation of aluminum-boron slurry.

Figure 4.4: Photograph of water-based solution.

Figure 4.5: Finished aluminum slurry.

Note that the mixture texture is like a shining paint.

Figure 4.6: Finished aluminum-boron slurry.

4.3.3 Slurry deposition

The samples were immersed in the slurry and left to dry for a night at room temperature. Figures 4.7, 4.8 and 4.9 show the drying process of the aluminum coating. If the pieces are left for more than 24h drying there are no side-effects. Nevertheless, for longer periods of time, the quality of the powder compaction may be worse.

Al-B slurry covered homogeneously the samples. In the case of the aluminum one, there were some uncovered zones due to gravity effects, although the slurry was optimized to minimize this issue. As indicated before, a brush can be used to give additional fresh slurry layers, if needed.

After that, the samples were heated up to 1000°C for 4 hours, in order to let diffuse the slurry. For that purpose, the covered samples were placed in a flat ceramic crucible over a bed of small balls of Zirconium dioxide, ZrO_2. This material is included to prevent the pieces from sticking to the crucible.

There were two reasons for choosing 1000°C as the temperature of diffusion. First, this value is below the eutectoid point for this alloy which is situated at 1158°C, hence the microstructure is not modified. Second, this temperature is high enough to let the slurry be chemically active or even in molten state[1] [2], and penetrate (diffuse) into the receptive substrate whose atoms are also energetically excited.

Figure 4.10 shows the thermal cycle used for this experiment. The heating and cooling rates were set to be $5°/min$ but, actually, the rate was even slower to protect the furnace.

Once the samples went out from the vacuum furnace (Fig. 4.11), they were cleaned (Fig. 4.12). First, the additional coating had to be removed; this did not diffuse and had a brittle texture. Second, samples were immersed in water and cleaned smoothly with a brush in order to eliminate free powder particles. It is important to avoid rubbing and scratching in this step. After that, they were placed in ethanol and subjected to vibration in an ultrasonic cleaner, similarly to the one used after grinding. Finally, they were again cleaned in water and dried with hot air.

[1] Aluminum melting temperature, $T_m = 660°C$.
[2] Boron melting temperature, $T_m = 2076°C$.

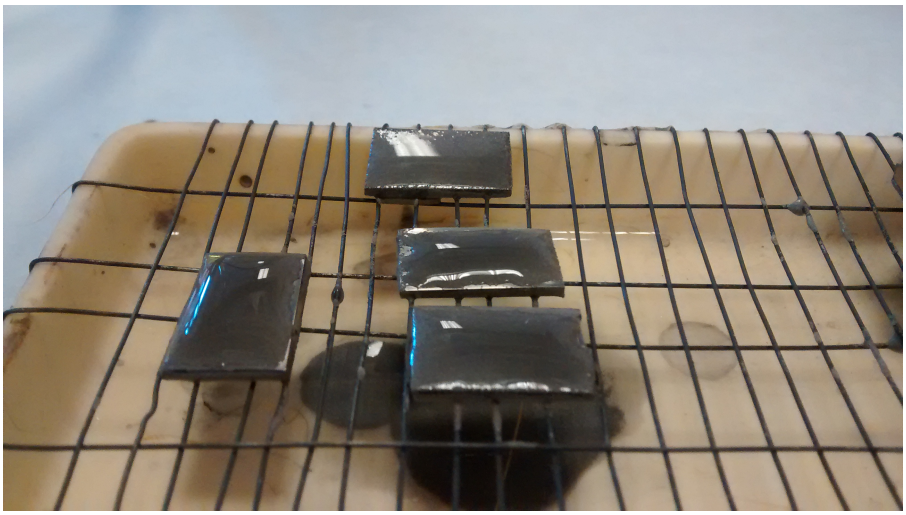

Figure 4.7: Aluminum slurry after application onto substrates.

Figure 4.8: Aluminum slurry coating applied onto substrates after half an hour drying.

Figure 4.9: Slurry coating after 24h drying at room temperature. Left: Al, Right: Al-B.

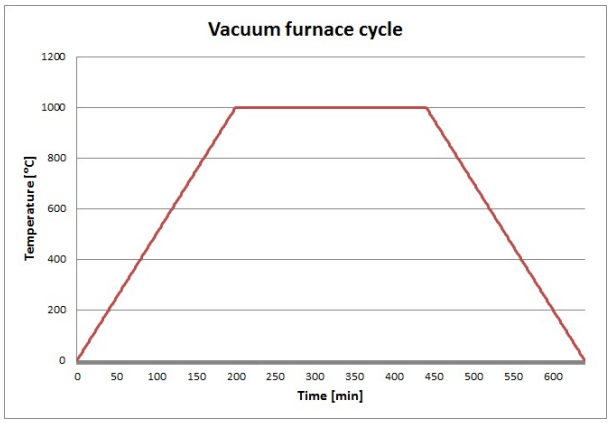

Figure 4.10: Vacuum furnace cycle.

Figure 4.11: Slurry coating after diffusion treatment in vacuum furnace for 4 hours at 1000°C. Left: Al, Right: Al-B.

Figure 4.12: Slurry coated samples after diffusion treatment in vacuum furnace for 4 hours at 1000°C and after cleaning. Up: Al, Down: Al-B.

4.4 Oxidation process

The oxidation test is the heart of the experimental part of this research. Recalling the introduction of this Chapter, a total of 18 samples were oxidized: 9 for each type of substrate (either HIP or CC), which were divided in 3 groups depending on the applied protection type: none, aluminum, aluminum-boron.

The samples were placed in a ceramic crucible that had a special metallic mesh attached to it. This mesh helps to sustain and give enhanced superficial exposure to the samples. Clearly, both the ceramic and the metal have to resist (not melt) at the oxidation temperature.

The performed oxidation test lasted for 300h at 800°C. It was an interrupted-type test; the pieces were heated and cooled several times during the 300h, in order to take mass-gain measurements, which will help to evaluate the oxide gain and the coating performance. Figure 8.3 in the appendix provides a view of the oxidation furnace.

These measurements were taken after 12, 24, 50, 100, 150 and 300 hours of oxidation at the selected temperature. Within these 300 hours, neither the ramp time (the time it takes for the furnace to heat and cool down in each time section), nor the dead time (the time after the furnace reaches room temperature and before being started again) were included (see Table 8.2 in the appendix).

Note that the oxidation test took a total of 17 days. Tables 8.1 and 8.2 in the appendix give an actual detailed schedule of this test.

At each time-step (interruption), the samples were weighed in a high precision balance. This data will be gathered and plotted in the *'Oxidation graphs'* that will be explained in section 5.3.

The method to create these graphs is that the values of the increment of mass are divided by the initial exposed-surface area, A_0, of each sample (see Table 8.3). The area is calculated by taking an average between the measurements collected in Table 8.7. The surface value can be obtained by the following expression (4.1) and assuming a tetragonal prisma shape:

$$A_0 = 2 \times (l \cdot w + l \cdot t + w \cdot t) \tag{4.1}$$

Where l, w and t are: length, width and thickness, respectively.

The dimensions of the values obtained are in g/mm^2, they are transformed into mg/cm^2 and an average is taken between the samples of the same type (Table 8.5).
Finally, Chapter 5 explains the effects of the oxidation process and its consequences.

4.5 Analysis of the samples

This section presents a brief theoretical background in order to understand the two different techniques used to analyze the samples. These were: X-Ray diffraction and the Scanning Electron Microscope. Samples with and without coating, as well as samples subjected or not subjected to the oxidation, were studied under these two devices.

4.5.1 X-Ray diffraction

X-Ray diffraction is one of the most extended techniques in the scientific community to analyze the crystalline structure and the phases present in a sample [113]. In other words, it analyzes how the atoms are organized within the material and the chemical elements that compose it. It is a quite reliable technique, since it has both precision and accumulated historical data, so that the results can be contrasted in many cases.

The technique consists of sweeping the sample surface with an X-Ray beam. Once this beam impinges the target, the rays are diffracted in several directions due to the symmetry of the atomic clusters of the material. A receiver collects all these diffracted rays and creates a 'pattern of intensities', which represents the place of the atoms in the crystal.

This pattern can be interpreted thanks to Bragg's law:

$$n\lambda = 2dsen\theta \tag{4.2}$$

Where:

- n = integer number.
- λ = wave length.
- d = interplanar structural distance of the sample.
- θ = incidence angle of the X-Rays.

A scheme of the configuration is shown in Figure 4.13.

Actually, the receiver captures energy peaks coming from the diffracted rays, creating what is known as 'diffraction diagram' or 'diffractogram'.

Furthermore, this representation permits to identify the different crystalline structures, associated with each phase, that compose the sample. Each one of these structures has its own characteristic diffractogram, so the identification can be performed by comparing the actual results with tabulated diagrams (historical data).

The X-Ray diffractometer used in this experiment was *Philips X-pert* using monochromatic Cu-K radiation (Philips X'pert MPD, $K_{\alpha(Cu)}$ radiation). The parameters set for this device can be found in table 4.4. Cycle 2 was created to get a higher accuracy with respect to cycle 1 when analyzing the samples.

	Cycle 1	Cycle 2
Initial inclination angle	20°	30°
Final inclination angle	100°	90°
Goniometer	0,02°	0,02°
Time step	1.7s	2.2s
Total process time	1h 53 min.	2h
Working intensity	40 mA	40 mA
Working voltage	40 kV	40 kV

Table 4.4: X-Ray adjusting parameters.

For the present experiment, the analysis of the chemical compounds present on the surface of the samples was performed by means of X-Ray Diffraction.

The output information (diffractograms) coming from *Philips X-Pert* device were treated with the software *X-Pert Highscore*. This program helps the user to identify the chemical compounds present on the surface of the work-piece.

The software marks the peaks of the diffractogram and compares the patterns obtained from the sample with the patterns of the expected components (included in the program database). Finally, the user has to make an educated selection of the matching compounds proposed by the program and then, identify the peaks.

The results of the analysis are presented in the *XRD-tables* of section 5.4. These are based on the information extracted from the diffractograms.

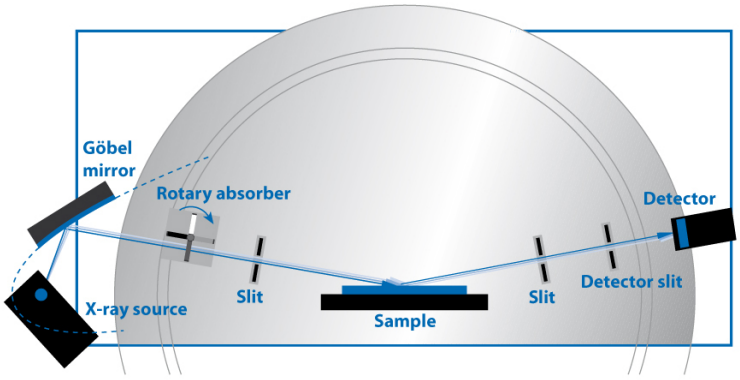

Figure 4.13: Theoretical display of the X-Ray diffraction.

Source: Bruker.

4.5.2 Scanning Electron Microscope

The Scanning Electron Microscope (SEM) uses a beam of electrons in order to create high resolution microscopic images of the sample surface.

The system works as follows: First, vacuum is created in the chamber where the sample is placed. Second, electrons forming a beam are accelerated in an electric field and bombard the material surface. Finally, these electrons interact with the atoms of the sample generating a signal that will determine the creation of the images.

There exists two electronic detectors that collect these signals: the detector for secondary electrons and the back-scatter electron detector.

The former receives low-energy electrons (few dozens of eV) coming from the upper-most part of the surface. This signal is the result of the inelastic interaction of the incident beam with the atoms of the sample and it contributes to obtain the topographic information of the surface.

The latter perceives the signal of the elastic collisions (i.e electrons released from the substrate) revealing the differences in the chemical composition of the sample. For instance, those elements with higher atomic weight will generate more intense signals –shining more–, since they deflect more. In other words, heavy atoms will appear clearer, whereas lighter atoms will appear darker. Thus, a difference in contrast can be established among the elements creating a high resolution image.

Finally, the SEM is also equipped with a third detector that is used to identify the composition and measure the abundance of chemical elements in the sample. This detector is based on interpreting the characteristic X-ray waves that are emitted from the atoms when the electron beam removes an inner shell electron from the sample. This removal causes a higher-energy electron to fill this shell, releasing energy (X-ray waves) when moving.

Figure 4.14 shows the working principle of this device.

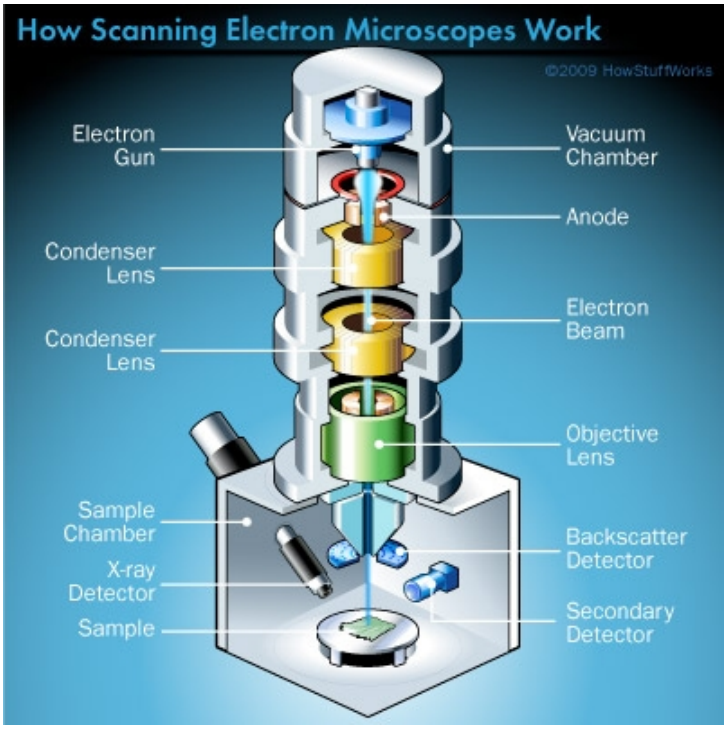

Figure 4.14: Scanning Electron Microscope configuration.

Source: HowStuffWorks.

The Scanning Electron Microscope gives a double information. First, it is able to take pictures of the topography and the microstructure of the sample surface, and second, it performs an analysis of the atomic composition of the material.

This analysis is performed by means of a technique called *Electron Dispersive Spectroscopy* (EDS). Its results can be given in both atomic and weight percentages (at.% and wt.%). The former provides information about the stoichiometric composition of the substance, whereas the latter gives information about their weight proportions.

EDS is a semiquantitative analysis technique; it indicates that the results are not a 100% precise, but it gives a first order approximation. In other words, SEM cannot provide the exact atomic and weight percentage of the elements present within the studied work-piece. Thus, the results can be understood to be incomplete if there is no other diagnostic technique. In this case, XRD plays an important role as complement.

The SEM device used for the analyses was a *Philips XL-30*. Its detection threshold is situated for atoms with an atomic number higher than Boron (Z=8).

4.5.3 Metallographic preparation for SEM observation

The steps for the metallographic preparation of the samples in order to observe under the SEM are as follows:

1. **Metallic coating:** A metallic coating was applied to the samples prior to cutting in order to protect the underlying coating/oxide during the metallographic preparation. For this reason, the pieces were previously protected by covering them, first with gold (Au) by sputtering, and then with copper (Cu) by electrodeposition.

   A thin layer of gold makes the sample an electrical conductor, so that the subsequent electrodeposition phenomenon can take place. This is specially indicated to the oxidized samples, because they are not conductive. Copper is added in order to protect the sample during the metallographic preparation. For example, it prevents the oxides lying in the surface from falling and getting lost.

   Electric and heat conduction of the sample inside the SEM is ensured by mounting[3] it in conductive resin.
   With this process, the work-piece is protected and becomes conductive. Besides, the resin provides a physical structure which allows it to be observed.

   (a) **Gold coating:** The process is known as *'Sputtering'*. The used device consists of a chamber in which a sample and a foil of gold are placed. Then, an electric field is created in order to accelerate and conduct atoms from the foil (anode) to the target (cathode), in this case the sample. Gaseous Argon (Ar) atoms are injected in the chamber, they impinge the foil and detaches the gold atoms that will fall and cover the sample.
   The entire process is performed under vacuum conditions.

   For this experiment, samples were sputtered for 9 minutes. See Figures 4.16 and 4.17.

   (b) **Copper coating:** The deposition process of copper is performed by electrodeposition that is similar to the working principle of a battery.

   The process takes place in an electrolytic solution in which a copper foil and the sample are immersed (see Figure 4.18). Copper acts as the anode and the sample as the cathode. By applying electric voltage difference, atoms of copper are able to detach and travel, hence covering the target specimen.

[3] Mounting process is detailed in page 56.

This step may take from 30 to 60 minutes. It ends once the sample has a coppery appearance. The composition of the electrolytic solution is the following:
For a 100 ml mixture, it is required:

- 22 grams of copper sulphate: $CuSO_4$.
- 3ml of sulfuric acid: H_2SO_4.
- Distilled water.

Water is added at the end until the whole solution achieves a 100 ml. A beaker can be used as a recipient for measuring and mixing.

Note: If copper does not cover the sample homogeneously, then the sample has to be bombarded with gold again.

2. **Cutting:** Samples were cut at low speed in a 'microcutter' with a disk, similar to the previous cutting step. They were cut from the middle section (in the thickness direction), thus showing their interior and preparing them for analysis.

3. **Mounting:** Samples were mounted in conductive resin. The process was performed at 170°C for 15 minutes. See Figure 4.15.

4. **Grinding:** Mounted samples must be grinded to achieve a good surface finish, and to ensure that the cross-section of the samples are free from some resin, that possibly attached during the mounting process.

5. **Polishing:** Samples were polished in order to achieve the necessary surface finish for observation in the SEM.
First, the samples were polished with a water-based monocrystalline diamond (abrasive particle) solution of a grain size of 1 μm, then with diamond paste of 0.1 μm grain size, and finally with a suspension of colloidal silica [4] of 0.06 μm. Water-based lubricant indicated for diamond suspension was applied during the whole process.

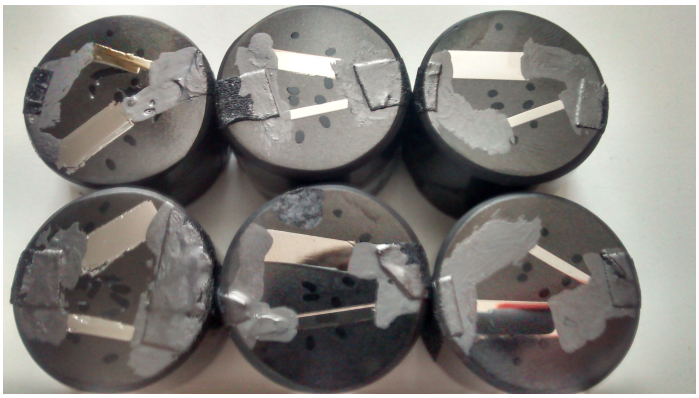

Figure 4.15: Mounted samples prepared for SEM observation.

[4] Silica: SiO_2

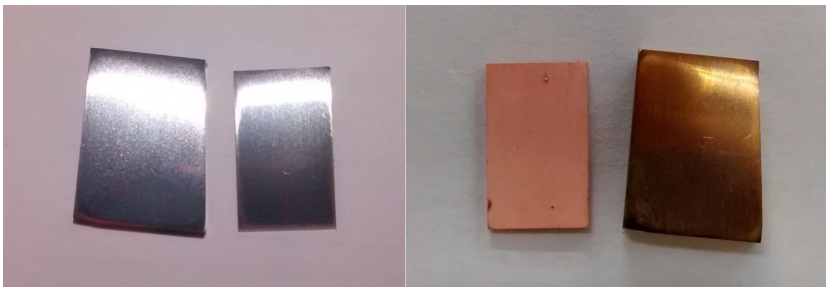

Figure 4.16: From left to right: Grinded surface of a CC and a HIP samples. Then, covered with gold and copper.

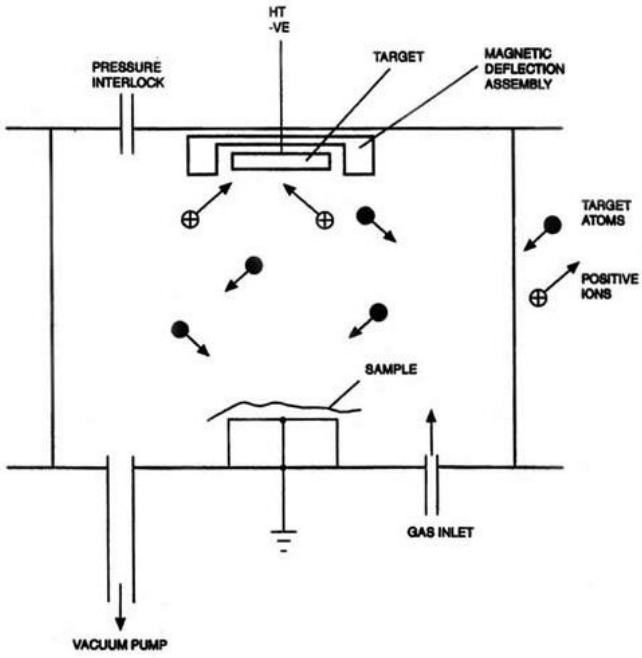

Figure 4.17: Sputtering process layout.

Source: Emsdiasum.com

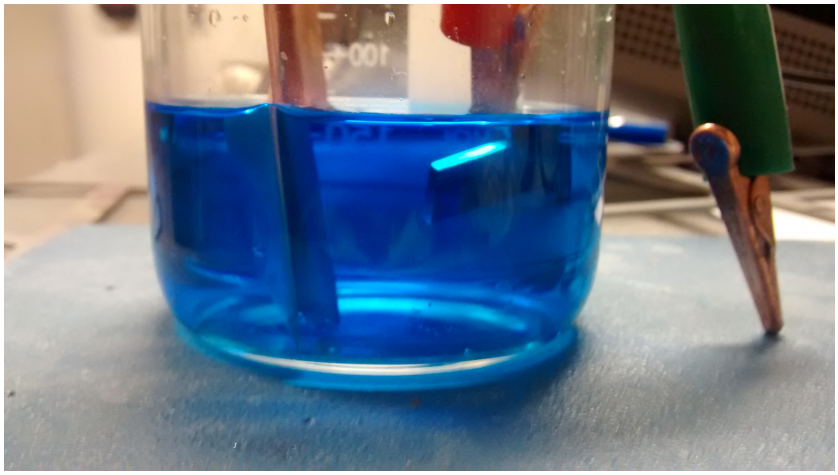

Figure 4.18: A sample while it was coated with copper by electrodeposition.

Chapter 5

Results & Discussion

A set of three techniques are used to analyze the results of the experiment: mass-gain oxidation graphs, X-Ray diffraction (XRD) and the Scanning Electron Microscope (SEM). All of them give an insight of the diffusion and oxidation phenomena.

5.1 Slurry optimization

There are not many references about the proportions of the different compounds that have to be used to obtain a high quality slurry. Therefore, this section describes the preliminary slurry optimization carried out for the present research. The slurry coating contains distilled water, aluminum and boron powders, a soluble binder and Dolapix. All these components as well as the production process are described in detail in section 4.3 and in Tables 4.2 and 4.3.

The three main aspects that were optimized are: proportion of solids (i.e. wt.%), type of binder and metal powder performance.

Metal Powder

It was observed that the main driving factor in the appearance, quality and deposition of the fresh slurry was the particle size of the metal powder. When the size is relatively large (around 20-50 μm), the particles did not adhere consistently to the work-piece surface and fell off leaving non-covered regions. If this happens then there will be no diffusion, due to the absence of coating, and hence no protection for that area.
In other words, a slurry coating has to be consistent enough so that the metal particles cover the entire sample surface homogeneously.

A second phenomenon can be observed when a slurry mixture with considerable particle size is left for a while in its container. Two different layers were formed in the vessel. The liquid solution remained at the top and the precipitated metal particles deposited at the bottom.

In principle, this deposition phenomenon does not affect any property of the slurry. Nevertheless, the mixture shall be stirred well before use, thus recovering its initial appearance.
In any case, it is recommended to apply the slurry once it has been prepared to avoid particle deposition in the vessel.

Binder

Choosing an appropriate binder is crucial for a good output. The binder shall be compatible with water and attain desired properties of intermediate and final products, that is, it has to enable the user to apply it without difficulty and it has to ensure that once the carrier fluid has evaporated, the metal particles will remain compacted over the work-piece surface.

The binder optimization process was done with PVA, CMC and PEG.

- **Polyvinyl Alcohol:** Literature regarding oxidation coatings like: [81, 87, 88, 97, 98, 99] use PVA. The ones which applied it for slurries coincide in pointing fair properties and stability. The optimization carried out for this research did not show fast and easy dissolution abilities, although water was heated up to $80°C$, or good performance, since it created foam bubbles. See Figure 5.1.

- **Carboxy Methyl Cellulose:** Its dissolution time is relatively quicker than that of PVA. The dissolution can be performed at room temperature. Moreover, this binder gave the highest viscosity, but the coating had a poor uniformity once it dried (see Figure 5.2) and did not adhere correctly. That is, the coating layer could be removed at once due to the binder properties (Figure 5.3). For these two reasons, it was discarded.

- **Polyethylene Glycol:** PEG was easily dissolved in water at room temperature. It did not give further complications, adhering correctly to the sample surface. Thus, PEG was chosen to be the binder of the slurry used for this experiment due to its good performance among the three candidates.

Weight-percentage of solids

In the case of the Aluminum slurry, it was observed that the adherence to the samples was not very good. Uncovered regions appeared due to the large size of the metal particles. Then, it was decided to increase the wt.% of both binder and metal powders. The optimization process was carried by fixing the wt.% of PEG, wt.% of powder and varying the other.

The binder proportion was varied from the usual 3% to 5% and 10% in weight (with respect to solids). This way a higher viscosity is achieved, in order to sustain larger powder particles and getting a better adherence. The latter prevents the

particles from falling off. Therefore, the best covering performance was achieved with the last value.

Regarding the metal proportion: The aim is to get the right amount of metal so that the particles cover the substrate completely. Then, the metal wt.% was varied from the common 60% to 70%. However, the appearance at that value was that of concrete. Water was completely absorbed by the metal powder, disabling the slurry from proper application.

In the case of Aluminum-Boron slurry, the particle was small enough (5 μm) to avoid these problems. Thus, it is not needed to exceed the 5 wt.% of binder if the particle size is small.

Further optimization

In general, slurry coatings have some disadvantages that need to be overcome by trying to improve the application techniques. The data from previous sections illustrate that the thickness of the coating is difficult to control. Further, if the particle size is relatively large, the slurry will tend to fall off, exposing certain areas while leaving others with more slurry accumulations. Hence, the homogeneity and uniformity have to be improved as well. Consequently, alternative deposition techniques like plasma spray are utilized, in some cases, with respect to slurries.

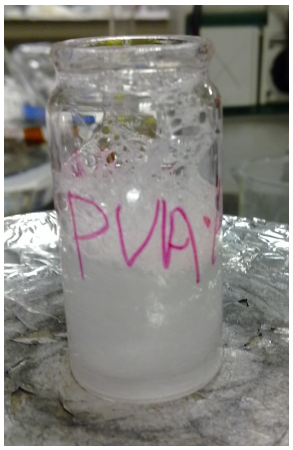

Figure 5.1: Appearance of the water-based solution while dissolving PVA.

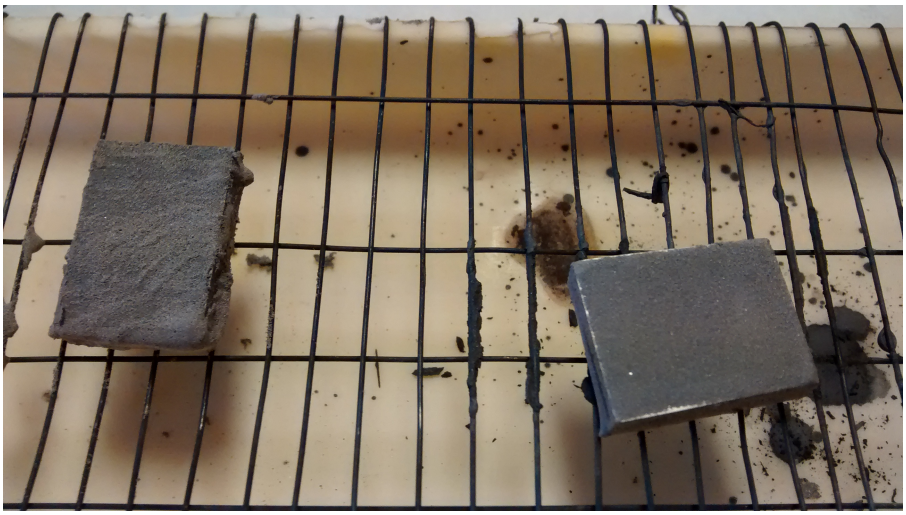

Figure 5.2: Appearance of aluminum based slurry with different binders after drying. Left: CMC. Right: PEG.

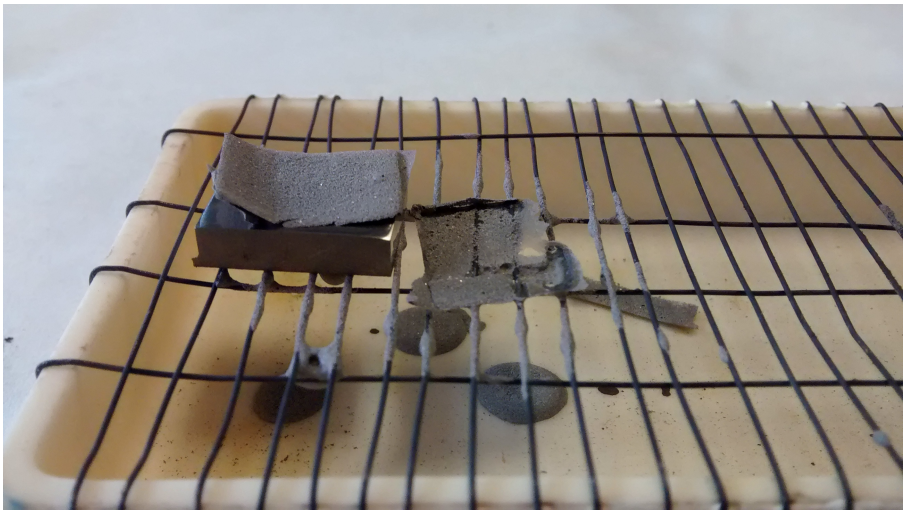

Figure 5.3: Appearance of aluminum based slurry with CMC binder after drying.

5.2 Post-diffusion state

This section is devoted to comment on the external appearance of the slurry coating once it has diffused in the substrate, that is, after the vacuum furnace step.

It was observed that the aluminum-boron slurry did not cover the sample homogeneously. There were areas where the coating was clearly present on the sample surface, while its presence was limited to a microscopic level in others (see Figures 4.12 and 5.4).

In principle, the slurry coating should appear uniformly distributed along the surface, without having high thickness. The beneficial effect of this kind of coatings is that there is not an important external presence of it, once it diffuses inwards. In other words, the protection function is achieved when the coating is located within the substrate (not like an overlay coating).

Figure 5.4: Al-B slurry appearance after diffusion.

Conversely, aluminum slurry coating gave an unexpected final appearance. The samples grew in size and there was even an additional layer in the boundaries of the samples. The thickness of this additional new layer was comparable in size with the thickness of the initial sample, hence creating a physical shield. This phenomenon was observed in both substrates: HIP and CC. The appearance of the coating was similar in both cases.

The possible causes of the undesired thickness might lie in the fact that the slurry coating was applied up to three times. This was made in order to cover the sample completely, since the particle size of the aluminum powders (see Figure 8.2) were relatively large (45 μm). Moreover, the diffusion phenomena was performed at 1000°C, which is a temperature well above the melting point of pure aluminum. The diffusivity of this metal is quite high in both liquid and solid state.

Therefore, the diffusion took place between reactive aluminum, which could be first solid and then liquid, and a solid-state substrate (solvent). When a substance is in a liquid state, its diffusion coefficient is much greater than when it

is in solid state [114]. Thus, the diffusional outcome can be expected to be more drastic.

An additional remarkable fact is that the work-piece lost its original dimensions. At the beginning, the sample's cross-sectional area had a rectangular shape. However, as it can be observed in Figure 5.5, the substrate area associated with the white color lost its smooth shape and acquired a wavy profile. There was also a transition (diffusion) are which surrounded this profile, and another area influenced by the coating, which had a darker color.

The loss of a uniform profile is due to the aggressiveness of the diffusion of the aluminum and the fact that the substrate behaved in a similar manner to a sponge. It absorbed the coating and merged with it (Figure 4.12).

Moreover, SEM analysis proved the existence of titanium atoms coming from the substrate in the outer-most layers of the coating. This means that the diffusion took place in both directions: inwards (i.e. towards the substrate) and outwards. Additionally, an analysis of the aluminum coating performance after oxidation is made in section 5.4.

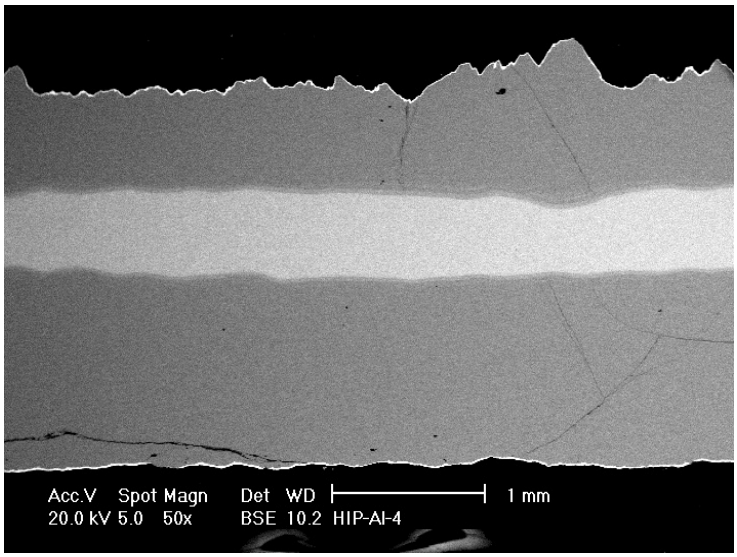

Figure 5.5: Aluminum slurry coating layout after diffusion in a HIP sample.

5.3 Oxidation process

Figure 5.6 shows the appearance of the samples before and after oxidation. It can be observed that the samples took a degraded appearance with green and yellow colored oxidation products arising on their surfaces.

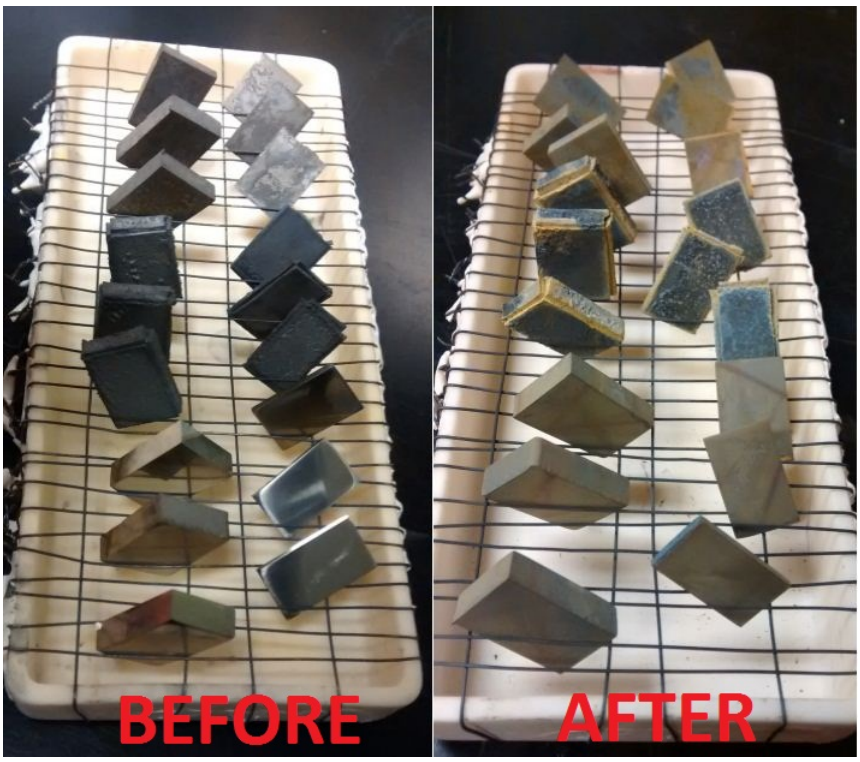

Figure 5.6: Samples evolution in the oxidation test.

CC samples form the left column and HIP the right. From the closest to the furthest part of the crucible: Slurry-free, Al and Al-B.

5.3.1 Oxidation Curves

A fairly good indicator of the oxidation evolution is the mass-gain curves. These graphs show the increment of mass of a sample over the initial exposed surface versus time. These plots are used to analyze the behavior of the base material as well as the effectiveness of the coating against oxidation.

The points that conform these curves were taken by weighing every sample at each time step of the oxidation process, that is, at 12, 24, 50, 100, 150 and 300 hours of accumulated exposure.

Some samples exhibited mass loss. This phenomenon is observed only in HIP work-pieces. The reason can be found in the oxide layer formed on the smaller faces of the samples. This accumulation was brittle and not adherent, so after

complete formation (long oxidation exposure) it fell off. Figure 5.7 shows this kind of shell.

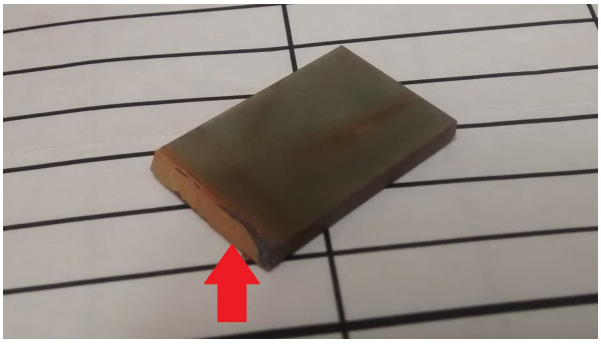

Figure 5.7: Photograph of spalled removable oxide layer appearing on the hot isostatic pressed samples.

There is a total of five oxidation curves. Two compare the coatings for the same substrate, and the other three compare the two substrates for the same coating. In the latter graphs, the oxidation curves of the uncoated samples are also included, so that one can observe the difference between applying and not applying a coating to the same substrate type.
The plots also include an error range at each point measurement. They indicate the standard deviation of the $\Delta m/A_o$ values.

Samples manufactured by hot isostatic pressing.

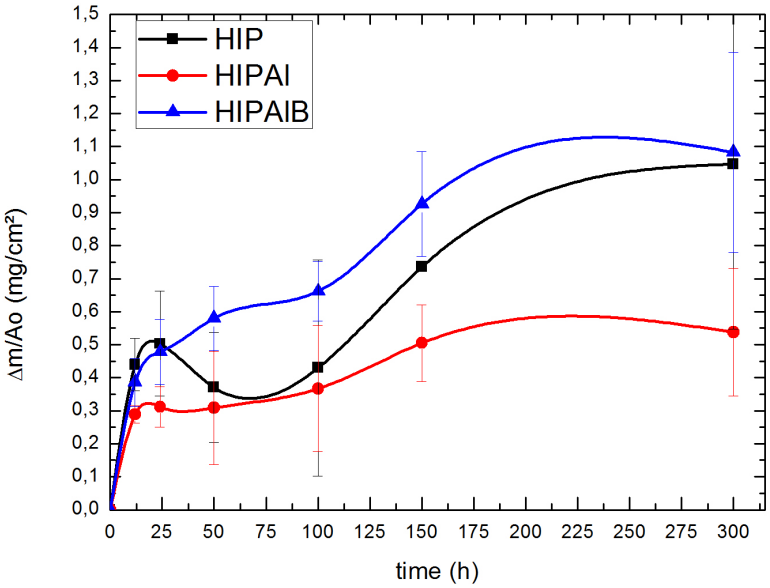

Figure 5.8: Oxidation curves of samples with and without slurry coating manufactured by hot isostatic pressing.

Figure 5.8 indicates that the best oxidation performance for the hot isostatic pressed samples was achieved with the aluminum slurry coating. The mass-gain with this protection was around 0.54 mg/cm^2, whereas with the aluminum-boron coating it reached up to 1.1 mg/cm^2, which is approximately the double.

The oxidation rate law of these curves can be assumed to be logarithmic at the very beginning, since they have a nearly vertical slope. Then, they adopt a parabolic behavior in which the oxide scale continues to grow with time.

After 50 hours of exposure to oxidation, 2 of the 3 HIP samples without any coating lost mass by releasing the oxidation shell mentioned above. This explains the concave aspect of the curve around that value of time.
After 150 hours, the sample that did not release anything, now lost its shell, and another sample lost it for the second time. In this case, since the final weight value of the samples was smaller than the initial one, then they were discarded for the calculation of that point of the graph.

Samples manufactured by centrifugal casting.

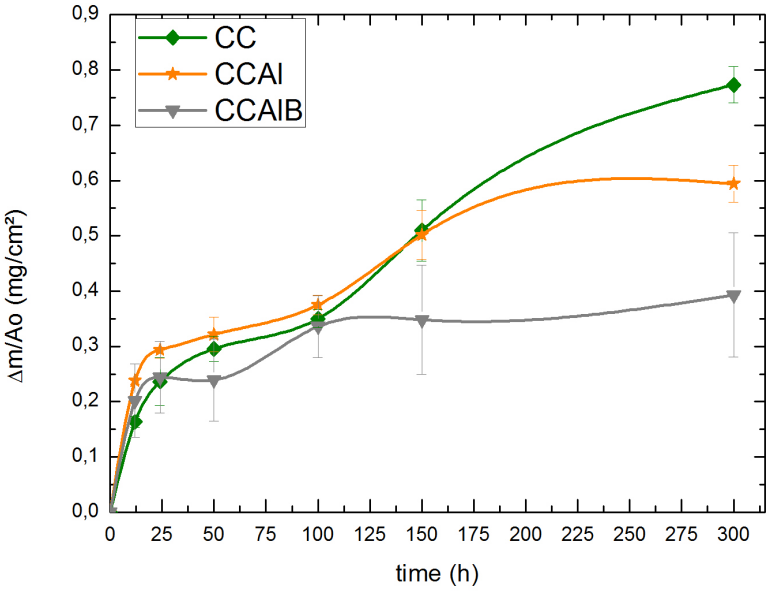

Figure 5.9: Oxidation curves of samples with and without slurry coating manufactured by centrifugal casting.

In this case, the aluminum-boron slurry coating gave the best oxidation resistance performance to the samples manufactured by centrifugal casting.
The maximum value of the mass-gain with this coating was 0.4 mg/cm^2, whereas its performance without coating achieved 1.1 mg/cm^2, more than the double.

The behavior of the samples is remarkable in the first 100 hours of oxidation. The curves are very similar, which indicates that the coating is not very effective early in the process. After that time, and in the case of the Al-B coating, there is a slight mass increase, so that the nature of this curve can be assumed to be nearly constant.

Figures 5.8 and 5.9 show that for the HIP substrate the Al slurry coating appears to show the best performance, whereas for the CC substrate the Al-B coating appears to show the best performance. This means that the microstructre, and so the manufacturing technique, affect to resulting coating deposition and behavior, although the overall nominal composition of the two substrates is the same.

Oxidation of the samples that were not coated.

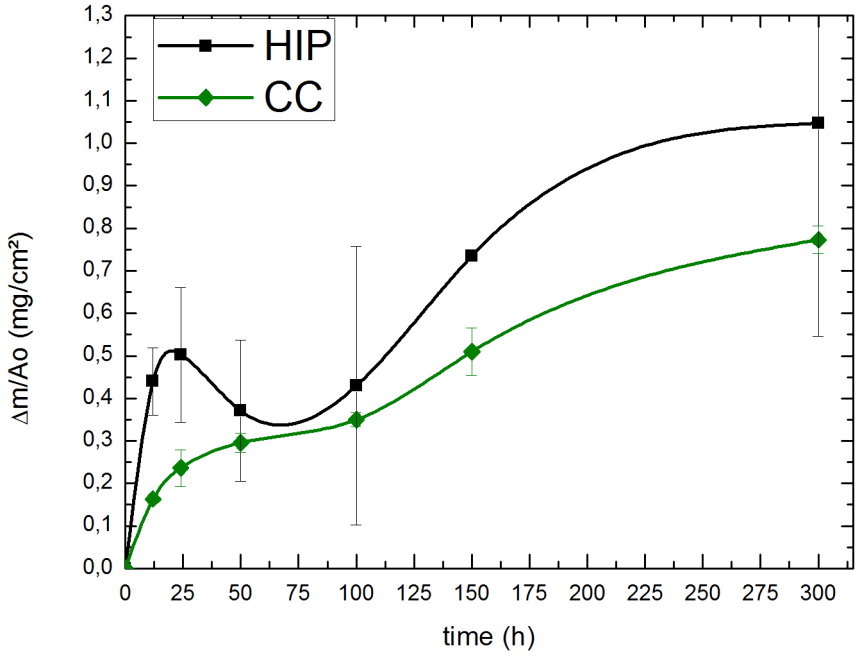

Figure 5.10: Oxidation curves of CC and HIP samples without coating.

Figure 5.10 indicates that the oxidation resistance of the samples manufactured by CC is better than those manufactured by HIP, although the samples present the same chemical composition.

The samples manufactured by HIP acquired a total average mass-gain of 1.0472 mg/cm^2, whereas those manufactured by CC got 0.7732 mg/cm^2. This difference is probably attributed to the type of microstructure of the starting substrates.

Oxidation of the samples that were coated with aluminum slurry.

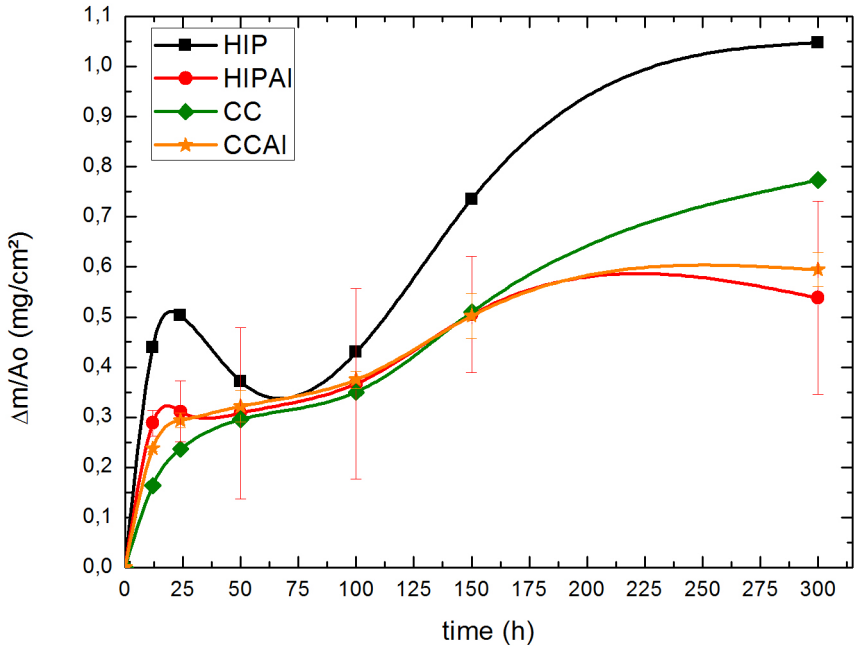

Figure 5.11: Oxidation curves of samples with aluminum slurry coating, compared to uncoated samples for both CC and HIP substrates.

Figure 5.11 shows a comparison of the Al slurry coatings with the uncoated substrates for both HIP and CC substrates. The curves indicate that the aluminum slurry coating protected both types of substrate for a long-term exposure.

In both cases, the mass gain is lower for the coated samples compared to the uncoated ones. HIP samples gained a total average mass of 0.5381 mg/cm^2, and CC 0.5942 mg/cm^2. These figures are collected in Table 8.5 in the appendix.

Oxidation of the samples that were coated with aluminum-boron slurry.

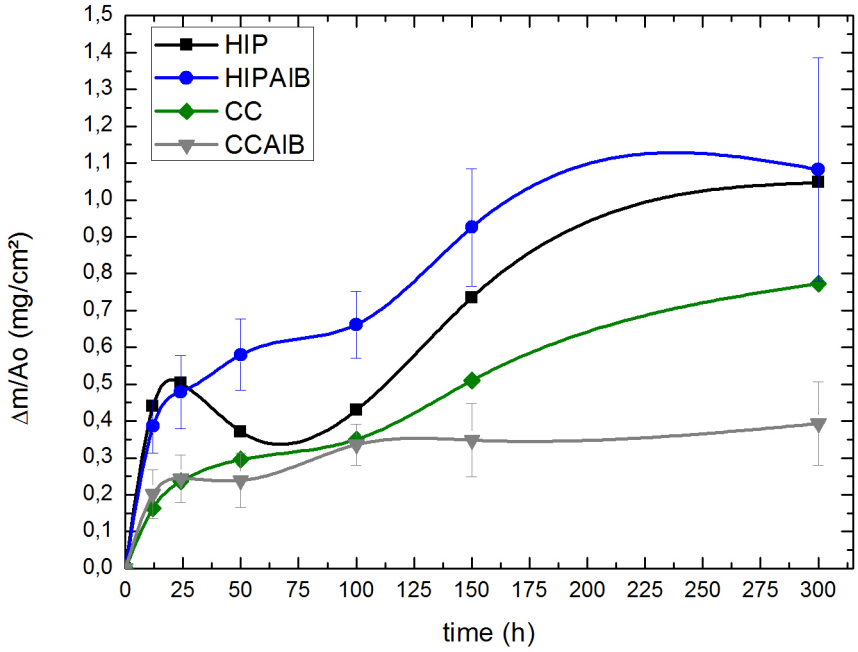

Figure 5.12: Oxidation curves of samples with aluminum-boron slurry coating, compared with uncoated samples, on both CC and HIP substrates.

Figure 5.12 shows a comparison between uncoated samples and samples coated with Al-B slurry for both HIP and CC substrates. The graph indicates that the Al-B coating does not consistently improve the oxidation behavior of the uncoated substrate. Since for the substrate manufactured by HIP, the mass-gain of the Al-B slurry coated sample is higher than that for the uncoated sample. However, for the case of the CC substrate coated with Al-B slurry, its mass-gain is lower than the one of the uncoated sample.

The exposed CC samples without coating performed even better than those manufactured by HIP and coated with the Al-B slurry. Moreover, there is a peak difference of 0.7 mg/cm^2 in mass-gain between the CC samples and the HIP samples, which are both coated with Al-B slurry coating.

The nearly constant behavior of CC samples coated with Al-B slurry means that the coating is very effective against oxidation, since it impedes further mass growth.

The stability of this coating as well as its interaction with the different substrates is studied in more detail in section 5.4.

5.4 Characterization of the coating

5.4.1 HIP and CC samples performance without any coating

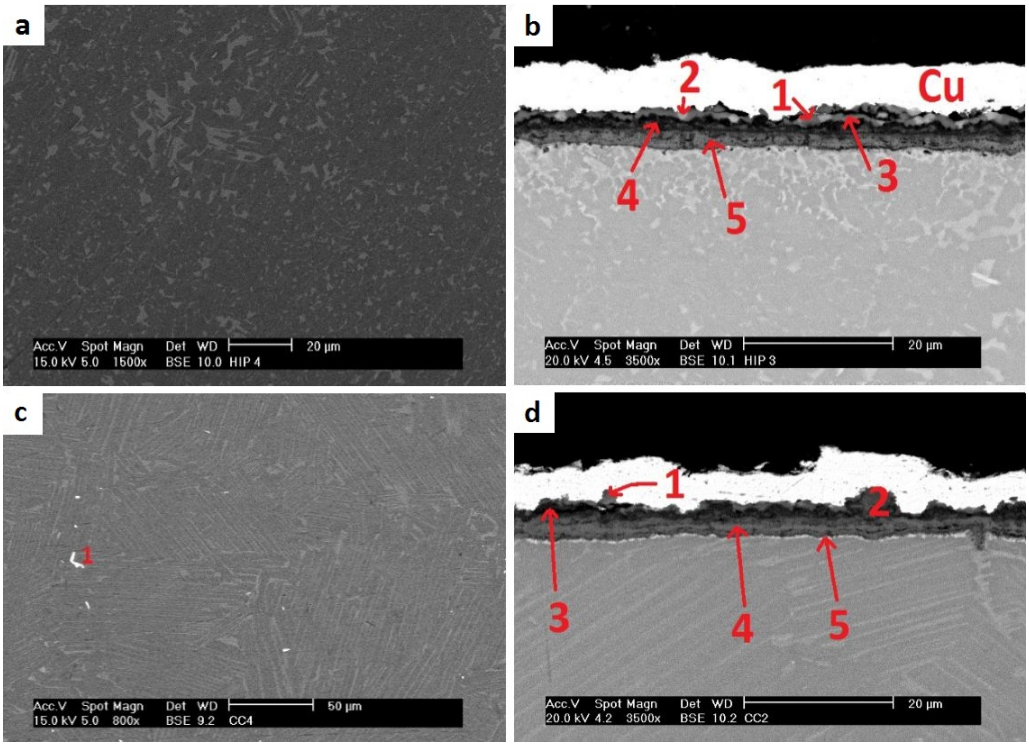

Figure 5.13: Cross section of HIP and CC samples substrates without any coating. (a) HIP substrate with near-γ microstructure, (b) HIP cross section after 300h of oxidation in air at 800°C, (c) CC substrate with lamellar microstructure, (d) CC cross section after 300h of oxidation in air at 800°C.

Figures 5.13 (a) and (c) show the microstructure of the raw material before adding any coating and prior to oxidation. In particular, the microstructure is composed by α_2 (Ti_3Al) and γ (TiAl) phases, which is explained in subsection 2.2.2.

It can be observed in Fig. 5.13(a) that the microstrucure of the samples manufactured by hot isostatic pressing is near-γ. The brighter zones indicate that the atomic weight of the elements present there is higher than the surroundings. Therefore, these regions contain a higher presence of titanium, because its atomic number is higher than that of aluminum. Thus, brighter zones can be associated with α_2 phase. Similarly, the microstructure of CC samples is composed by alternating lamellae with different brightness (Figure 5.13 (c)). Indeed, this reflects the difference between an α_2 lamella and a γ lamella.

The XRD analysis (Table 5.1) performed to the substrates before oxidation corroborates the presence of Ti_3Al and TiAl compounds (i.e. α_2 and γ phases).

Detected species			
Hot Isostatic Pressing		**Centrifugal Casting**	
Before Oxidation	**After Oxidation**	**Before Oxidation**	**After Oxidation**
TiAl	TiAl	TiAl	TiAl
Ti_3Al	TiO_2	Ti_3Al	TiO_2
	Al_2O_3		Al_2O_3

Table 5.1: XRD results: HIP and CC without any coating.

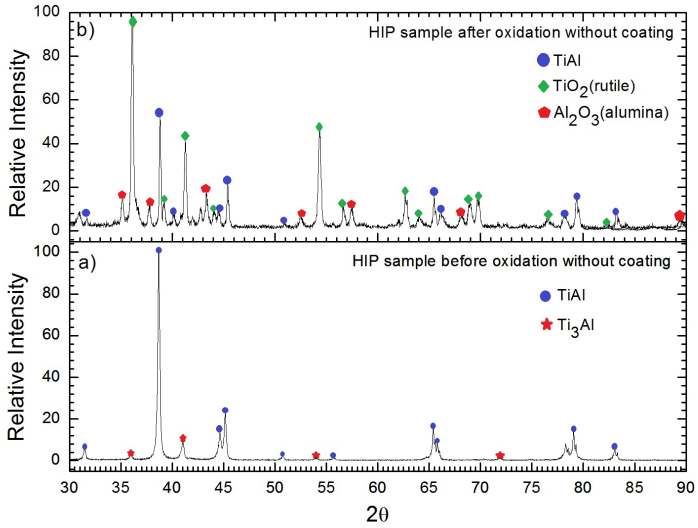

Figure 5.14: Diffractogram: HIP sample before and after oxidation in air for 300h at 800°C without coating.

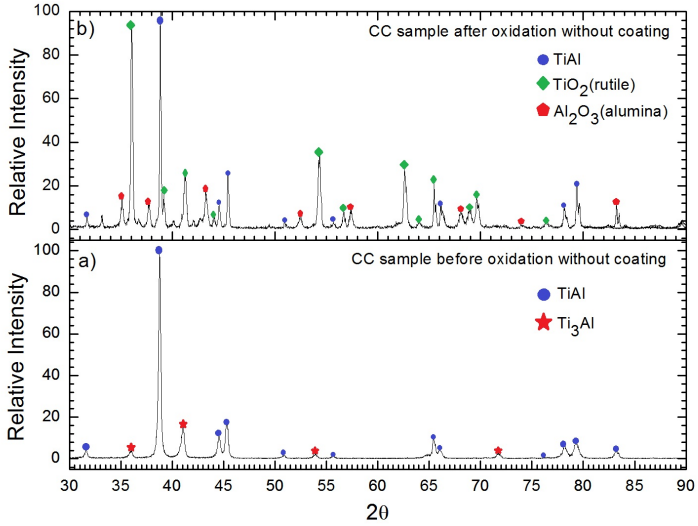

Figure 5.15: Diffractogram: CC sample before and after oxidation in air for 300h at 800°C without coating.

It can also be observed the existence of small white points appearing in the CC microstrucure, which is depicted in Figure 5.13 (c). The Electron Dispersive Spectroscopy (EDS) analysis shows the existence of yttrium (Table 5.2). This metal is not expected to appear, since the base alloy does not have any reported content of it. Tracing back the possible causes of this contamination, it is found that yttria was used as an anti-adherent agent of the cast mold at processing. Hence, this compound mixed with the molten alloy and remained trapped upon solidifaction.

EDS composition analysis						
Point	**Element (at.%)**					**Observations**
	Ti	**Al**	**Nb**	**Mn**	**O**	
1	43.71	39.18	-	1.71	15.40	Yttrium colonies

Table 5.2: EDS analysis of CC uncoated sample (Figure 5.13 (c))

The presence of yttrium coincides with the disappearance of niobium. This incompatibility could lie in the fact that these two substances are immiscible in liquid state. Moreover, no stable intermetallic phases of Y-Nb have been found in solid state [115].

Figures 5.13 (b) and (d) show the cross section of the grinded surface of the samples with an adhered oxide scale after 300h of oxidation at 800°C.
It has been observed that the surface finish influences the oxide scale thickness and adherence. If the surface is not grinded, the thickness is greater. However, this roughness gives a better adherence of the oxide layer to the substrate.

The thickness of the oxide scale present in the grinded surface of both types of substrate is around 4.5 μm, otherwise it oscillates between 4-6 μm. In any case, the oxide layer has a homogeneous and compact appearance with no cracks.

Regarding the microstructure, the lamellar colonies of the CC samples close to the surface remain unperturbed after oxidation. However, in the case of the CC samples, it can be clearly observed that the areas of the substrate next to the oxide layer are brighter. Hence, there is a higher content in titanium, that is, aluminum depleted zones are formed.

Additionally, these bright zones can be associated with a high presence of manganese oxide (MnO) in the outer-most layer of the substrates. EDS analysis provides numerical values that are reflected in Tables 5.3 and 5.4 (point 6 for the HIP and point 5 for the CC).

Note that in the case of HIP samples, pure manganese represents a 16% of the total present atoms. This is 8 times greater than the atomic percentage of Mn in the alloy substrate, which is a 2%. Conversely, CC samples contains a 4%, which is double the amount present in the substrate, but 4 times smaller than the amount found in the HIP samples.

EDS composition analysis						
Point	**Element (at.%)**					**Observations**
	Ti	**Al**	**Nb**	**Mn**	**O**	
1	28.78	13.21	-	-	58.01	Higher content of TiO_2 than Al_2O_3
2	26.40	14.23	-	1.62	57.75	
3	17.20	32.35	-	0.58	49.87	
4	40.71	27.92	-	2.28	48.28	Dark layer
5	13.68	36.01	-	0.59	49.72	Higher content of Al_2O_3 than TiO_2
6	11.19	24.20	-	16.33	30.02	

Table 5.3: EDS analysis of HIP substrate oxide scale without coating after oxidation in air for 300h at 800°C. Figure 5.13 (b).

EDS composition analysis						
Point	**Element (at.%)**					**Observations**
	Ti	**Al**	**Nb**	**Mn**	**O**	
1	34.25	3.23	-	0.88	61.65	Higher content of TiO_2 than Al_2O_3
2	32.17	33.27	-	1.33	33.23	Mixed grains of TiO_2 and Al_2O_3
3	26.66	29.20	-	1.06	43.07	
4	34.09	6.33	-	0.57	55.68	
5	39.52	43.16	-	3.86	13.46	Higher content of Al_2O_3 than TiO_2

Table 5.4: EDS analysis of CC substrate oxide scale without coating after oxidation in air for 300h at 800°C. Figure 5.13 (d).

According to the XRD and EDS analyses (Tables 5.1, 5.3 and 5.4), the oxide scale, which formed after oxidation for 300h at 800°C in air, is composed of a mixture of alumina (Al_2O_3) and rutile (TiO_2). This coincides with the results found in literature [6, 15, 16, 17, 56, 57] and introduced in Chapter 2.
The different atomic percentages presented in Tables 5.3 and 5.4 show that the outer-most oxide layer is dominated by the existence of rutile and then below alumina.

The presence of alumina at the bottom layer of the oxide scale indicates that the outer-most region of the substrate, the one next to the oxide, is depleted of aluminum. Moreover, there is a slightly higher content of manganese where rutile is located, and a lower content of alumina.

Finally, there is no detectable niobium (Nb) content throughout the oxide scale. This is observed in both CC and HIP samples.

5.4.2 HIP and CC samples performance with aluminum slurry coating

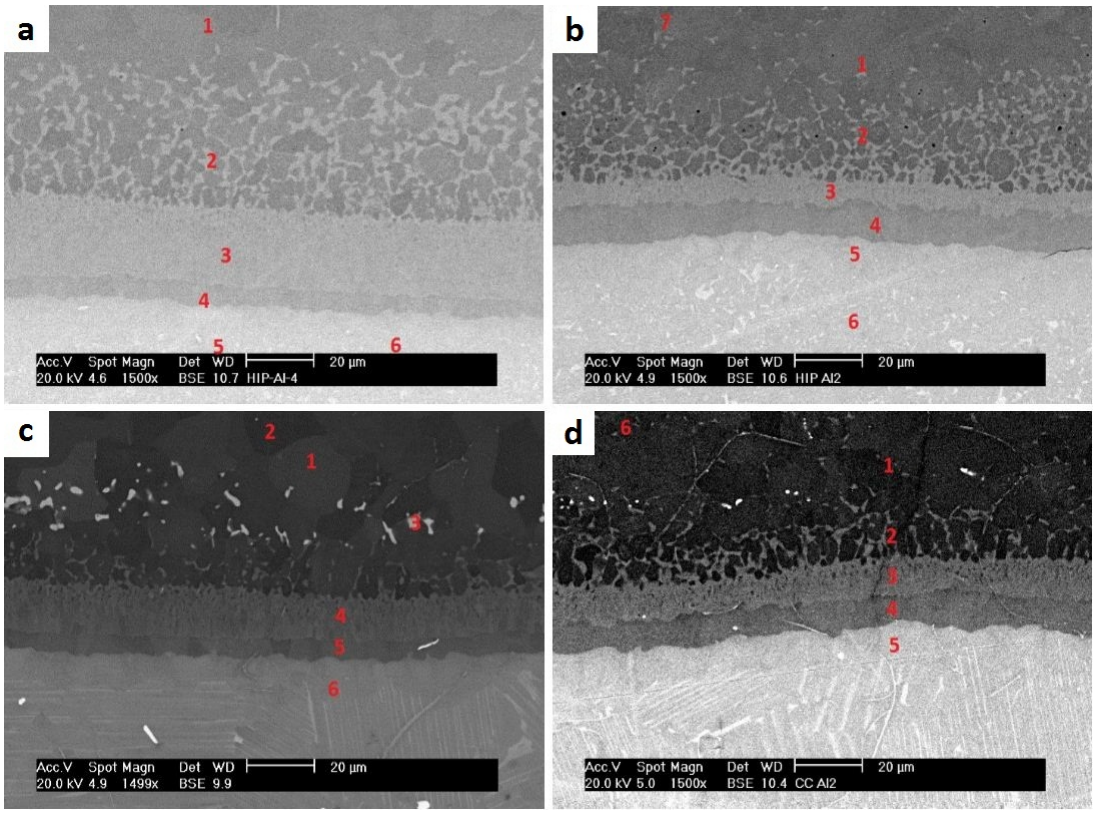

Figure 5.16: HIP and CC samples with aluminum slurry coating before and after oxidation in air for 300h at 800°C. Cross-sectional view.
(a) HIP sample before oxidation, (b) HIP sample after oxidation, (c) CC sample before oxidation, (d) CC sample after oxidation.

It can be observed in Figures 5.16 (a) and (c) that the coating forms several interdiffusion zones with the substrate. This indicates that the coating has well diffused and is well adhered. The layout of the diffusion layers is similar in both types of substrate: HIP and CC.

XRD (Table 5.7) and EDS analyses (Tables 5.5 and 5.6) allow obtaining the data on the porportions of the elements composing the different regions, and hence the formed compounds. The following sequence is found:

$$\mathsf{TiAl_3} \rightarrow \mathsf{TiAl_2} \rightarrow \mathsf{TiAl}\ \text{(substrate)}.$$

It is expected to have $\mathsf{TiAl_3}$ in the outer layers, since the coating is made of aluminum. The closer the aluminum atoms to the substrate, the less predominant the metal becomes. The TiAl substrate is able to provide, by diffusion, enough Ti atoms that will combine with Al in higher proportions, creating $TiAl_2$.

EDS composition analysis					
Point	**Element (at.%)**				**Observations**
	Ti	**Al**	**Nb**	**Mn**	
1	23.15	75.32	0.85	0.67	$TiAl_3$
2	49.23	46.51	2.14	2.12	TiAl
3	22.85	73.24	0.85	3.07	$TiAl_3$
4	24.68	68.40	0.90	6.02	
5	31.40	65.63	1.42	1.55	$TiAl_2$
6	43.73	52.62	2.08	1.57	TiAl

Table 5.5: EDS analysis of HIP substrate and interdiffusion zone with Al slurry coating before oxidation. Figure 5.16 (a).

EDS composition analysis						
Point	**Element (at.%)**					**Observations**
	Ti	**Al**	**Nb**	**Mn**	**Y**	
1	21.75	76.07	0.73	1.46	-	$TiAl_3$
2	21.83	75.41	0.84	1.93	-	
3	9.42	71.11	-	13.99	5.49	Yttrium-manganese colonies
4	23.94	69.93	0.96	5.17	-	
5	30.98	66.41	1.40	1.21	-	$TiAl_2$
6	47.99	47.89	2.08	2.05	-	

Table 5.6: EDS analysis of CC substrate and interdiffusion zone with Al slurry coating before oxidation. Figure 5.16 (c).

Taking a look at the different interdiffusion layers before oxidation, the outermost region is made of a combination of $TiAl_3$ and TiAl. The latter is brighter (weighs more), creating interconnected colonies with a similar appearance to flowing lava. The presence of TiAl in this outer region, relatively far from the substrate, could be associated with the fact that the coating was absorbed by the substrate. Hence, the sample lost its rectangular profile as observed in Figure 5.5.

Another observed phenomenon in both type of substrates is that the external surface region (i.e. the bottom layer of the interdiffusion zone) and the layer above it, which is darker, are mainly formed by $TiAl_2$. Moreover, at the interface between the substrate and the coating, the microstructural features of the substrate are no longer present. Instead, a zone without a defined microstructure appeared.

CC samples before oxidation also have an area with an important amount of bright grains (Table 5.6, point 3). Again, this is due to the presence of yttrium. It is important to note that there is a lack of Nb in the colonies, but a high content of Mn. Manganese presence accounts for about 14 at.%, which is 7 times greater than the percentage contained in the base alloy. The presence of Y and Mn indicate certain chemical and diffusional affinity and stability.

Detected species			
Hot Isostatic Pressing		**Centrifugal Casting**	
Before Oxidation	**After Oxidation**	**Before Oxidation**	**After Oxidation**
$TiAl_3$	$TiAl_3$	$TiAl_3$	$TiAl_3$
TiO_2	$TiAl_2$	TiO_2	TiO_2
	TiO_2	Al_2O_3	Al_2O_3
	Al_2O_3		

Table 5.7: XRD results: HIP and CC with aluminum slurry coating before and after oxidation in air for 300h at 800°C.

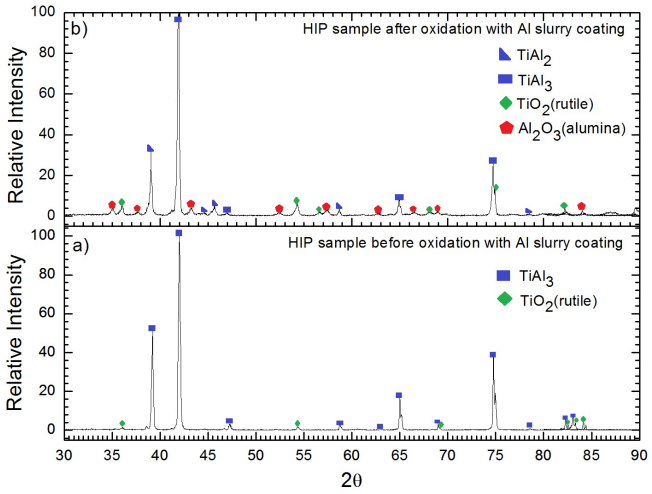

Figure 5.17: Diffractogram: HIP sample before and after oxidation in air for 300h at 800°C with aluminum slurry coating.

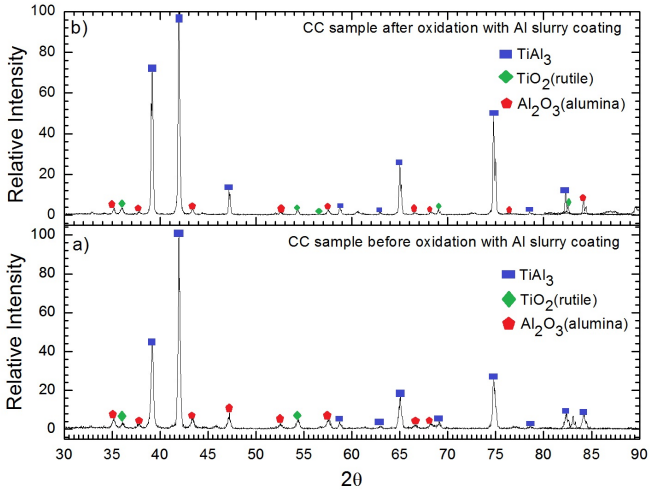

Figure 5.18: Diffractogram: CC sample before and after oxidation in air for 300h at 800°C with aluminum slurry coating.

After the isothermal oxidation, the diffusion layers have the same compound sequence: $TiAl_3 \rightarrow TiAl_2 \rightarrow TiAl$ (substrate). In other words, the coating composition remains the same after oxidation. Hence, it can be said that coatings rich in aluminum have a stable performance. This is in agreement with the oxidation curves discussed in section 5.3.1, where Al-slurry coatings in general showed better performance than uncoated samples.

EDS composition analysis						
Point	**Element (at.%)**					**Observations**
	Ti	**Al**	**Nb**	**Mn**	**O**	
1	23.49	74.68	0.96	0.86	-	$TiAl_3$
2	24.32	72.35	1.00	2.33	-	
3	25.04	67.07	1.16	6.73	-	
4	32.57	64.41	1.34	1.69	-	$TiAl_2$
5	47.23	49.28	1.96	1.53	-	TiAl
6	50.00	45.73	2.05	2.21	-	
7	9.83	55.08	0.66	0.23	34.20	Analysis of the oxide scale in a point. Predominance of Al_2O_3 over TiO_2

Table 5.8: EDS analysis of HIP substrate and interdiffusion zone with Al slurry coating after oxidation in air for 300h at 800°C. Figure 5.16 (b).

EDS composition analysis						
Point	**Element (at.%)**					**Observations**
	Ti	**Al**	**Nb**	**Mn**	**O**	
1	23.19	74.38	0.86	1.57	-	$TiAl_3$
2	24.19	72.84	0.73	2.24	-	
3	24.84	68.11	1.09	5.96	-	
4	32.64	64.48	1.43	1.44	-	$TiAl_2$
5	47.53	49.17	1.99	1.32	-	TiAl
6	6.17	38.87	1.49	-	53.47	Analysis of the oxide scale in a point. Predominance of Al_2O_3 over TiO_2

Table 5.9: EDS analysis of CC substrate and interdiffusion zone with Al slurry coating after oxidation in air for 300h at 800°C. Figure 5.16 (d).

The darker intermediate $TiAl_2$ layer, which corresponds to point 4 in Figures 5.16 (a) and (b), grew, whereas the $TiAl_3$ zone decreased in size. This can be associated with the diffusion of Al atoms towards the exterior, where oxygen is present. Besides, the TiAl grains descreased in influence. Thus the Ti atoms, that were there, also diffused. Yttrium-manganese colonies went down in size and number as well. This indicates that they had a similar behavior as TiAl compounds.

The composition of the oxide scale is expected to be formed by rutile and alumina as reported by the XRD analysis (Table 5.7). Nevertheless, alumina should predominate, since the coating was made of aluminum. This fact is reflected

in the at.% obtained by EDS analysis (Tables 5.8 and 5.9) and by the different atomic movements observed after oxidation.

Finally, the thickness of the oxide scale of the HIP samples is smaller than 1 μm. This figure indicates a good effectiveness of this coating combined with this substrate. Oxidation curves (Figs. 5.8 and 5.11) also coincide with this statement. The oxide layer of the CC samples measures around 1-1.5 μm. This is a good thikcness too. In this case, there is no manganese content in the upper-most surface, although HIP samples have a low amount.

5.4.3 HIP and CC samples performance with aluminum-boron slurry coating

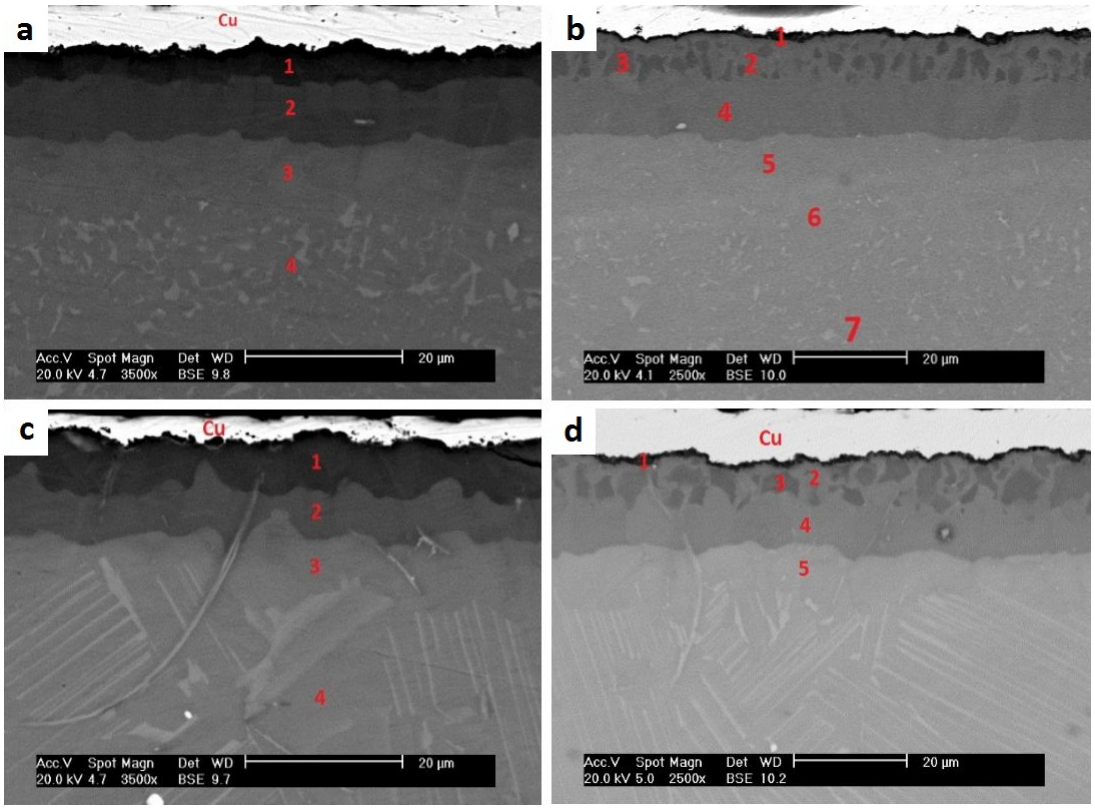

Figure 5.19: HIP and CC samples with aluminum-boron slurry coating before and after oxidation in air for 300h at 800°C. Cross-sectional view.
(a) HIP sample before oxidation, (b) HIP sample after oxidation, (c) CC sample before oxidation, (d) CC sample after oxidation.

Figures 5.19 (a) and (c) indicate that the coating configuration before oxidation is the same for both types of substrate. Thus, the microstructure does not appear to influence the formation of the aluminum-boron coating.

After oxidation (Figs. 5.19 (b) and (d)), the coating varies with respect to the previous state, but it keeps the same layout with both types of substrate.

It was observed that the coating is dense, compact and homogeneous, but there were uncovered parts on the sample surface. However, in this case, the coating was good enough to be considered as protective. Moreover, the coating has deposited, in general, better in the not-grinded surfaces, which had better adherence. The entire diffusion layer has an approximate thickness of 32 μm.

EDS and XRD analyses report a progressive enrichment in Al of the coating going from the substrate. This means, that the coating composition sequence is similar to the one observed in the aluminum coating. From the copper (Cu) layer to the substrate, this is:

$$TiAl_3 \rightarrow TiAl_2 \rightarrow TiAl \text{ (substrate)}.$$

The formation of these compounds is related to the aluminum powders contained in this slurry-coating (see observations in Tables 5.10 and 5.11).

EDS composition analysis					
Point	**Element (at.%)**				**Observations**
	Ti	**Al**	**Nb**	**Mn**	
1	23.49	75.10	1.41	-	$TiAl_3$
2	32.00	66.73	1.27	-	$TiAl_2$
3	45.15	51.30	2.09	1.46	TiAl
4	48.75	47.46	1.95	1.84	

Table 5.10: EDS analysis of HIP substrate and interdiffusion zone with Al-B slurry coating before oxidation. Figure 5.19 (a).

EDS composition analysis					
Point	**Element (at.%)**				**Observations**
	Ti	**Al**	**Nb**	**Mn**	
1	24.96	73.91	0.86	0.28	$TiAl_3$
2	33.56	64.62	1.15	0.66	$TiAl_2$
3	46.90	49.84	2.00	1.26	TiAl
4	50.15	45.77	1.77	2.31	

Table 5.11: EDS analysis of CC substrate and interdiffusion zone with Al-B slurry coating before oxidation. Figure 5.19 (c).

Detected species			
Hot Isostatic Pressing		**Centrifugal Casting**	
Before Oxidation	**After Oxidation**	**Before Oxidation**	**After Oxidation**
TiAl	TiAl	TiAl	TiAl
$TiAl_2$	$TiAl_2$	$TiAl_2$	$TiAl_2$
$TiAl_3$	$TiAl_3$	$TiAl_3$	$TiAl_3$
TiB_2	Al_2O_3	TiB_2	Al_2O_3
	TiO_2		TiO_2

Table 5.12: XRD results: HIP and CC with aluminum-boron slurry coating before and after oxidation in air for 300h at 800°C.

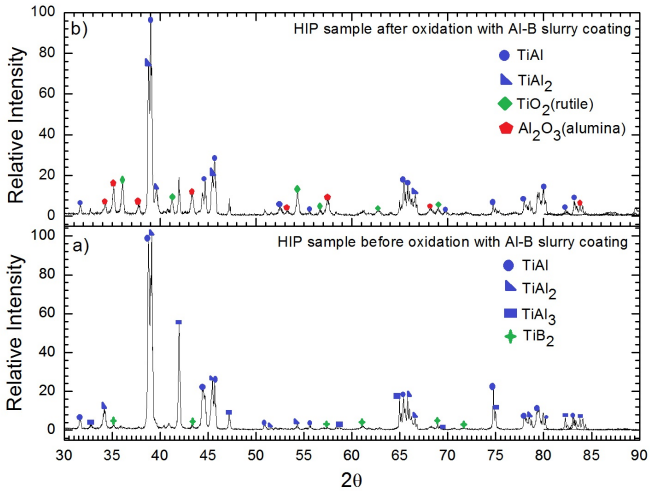

Figure 5.20: Diffractogram: HIP sample before and after oxidation in air for 300h at 800°C with aluminum-boron slurry coating.

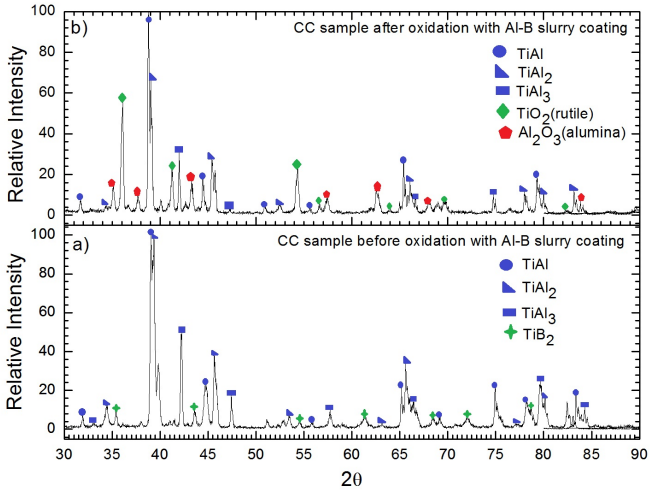

Figure 5.21: Diffractogram: CC sample before and after oxidation in air for 300h at 800°C with aluminum-boron slurry coating.

XRD analysis detected the presence of boron (see Table 5.12) in the form of titanium diboride (TiB_2). This cannot be corroborated by EDS analysis, since the SEM device is constrained by its own detection threshold. Nevertheless, the darkest layer in the outer-most part of the coating, below the copper deposited zone, must be composed by light atoms. Hence, this layer has an important presence of boron, which is an element with a small atomic number.
Al-B coating also created a layer with a non-defined microstructure at the interface between the substrate and the coating. This phenomenon is observed in both types of substrate.

The Al-B coating after oxidation remained compact and similar to the one before the treatment. Although the coating has a similar configuration for both substrates (HIP and CC), it performed oppositely with respect to oxidation resistance. In the case of CC samples, it gave the best oxidation resistance (see Figures 5.9 and 5.12), but not for HIP samples. This could possibly be attributed to the non-homogeneous covering by the Al-B slurry of some of the HIP samples.

EDS composition analysis						
Point	**Element (at.%)**					**Observations**
	Ti	**Al**	**Nb**	**Mn**	**O**	
1	9.98	38.16	-	-	51.85	Predominance of Al_2O_3 over TiO_2
2	29.77	66.34	0.79	-	3.11	
3	25.04	72.41	1.02	-	1.54	
4	30.22	64.57	1.21	1.02	2.98	
5	31.19	66.50	1.26	1.05	-	$TiAl_2$
6	45.09	52.38	1.95	0.57	-	TiAl
7	49.07	46.56	2.36	2.02	-	

Table 5.13: EDS analysis of HIP substrate and interdiffusion zone with Al-B slurry coating after oxidation in air for 300h at 800°C. Figure 5.19 (b).

EDS composition analysis						
Point	**Element (at.%)**					**Observations**
	Ti	**Al**	**Nb**	**Mn**	**O**	
1	15.21	31.03	-	-	53.76	Analysis of the oxide scale in a point. Predominance of Al_2O_3 over TiO_2
2	29.36	69.56	1.08	-	-	$TiAl_3$
3	23.86	74.89	1.24	-	-	
4	31.15	66.49	1.44	0.92	-	$TiAl_2$
5	45.59	50.82	2.04	1.54	-	TiAl

Table 5.14: EDS analysis of CC substrate and interdiffusion zone with Al-B slurry coating after oxidation in air for 300h at 800°C. Figure 5.19 (d).

After oxidation, it is found that Nb and Mn are not present anymore on the surface in contact with air of both substrates (Tables 5.13 and 5.14, point 1).

Additionally, the darkest layer vanished. Instead, it transformed into small black regions in the form of islands. Hence, the presence of boron decreased and so, it is no longer detectable by the XRD technique. Conversely, there are not 'Yttrium-Manganese' colonies above the diffusion layers of the CC samples, as it happened in the case of the aluminum slurry.

The concentration of $TiAl_3$ also decreased with this coating. Thus, the formation of $TiAl_2$ was promoted. This can be appreciated in the Figures 5.19 (b) and (d), where brighter zones appear, and in the data collected by the EDS analysis (Tables 5.13 and 5.14). The loss of aluminum atoms can be associated with the formation of alumina (see Table 5.12).

The oxide scale of both substrates is composed of alumina and rutile as reflected by the XRD analysis. In the case of HIP samples, the thickness of the oxide layer is about 1.5–2 μm. Whereas the measure of this scale in the CC samples was from 0.4-0.8 μm. The latter range is observed to be the smallest thickness among the studied samples. Also, this is the coating that had the lower mass gain, which indicates that a stable protective oxide has formed.

Finally, taking a look at the EDS analysis, CC samples exhibited oxygen only in the outer-most layer. Hence, oxygen could not penetrate in the coating. This fact could lead to the best oxidation performance shown by the oxidation curves of Figures 5.9 and 5.12. Therefore, this coating is highly protective when combined with samples manufactured by CC.

5.5 Detected cracks in the aluminum slurry coating after oxidation

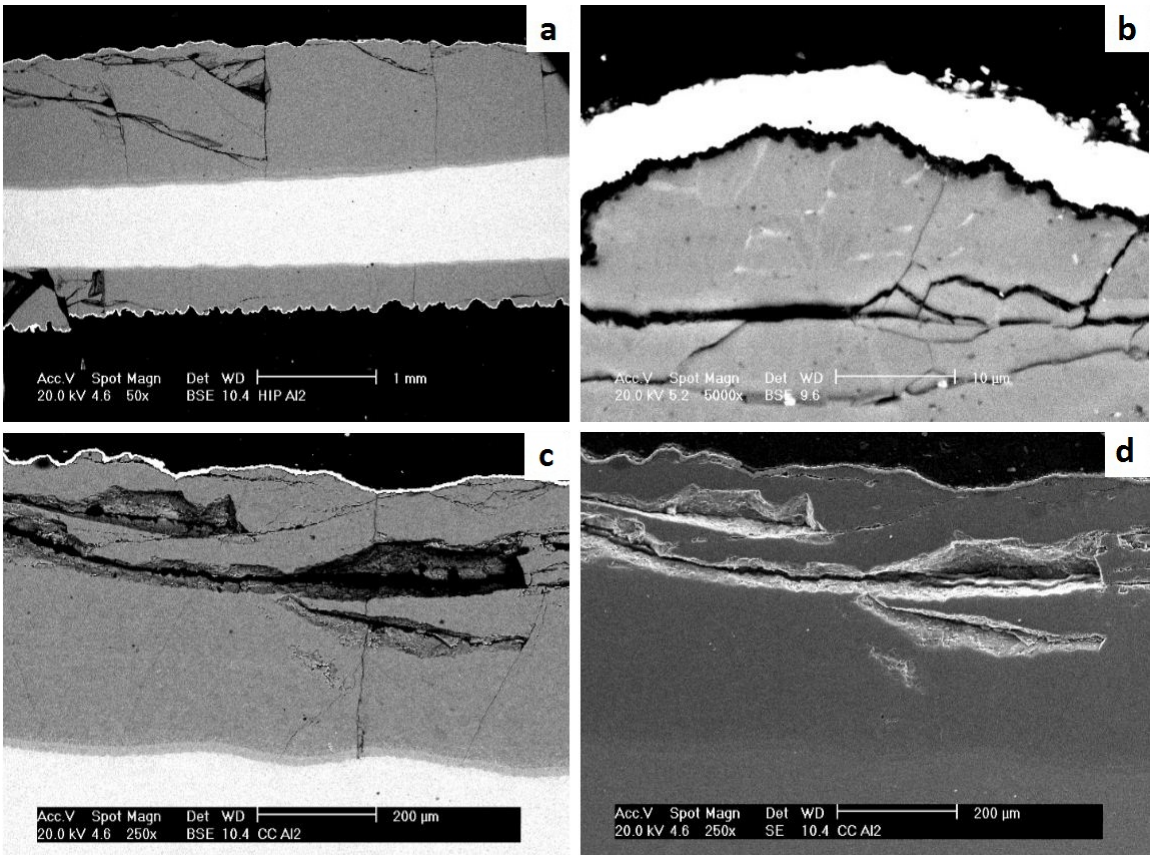

Figure 5.22: Cracks observed in aluminum slurry coated samples arising after oxidation in air for 300h at 800°C.

(a) Cracks in the coating of a Al slurry coated HIP sample, (b) Higher magnification of a crack in HIP Al-slurry sample, (c) Cracks in the coating of a CC sample, (d) Topography of internal cracks in the CC sample coated with Al slurry.

Figure 5.22 shows cracks that were observed in the samples coated with Al slurry after oxidation in static air for 300h at 800°C.

A first indicator of the appearance of cracks could be a PBR ratio greater than one (section 2.2.6). This ratio explains that the volume of the formed oxide scale is greater than the volume of the consumed metal. Thus, the oxide buckles and brakes.

This theoretical principle can be also extrapolated to the case of the coating, that is, the volume of the coating is larger than the volume of the substrate. This fact creates internal stresses that make the cracks appear and grow.

Another factor for the crack existence and growth is the difference in the values of the coefficient of thermal expansion (CTE) of the substrate and the coating. Pure aluminum has a CTE = $23 \cdot 10^{-6}$ K^{-1} at 20°C, whereas pure titanium has a CTE = $8.6 \cdot 10^{-6}$ K^{-1}. This means that aluminum expands quicker than titanium, which has a lower CTE value. These differences could create thermal stresses and bending moments that originate cracks.

Note that these numbers do not represent the real case, since the substrate material is a TiAl alloy and the coating is not pure aluminum, since it has some traces of titanium (diffused atoms). Therefore, the numbers vary, but not the theoretical principle behind it, which is: different materials have different CTEs.

Additionally, the samples were subjected to an isothermal interrupted test. The cyclic heating and cooling of the samples started and enhanced a thermal fatigue phenomenon. Thermal stresses appeared and helped in the development of cracks.

Therefore, a PBR>1, a difference between CTEs, a lack of residual stresses in the coating and a thermal fatigue cycle led to the formation and propagation of cracks. This detrimental effect may cause a total loss of the coating and the overlying oxides, hence accelerating the oxidation of the work-piece.
However, all the coated samples preformed better than the uncoated ones. Therefore, optimization of the coating thickness is believed to minimize the observed cracking and protect the substrate adequately.

Chapter 6

Conclusions

The current research project studied the isothermal oxidation performance at high temperature (800°C) of the alloy Ti 45Al 2Nb 2Mn 0.8% vol. TiB_2 coated with two novel slurry coatings.

This alloy is classified as a $\gamma-$TiAl type. The experiment was carried out with samples manufactured by Hot Isostatic Pressing (HIP) with a near-γ microstructure and Centrifugal Casting (CC) with a nearly lamellar microstructure.

Two types of slurry coatings were created and deposited by diffusion in order to enhance the oxidation resistance of the alloy. One type of coating was based on aluminum powders and the other was based on a mixture of aluminum-boron powders.

The research led to the following conclusions:

- Regarding the slurry production and optimization, PEG showed the best performance among the three tested slurry binders: PVA, PEG and CMC. In order to obtain a high quality slurry, the best proportion of metal powders was found to represent a 60 wt.% of the total mixture weight. Nonetheless, the amount of binder depends on the metal particle size, but it can vary from 0-6 wt.%.

- If the sample is not coated, the surface roughness is important for the thickness control of the oxide scale. Grinded surfaces showed worse oxide adherence, but smaller (less thick) and more uniform oxide scales. If the sample is coated, then neither the oxidation performance nor the properties of the coating (diffusion mechanisms and display) are affected by the surface finish.

- The oxides formed on the coated and uncoated samples were rutile (TiO_2) and alumina (Al_2O_3). In general, they created a compact, stable, uniform and protective oxide scale which prevented further oxidation of the material substrate. Thus, the Pilling-Bedworth Ratio can be considered to be close to unity in the uncoated samples.

According to the oxidation curves, samples manufactured by CC performed, in general, better than those manufactured by HIP. The aluminum slurry gave the best protectiveness (lowest mass-gain) to HIP samples, whereas the aluminum-boron coating gave the best performance to CC samples.

- The interdiffusion zones of the same coating have a similar layout independent of the work-piece substrate type. Additionally, a layer without a defined microstructure situated at the interface between the substrate and the coating was formed after diffusion. This region appeared with both types of coating and in both types of substrate microstrucure (near-γ and lamellar).

- CC samples have detectable yttrium in their substrate. This element only diffused outwards with the aluminum slurry coating. It appeared creating grains with a high content in manganese and with a total lack of niobium (showing a high incompatibility between both metals: Nb and Y).

- Niobium is not present in any of the oxide scales formed on the non-protected samples. It remained in the substrate independent of the microstructure type. Nevertheless, Nb diffuses through the coatings and appears in the oxide scales of the protected samples.

- A layer of manganese oxide, MnO, is created in the interface between the oxide scale and the substrate of the uncoated samples manufactured by CC and HIP. In the case of the latter, the Mn content is 8 times greater than that found in the base alloy.

- The aluminum slurry coating had an undesired excessive thickness. To avoid this, the particle size of the metal powder used when creating the slurry coating should be lower than that employed in this work, which was 45 μm.

- The aluminum coating developed cracks after oxidation. The reasons for this to happen could be: a high coating volume, an important difference between the thermal expansion coefficients of the coating and the substrate, and the fact that the coating and substrate were subjected to a thermal fatigue cycle. Nevertheless, the Al slurry coating improved the oxidation behavior of the substrate in all the studied cases.

- Deposition of Al-B slurry coating resulted in the formation of a diffusion layer that consisted of titanium aluminides and TiB_2. The deposition of this type of coating on γ-TiAl alloys has not been previously reported.
  The aluminum-boron slurry coating formation and layout are not influenced by the type of substrate microstructure. However, further work is needed to achieve a better deposition. Moreover, there are no traces of Nb or Mn in the oxide scales formed after oxidation of the samples covered with this coating. Additionally, the Al-B slurry coating showed the best oxidation behavior. It generated a thin stable oxide layer when it was deposited onto the CC samples.

Chapter 7

Future trends

This chapter points out various unfinished issues with respect to both slurry coatings and titanium-aluminide intermetallics that need further analysis, especially their interaction and performance.

- ⋆ One of the difficulties found in the industry when applying slurry coatings is the thickness control. It is required to develop methods for applying these coatings uniformly, and mainly to large and complex shape pieces.
  A practical application is found in the size and geometry of the internal passages and cooling holes of air-cooled components, which are critical to maintain the required amount of coolant flow. Hence, the processes by which diffusion coatings are deposited on the external and internal surfaces of air-cooled components should be capable of producing coatings of uniform thickness and leave minimal residue [92].
  Another example is the results from the samples that were coated with aluminum slurry in this research. The sample surface and its size varied completely (section 5.2) and cracks developed within the coating.

- ⋆ As mentioned above, thickness control also implies coating uniformity. The thicker the coating, the greater the protective reservoir, but the lower the thermal fatigue resistance and the higher the work-piece weight. Hence a trade-off study should be set.

- ⋆ When aluminide diffusion coatings are modified with further elements especially with Pt (one of the most expensive metals), the endurance at high temperatures can be significantly improved.
  Platinum was shown to significantly improve the oxidation resistance of both low-activity and high-activity PtAl-coatings. This is an industrially well-established process in combination with low-activity coatings for application temperatures higher than 1050°C [66]. Future work could involve adding an amount of this alloying element to the slurry and checking its response with a TiAl substrate.

- ⋆ Another important aspect is related to the optimization of the slurry. Further work is needed to obtain more complex slurry coatings from these

presented in this document. This can be achieved by pouring additives to the mixture and trying to combine, for example, more than one binder or metal powder.
It is also important to investigate and try to implement those additives used for enhancing the adherence of paints in slurry coatings.

- ⋆ Another mechanism to take into account for a better slurry behavior is the pH of the suspension. This has to be controlled in order to avoid possible chemical attack in the substrate and hence degradation of the material.

- ⋆ An important point to study is the implementation of the slurry coating diffusion step within the manufacturing process, that is, when the coating should be applied.
  After the production of a work-piece, for example, a turbine blade, which is subjected to several heat treatments that enhance its mechanical properties, such as annealing or quenching.
  After that, surface treatments usually take place. There are many available techniques in this field. For example: shot peening which increases the amount of residual stresses of the work-piece, making the crack propagtion caused by fatigue phenomena to be more difficult. Also, thermal barrier coating (already commented in section 2.3.2) that protect and increase the operative temperature of the material, or slurry coatings, which prevent oxidation, etc. The compatibility of the different application techniques as well as the used coatings should be analyzed in more detail.
  Production engineering is essential for this point.

Chapter 8

Appendix

8.1 Definitions

- **Alloying Elements:** Metallic or non-metallic elements suitable to modify, up to a certain point, the mechanical and chemical properties of a base-alloy.
- **Binder:** Polymer resin compounds with varying molecular weight and properties, and whose primary function is to work as an adhesive between metal powders and substrate as well as a slurry homogenizer.
- **Component:** Chemical substance or compound with fixed composition.
- **Creep:** Permanent (plastic) deformation of a material which is subjected to the influence of a constant mechanical stress.
- **Crystal Lattice:** Three-dimensional pattern consisting of atoms or groups of atoms in ordered and repeated symmetrical arrangements.
- **Diffusion in solids:** It is a thermally activated phenomenon associated with the mass (atoms) transport within a solid matter.
- **Eutectoid:** Invariant reaction in which a solution in solid-state forms a single phase above the transformation point and two phases below it.
- **Fatigue:** Irreversible phenomenon by which cycling loading will produce permanent localized progressive structural damage in the form of cracks and crack growth, that can lead to fracture due to insufficient residual strength.
- **Grain boundary:** Interface between two grains, or crystallites, in a polycrystalline material. They are defects in the crystal structure and tend to control several physical properties of the material. Grain boundaries have, for example, special influence in characteristics like: creep resistance, electrical and thermal conductivity and stength (since they impede the dislocation (deffect) movement along the crystal lattice, thus increasing the material strength).

- **Halide:** A halide is a binary compound, of which one part is a halogen (F, Cl, Br, I and At) atom and the other part is an element or radical that is less electronegative (or more electropositive) than the halogen, making a fluoride, chloride, bromide, iodide, or astatide compound.
- **Heat treatment:** Heat treatments are intermanufacturing processes applied to a work-piece in order to improve its mechanical and phyisical properties by solid-state equilibrium transformations. Usually, these techniques are thermally activated so that they can change the microstructure and the crystilline order of a material. There exists a wide range of heat treatments, each pursuing specific outcomes. It is important to mention that the working temperature of the material should not overpass that of the heat treatment. If that happens, the beneficial effects of the treatment would be lost.
- **Intermetallic:** Alloy formed by two or more metals combined in stoichiometric proportions. These metals form an ordered crystalline net where atoms are joined by ionic or covalent bonds, providing intermediate properties between metals and ceramics.
- **Interstitial void:** Vacancy appearing within the crystal lattice of a material.
- **Invariant reaction:** Point in which one or more phases react at a particular temperature, on cooling or heating, to produce one or more new phases.
- **Microconstituent:** Each one of the different structures that can be observed on a polished surface of the material. It can be formed by one or more phases.
- **Microstructure:** Observable structure in a microscope of a prepared material surface.
- **Phase:** Chemically and structurally homogeneous area that forms part of the microstrucure. A phase can be formed by one or more components.
- **Phase Diagram:** It is a representation that provides the variation of the phases of an alloy with respect to a change in temperature and in the content of the elements.
- **Slurry coating:** It is a compound used for oxidation protection of metallic materials at high temperatures.
- **Superalloy:** Metallic alloy which can be used at unusual high temperature, often above 0.8Tm, preserving its mechanical properties.
- **Thermal fatigue:** Secondary failure mechanism. Temperature differentials create thermal stresses, that after cycling, they may lead to a structure collapse.

8.2 Nomenclature

- Acetone: $\mathsf{CH_3-\overset{\overset{\mathsf{O}}{\|}}{C}-CH_3}$
- Aluminum: Al
- Aluminum oxide - Alumina: $\mathsf{Al_2O_3}$
- Atomic percent: **at.%**
- Atomic number: **Z**
- Boron: B
- Carboxilic acid: $\mathsf{R-\overset{\overset{\mathsf{O}}{\|}}{C}-OH}$
- Carboxymethyl Cellulose: CMC
- Carboxymethyl group: $\mathsf{-CH2-COOH}$
- Chemical Vapor Deposition (CVD)
- Coefficient of Thermal Expansion: CTE
- Commercial carboxylic acid solution: DOLAPIX CE 64
- Copper: Cu
- Centrifugal Casting: CC
- Chemical Vapor Deposition: CVD
- Coefficient of Thermal Expansion: CTE
- Copper sulphate: $\mathsf{CuSO_4}$
- Electron Dispersive Spectroscopy: EDS
- Ethanol: $\mathsf{CH_3-CH_2-OH}$
- Gamma (Greek letter): γ
- Gold (Aurum): Au
- High-Pressure Compressor: HPC
- High-Pressure Turbine: HPT
- Hot Isostatic Pressing: HIP
- Low-Pressure Compressor: LPC

– Low-Pressure Turbine: LPT

– Manganese: Mn

– Manganese oxide: MnO

– Niobium: Nb

– Oxygen: O

– Polyethylene Glycol –PEG: $\mathsf{H-O-CH_2-CH_2-OH}$

– polyethylene Oxide: PEO

– Polyvinyl Alcohol: PVA

– Pilling-Bedworth Ratio: PBR

– Scanning Electron Microscope: SEM

– Silicon Carbide: SiC

– Sodium sulphate: $\mathsf{Na_2SO_4}$

– Sulfuric acid: $\mathsf{H_2SO_4}$

– Thermal Barrier Coatings: TBC

– Titanium-aluminide alloy: TiAl

– Titanium diboride: $\mathsf{TiB_2}$

– Titanium dioxide – Titania – Rutile: $\mathsf{TiO_2}$

– Titanium tetrachloride: $\mathsf{TiCl_4}$

– Weight percent: **wt.%**

– X-Ray Diffraction: XRD

– Yttrium: Y

– Yttrium Oxide (III) – Yttria: $\mathsf{Y_2O_3}$

– Yttria Stabilized Zirconia: YSZ

– Zirconium dioxide – Zirconia: $\mathsf{ZrO_2}$

8.3 Additional tables

Date. Year 2014	Local Time	Accumulated Time [h]	Temperature [°C]
Monday, March 24^{th}	15 h	0.00	0
	17:40 h	2.67	800
Tuesday, March 25^{th}	5:40 h	14.67	800
	8:20 h	17.33	0
	18:20 h	27.33	0
	21h	30.00	800
Wednesday, March 26^{th}	9 h	42.00	800
	11:40 h	44.67	0
	16 h	49.00	0
	18:40 h	51.67	800
Thursday, March 27^{th}	20:40 h	77.67	800
	23:20 h	80.33	0
Friday, March 28^{th}	16:30 h	97.50	0
	19:10 h	100.17	800
	21:10 h	150.17	800
Monday, March 31^{st}	23:50 h	152.83	0
	16:45 h	169.75	0
	19:25 h	172.42	800
Wednesday, April 2^{nd}	21:25 h	222.42	800
Thursday, April 3^{rd}	00:05 h	225.08	0
	16:30 h	241.50	0
	19:10 h	244.17	800
Thursday, April 10^{th}	1:10 h	394.17	800
	3:50 h	396.83	0
	15 h	408.00	0

Table 8.1: Oxidation test detailed schedule.

Allotted hours	
Oxidation time	300 h
Dead time	76 h
Ramp time	32 h
Total process time	408 h (17 days)

Table 8.2: Times allotted for each time phase of the oxidation process.

Sample ID	Mass measurements [g]							A_0 [mm^2]
	Initial	**12h**	**24h**	**50h**	**100h**	**150h**	**300h**	
HIP 1	0.9371	0.9387	0.9385	0.9393	0.9404	0.9364	0.9385	412.52
HIP 2	0.9428	0.9449	0.9454	0.9443	0.9435	0.9418	0.9385	396.11
HIP 3	1.0793	1.0811	1.0816	1.0802	1.0807	1.0826	1.084	448.83
HIP Al 1	1.3099	1.3113	1.3112	1.3105	1.3107	1.3119	1.3116	538.77
HIP Al 2	1.5629	1.5647	1.5649	1.5653	1.5658	1.5662	1.5667	583.34
HIP Al 3	1.5476	1.5493	1.5496	1.5499	1.5502	1.5509	1.5513	571.49
HIP Al-B 1	1.3841	1.3864	1.387	1.3875	1.3878	1.3895	1.3832	491.71
HIP Al-B 2	1.076	1.0777	1.0781	1.0785	1.0787	1.0797	1.0801	472.04
HIP Al-B 3	1.0171	1.0185	1.0188	1.0193	1.0199	1.0209	1.0226	424.16
CC 1	4.0517	4.0528	4.0531	4.0537	4.0541	4.0551	4.0572	723.09
CC 2	4.4421	4.4434	4.4439	4.4443	4.4448	4.4458	4.4478	761.76
CC 3	3.9972	3.9984	3.9992	3.9995	3.9998	4.0013	4.003	715.59
CC Al 1	3.9337	3.9355	3.9359	3.9361	3.9366	3.9379	3.9385	761.54
CC Al 2	4.4849	4.4868	4.4872	4.4873	4.4878	4.4887	4.4895	816.03
CC Al 3	4.3294	4.3316	4.3322	4.3326	4.3329	4.3338	4.3347	900.52
CC Al-B 1	4.1732	4.1752	4.1754	4.1755	4.1761	4.1766	4.1771	761.77
CC Al-B 2	4.2921	4.2931	4.2934	4.2933	4.2948	4.294	4.2943	764.00
CC Al-B 3	2.8794	2.8808	2.8812	2.8811	2.8812	2.8817	2.8819	658.52

Table 8.3: Mass gain measurements.

Sample ID	Mass measurements [g]						
	Initial	**12h**	**24h**	**50h**	**100h**	**150h**	**300h**
HIP 1	0	0.0016	0.0014	0.0022	0.0033	-0.0007	0.0014
HIP 2	0	0.0021	0.0026	0.0015	0.0007	-0.001	-0.0043
HIP 3	0	0.0018	0.0023	0.0009	0.0014	0.0033	0.0047
HIP Al 1	0	0.0014	0.0013	0.0006	0.0008	0.002	0.0017
HIP Al 2	0	0.0018	0.002	0.0024	0.0029	0.0033	0.0038
HIP Al 3	0	0.0017	0.002	0.0023	0.0026	0.0033	0.0037
HIP Al-B 1	0	0.0023	0.0029	0.0034	0.0037	0.0054	-0.0009
HIP Al-B 2	0	0.0017	0.0021	0.0025	0.0027	0.0037	0.0041
HIP Al-B 3	0	0.0014	0.0017	0.0022	0.0028	0.0038	0.0055
CC 1	0	0.0011	0.0014	0.002	0.0024	0.0034	0.0055
CC 2	0	0.0013	0.0018	0.0022	0.0027	0.0037	0.0057
CC 3	0	0.0012	0.002	0.0023	0.0026	0.0041	0.0058
CC Al 1	0	0.0018	0.0022	0.0024	0.0029	0.0042	0.0048
CC Al 2	0	0.0019	0.0023	0.0024	0.0029	0.0038	0.0046
CC Al 3	0	0.0022	0.0028	0.0032	0.0035	0.0044	0.0053
CC Al-B 1	0	0.002	0.0022	0.0023	0.0029	0.0034	0.0039
CC Al-B 2	0	0.001	0.0013	0.0012	0.0027	0.0019	0.0022
CC Al-B 3	0	0.0014	0.0018	0.0017	0.0018	0.0023	0.0025

Table 8.4: Mass increment during oxidation.

Sample	Δ**m** $/A_o$ **[mg/cm^2]**						
	Initial	**12h**	**24h**	**50h**	**100h**	**150h**	**300h**
HIP	0	0.4397	0.5027	0.3708	0.4295	0.7352	1.0472
HIP Al	0	0.2886	0.3114	0.3084	0.3669	0.5048	0.5381
HIP Al-B	0	0.3860	0.4785	0.5799	0.6615	0.9260	1.0827
CC	0	0.1635	0.2365	0.2956	0.3499	0.5096	0.7731
CC Al	0	0.2378	0.2939	0.3215	0.3750	0.5019	0.5942
CC Al-B	0	0.2020	0.2441	0.2391	0.3358	0.3481	0.3932

Table 8.5: Final mass-gain values used to create the oxidation curves.

Note: The mass loss with respect to the initial sample mass, which is reflected in table 8.4, has been omitted in the calculation of these averages.

Sample	XRD	SEM	Not oxidized	Oxidized - Spare
HIP	1	3	4	2
HIP Al	2	3	4	1
HIP Al-B	2	3	4	1
CC	3	2	4	1
CC Al	3	2	4	1
CC Al-B	2	3	4	1

Table 8.6: The use given to each sample.

Initial	**Sample size measurements**																	
	HIP 1	HIP 2	HIP 3	HIP Al 1	HIP Al 2	HIP Al 3	HIP Al-B 1	HIP Al-B 2	HIP Al-B 3	CC 1	CC 2	CC 3	CC Al 1	CC Al 2	CC Al 3	CC Al-B 1	CC Al-B 2	CC Al-B 3
Length	17.2	16.08	16.64	18	17.96	16.91	15.96	17.46	15.16	17.9	17.6	17.12	18.55	17.38	19.54	16.99	18.27	18.23
	17.25	16.1	16.67	17.95	17.96	17.38	15.97	17.64	14.81	17.89	17.68	17.21	19	18	18.62	16.98	18.31	18.41
	17.27	16.14	16.72	18.14	18.21	17.07	15.94	17.39	14.76	17.85	17.71	17.3	18.72	16.62	19.47	17.71	18.29	18.29
Width	9.82	9.84	10.84	10.5	11.49	12.17	12.17	10.95	11.4	12.7	13.35	11.78	11.29	13.53	13.4	13.6	12.17	12.95
	9.84	9.87	10.96	11.07	11.74	12.66	12.2	11.27	11.57	12.2	13.19	13.15	12.44	13.26	12.6	14.33	13.62	12.61
	9.87	9.92	11.11	11.25	11.95	12.68	12.22	11.24	11.6	12.21	13.21	13.19	12.81	13.9	13.48	13.93	12.84	11.69
Thickness	1.39	1.49	1.5	2.35	2.64	2.27	1.76	1.47	1.43	4.65	4.74	4.63	4.86	5.71	5.72	4.46	4.74	3.38
	1.34	1.5	1.5	2.47	2.76	2.43	1.85	1.45	1.6	4.621	4.7	4.67	4.94	5.51	6.25	4.54	4.67	3.27
	1.32	1.51	1.5	2.65	2.67	2.56	1.85	1.36	1.54	4.65	4.81	4.65	4.97	5.57	6.33	4.52	4.69	3.3
Average	**Sample average size**																	
	HIP 1	HIP 2	HIP 3	HIP Al 1	HIP Al 2	HIP Al 3	HIP Al-B 1	HIP Al-B 2	HIP Al-B 3	CC 1	CC 2	CC 3	CC Al 1	CC Al 2	CC Al 3	CC Al-B 1	CC Al-B 2	CC Al-B 3
Length	17.24	16.11	16.68	18.03	18.04	17.12	15.96	17.50	14.91	17.88	17.66	17.21	18.76	17.33	19.21	17.23	18.29	18.31
Width	9.84	9.88	10.97	10.94	11.73	12.50	12.20	11.15	11.52	12.37	13.25	12.71	12.18	13.56	13.16	13.95	12.88	12.42
Thickness	1.35	1.50	1.50	2.49	2.69	2.42	1.82	1.43	1.52	4.64	4.75	4.65	4.92	5.60	6.10	4.51	4.70	3.32
Surface [mm^2]	412.52	396.11	448.83	538.77	583.34	571.49	491.71	472.04	424.16	723.09	761.76	715.59	761.54	816.03	900.52	761.77	764.00	658.52

Table 8.7: Sample size measurements.

8.4 Complementary pictures

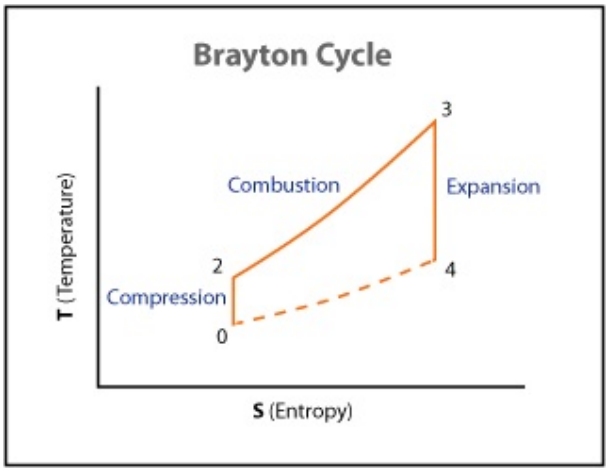

Figure 8.1: Ideal Brayton cycle.

Source: wikibooks.com

Figure 8.2: Samples covered with Al-slurry before diffusion.

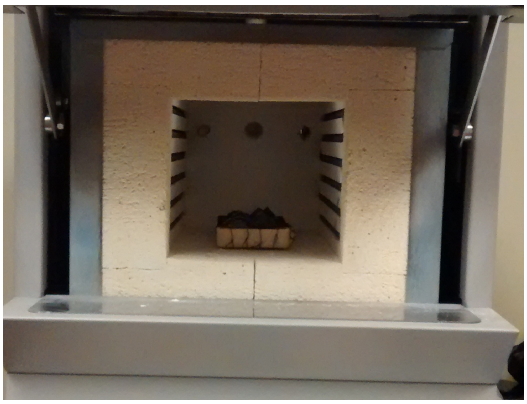

Figure 8.3: Oxidation furnace containing the crucible with the samples.

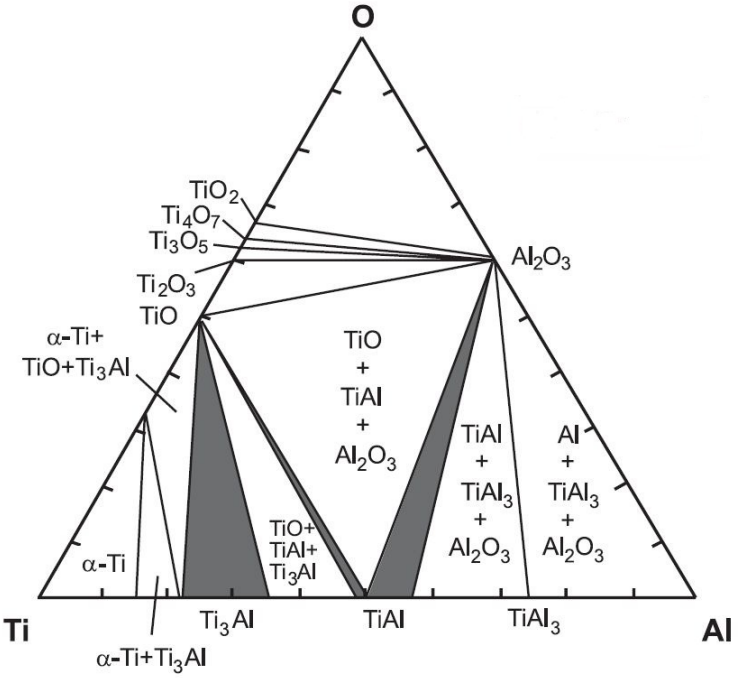

Figure 8.4: Isothermal section of the Ti-Al-O phase diagram at 800°C.

Source: Leyens & Peters [6].

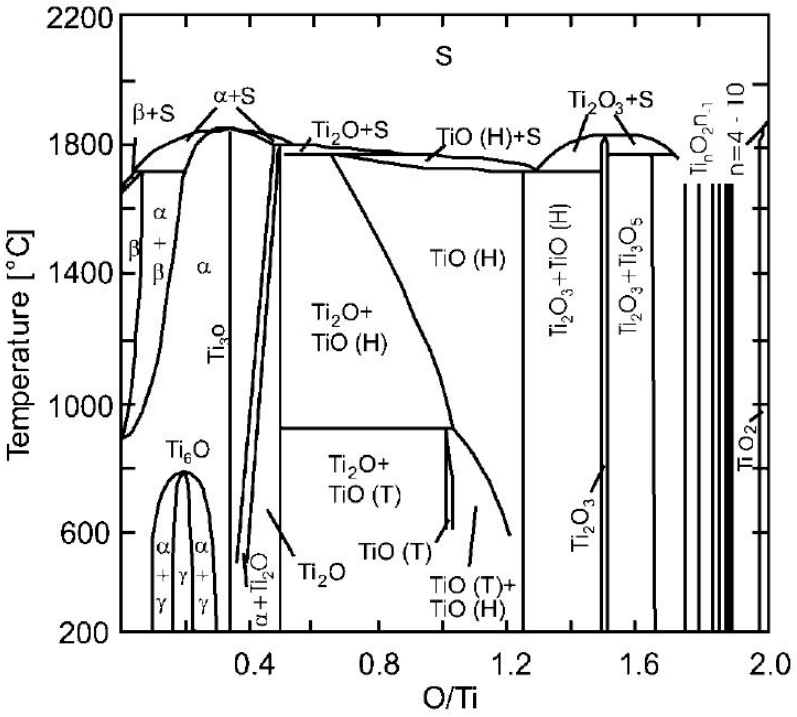

Figure 8.5: Oxides Temperature diagram. Oxide formation.

Source: Leyens & Peters [6].

List of Figures

List of Tables

Bibliography

[1] W.-b. Li, C.-y. Yan, W.-l. Huang, Z.-l. WANG, and Z.-f. YUAN, "Titanium pigment material: history, present situation and development," *Modern Chemical Industry*, vol. 22, no. 12, pp. 5–9, 2002.

[2] C. Woodford, *Titanium*. Marshall Cavendish Corporation, 2003.

[3] M. J. Donachie, *Titanium: A technical guide*. ASM International - The materials Information Society, 2000.

[4] G. Roza, *Titanium*. The Rosen publishing group, 2008.

[5] J. C. W. Gerd Ltjering, *Titanium*. The Rosen publishing group, 2008.

[6] C. Leyens and M. Peters, *Titanium and titanium alloys*. Wiley Online Library, 2003.

[7] V. Sikka, S. Deevi, S. Viswanathan, R. Swindeman, and M. Santella, "Advances in processing of ni3al-based intermetallics and applications," *Intermetallics*, vol. 8, no. 911, pp. 1329 – 1337, 2000.

[8] M. Yamaguchi, H. Inui, and K. Ito, "High-temperature structural intermetallics," *Acta materialia*, vol. 48, no. 1, pp. 307–322, 2000.

[9] J. Esslinger, "Titanium in aero engines," *MTU Aero Engines, Munich, Germany*, 1960.

[10] A. Donchev, E. Richter, M. Schütze, and R. Yankov, "Improvement of the oxidation behaviour of tial-alloys by treatment with halogens," *Intermetallics*, vol. 14, no. 10, pp. 1168–1174, 2006.

[11] D. Dimiduk, "Gamma titanium aluminide alloysan assessment within the competition of aerospace structural materials," *Materials Science and Engineering: A*, vol. 263, no. 2, pp. 281–288, 1999.

[12] F. Appel, J. D. H. Paul, and M. Oehring, *Gamma titanium aluminide alloys: science and technology*. John Wiley & Sons, 2011.

[13] R. Reddy, X. Wen, and M. Divakar, "Isothermal oxidation of tial alloy," *Metallurgical and Materials Transactions A*, vol. 32, no. 9, pp. 2357–2361, 2001.

[14] C. Zhou, H. Xu, S. Gong, and K. Young Kim, "A study of aluminide coatings on tial alloys by the pack cementation method," *Materials Science and Engineering: A*, vol. 341, no. 1, pp. 169–173, 2003.

[15] S. Kekare and P. Aswath, "Oxidation of tial based intermetallics," *Journal of materials science*, vol. 32, no. 9, pp. 2485–2499, 1997.

[16] V. Chuprina and I. Shalya, "Oxidation of tial intermetallic," *Powder Metallurgy and Metal Ceramics*, vol. 46, no. 11-12, pp. 582–588, 2007.

[17] Z. Li and W. Gao, *High temperature corrosion of intermetallics*. Nova Science Publishers, 2009.

[18] S. Sarkar, S. Datta, S. Das, and D. Basu, "Oxidation protection of gamma-titanium aluminide using glass–ceramic coatings," *Surface and Coatings Technology*, vol. 203, no. 13, pp. 1797–1805, 2009.

[19] S. Teng, W. Liang, Z. Li, and X. Ma, "Improvement of high-temperature oxidation resistance of tial-based alloy by sol–gel method," *Journal of Alloys and Compounds*, vol. 464, no. 1, pp. 452–456, 2008.

[20] H. Xiong, Y. Xie, W. Mao, W. Ma, Y. Chen, X. Li, and Y. Cheng, "Improvement in the oxidation resistance of the tial-based alloy by liquid-phase siliconizing," *Scripta materialia*, vol. 49, no. 11, pp. 1117–1122, 2003.

[21] Y. Jiang, Y. He, N. Xu, J. Zou, B. Huang, and C. Liu, "Effects of the al content on pore structures of porous ti–al alloys," *Intermetallics*, vol. 16, no. 2, pp. 327–332, 2008.

[22] Y.-W. Kim, "Intermetallic alloys based on gamma titanium aluminide," *Jom*, vol. 41, no. 7, pp. 24–30, 1989.

[23] M. Peters, J. Kumpfert, C. H. Ward, and C. Leyens, "Titanium alloys for aerospace applications," *Advanced Engineering Materials*, vol. 5, no. 6, pp. 419–427, 2003.

[24] J. C. Schuster and M. Palm, "Reassessment of the binary aluminum-titanium phase diagram," *Journal of phase equilibria and diffusion*, vol. 27, no. 3, pp. 255–277, 2006.

[25] F.-S. Sun, C.-X. Cao, M.-G. Yan, S.-E. Kim, *et al.*, "Alloying mechanism of beta stabilizers in a tial alloy," *Metallurgical and Materials Transactions A*, vol. 32, no. 7, pp. 1573–1589, 2001.

[26] Y. Shida and H. Anada, "The effect of various ternary additives on the oxidation behavior of tial in high-temperature air," *Oxidation of Metals*, vol. 45, no. 1-2, pp. 197–219, 1996.

[27] V. Haanappel, H. Clemens, and M. Stroosnijder, "The high temperature oxidation behaviour of high and low alloyed tial-based intermetallics," *Intermetallics*, vol. 10, no. 3, pp. 293–305, 2002.

[28] D. McKee and S. Huang, "The oxidation behavior of gamma-titanium aluminide alloys under thermal cycling conditions," *Corrosion science*, vol. 33, no. 12, pp. 1899–1914, 1992.

[29] R. Imayev, V. Imayev, M. Oehring, and F. Appel, "Alloy design concepts for refined gamma titanium aluminide based alloys," *Intermetallics*, vol. 15, no. 4, pp. 451–460, 2007.

[30] B. Inkson, C. Boothroyd, and C. Humphreys, "Microstructure of a γ-α_2-β tial alloy containing iron and vanadium," *Acta metallurgica et materialia*, vol. 41, no. 10, pp. 2867–2876, 1993.

[31] D. Larsen, L. Christodoulou, S. Kampe, and R. Sadler, "Investment-cast processing of xd¡ sup¿ tm¡/sup¿ near-γ titanium aluminides," *Materials Science and Engineering: A*, vol. 144, no. 1, pp. 45–49, 1991.

[32] T. Cheng, "The mechanism of grain refinement in tial alloys by boron additionan alternative hypothesis," *Intermetallics*, vol. 8, no. 1, pp. 29–37, 2000.

[33] E. L. Hall and S.-C. Huang, "Stoichiometry effects: on the deformation of binary tial alloys," *Journal of Materials Research*, vol. 4, no. 03, pp. 595–602, 1989.

[34] Y.-W. Kim, "Ordered intermetallic alloys, part iii: gamma titanium aluminides," *Jom*, vol. 46, no. 7, pp. 30–39, 1994.

[35] N. M. W. K. Kothari, R. Radhakrishnan, "Advances in gamma titanium aluminides and their manufacturing techniques.," -, vol. 55, pp. 1–16, 2012.

[36] F. A. U. B. U. C. S. E. S. J. U. L. J. M. M. O. J. D. H. Paul, *Recent progress in the development of gamma titanium aluminide alloys*. Wiley-VCH Verlag GmbH, 2000.

[37] R. M. Moreno., *In situ analysis of the high temperature deformation and fracture mechanisms of a TiAl alloy*. PhD thesis, Universidad Carlos III de Madrid, april 2014.

[38] H. Clemens and S. Mayer, "Design, processing, microstructure, properties, and applications of advanced intermetallic tial alloys," *Advanced Engineering Materials*, vol. 15, pp. 191–215, 2013.

[39] F. Appel, U. Brossmann, U. Christoph, S. Eggert, P. Janschek, U. Lorenz, J. Müllauer, M. Oehring, and J. D. Paul, "Recent progress in the development of gamma titanium aluminide alloys," *Advanced Engineering Materials*, vol. 2, no. 11, pp. 699–720, 2000.

[40] L. Christodoulou, P. Parrish, and C. Crowe, "Xd titanium aluminide composites," in *MRS Proceedings*, vol. 120, Cambridge Univ Press, 1988.

[41] K. Kumar and J. Whittenberger, "Discontinuously reinforced intermetallic matrix composites via xd synthesis," *Materials science and technology*, vol. 8, no. 4, pp. 317–330, 1992.

[42] C. Yang, D. Hu, X. Wu, A. Huang, and M. Dixon, "Microstructures and tensile properties of hot isostatic pressed ti4522xd powders," *Materials Science and Engineering: A*, vol. 534, pp. 268–276, 2012.

[43] H. M. Saari, *The processing of gas turbine engine hot section materials through directional solidification*. PhD thesis, Carleton University, 1999.

[44] G. Aviation, "Genx," 2014. `ttp://www.geaviation.com/engines/commercial/genx/genx-2b.`tml.

[45] W. Voice, "The future use of gamma titanium aluminides by rolls-royce," *Aircraft Engineering and Aerospace Technology*, vol. 71, no. 4, pp. 337–340, 1999.

[46] M. Koizumi, *Hot isostatic pressing: theory and applications: proceedings of the third international conference, Osaka, Japan, 10-14 June 1991*. Kluwer Academic Pub, 1992.

[47] M. Abouaf, J. Chenot, G. Raisson, and P. Bauduin, "Finite element simulation of hot isostatic pressing of metal powders," *International Journal for Numerical Methods in Engineering*, vol. 25, no. 1, pp. 191–212, 1988.

[48] S. Kofune, C. Manabe, and T. Fujikawa, "Developments and applications of high-temperature hot isostatic pressing," in *ISO 3: 3 rd International Conference on Isostatic Pressing.*, vol. 2, p. 27, 1986.

[49] U. A.-Q. University, "Metal casting processes," 2014. `http://uqu.edu.sa/files2/tiny_mce/plugins/filemanager/files/4290426/manufacturing_technology_2/solutions_manual_SM_Ch11-20.pdf`.

[50] M. Bocanegra-Bernal, "Hot isostatic pressing (hip) technology and its applications to metals and ceramics," *Journal of Materials Science*, vol. 39, no. 21, pp. 6399–6420, 2004.

[51] S. . Mussman, *Mater. World.* 7, 667, 1999.

[52] S. V. A. Royer, *Casting, Metals Handbook*. 9th ed. ASM International, 2007.

[53] K. Liu, Y. Ma, M. Gao, G. Rao, Y. Li, K. Wei, X. Wu, and M. Loretto, "Single step centrifugal casting tial automotive valves," *Intermetallics*, vol. 13, no. 9, pp. 925–928, 2005.

[54] J. Leggett, *Elevated temperature oxidation and corrosion of a titanium aluminide alloy*. PhD thesis, Cranfield University, October 1997.

[55] S. Bosel, *High Temperature Coatings*. Butterworth Heinemann, 2007.

[56] I. Okafor and R. Reddy, "The oxidation behavior of high-temperature aluminides," *JOM*, vol. 51, no. 6, pp. 35–40, 1999.

[57] C. Wang, W. Wang, S. Zhu, and F. Wang, "Oxidation inhibition of γ-tial alloy at 900 c by inorganic silicate composite coatings," *Corrosion Science*, vol. 76, pp. 284–291, 2013.

[58] C. Xu and W. Gao, "Pilling-bedworth ratio for oxidation of alloys," *Material Research Innovations*, vol. 3, no. 4, pp. 231–235, 2000.

[59] A. Mozalev, S. Magaino, and H. Imai, "The formation of nanoporous membranes from anodically oxidized aluminium and their application to li rechargeable batteries," *Electrochimica Acta*, vol. 46, no. 18, pp. 2825–2834, 2001.

[60] N. Hussain, *Oxidation behaviour of superalloys at elevated temperatures under different oxidizing atmospheres*. PhD thesis, University of the Punjab, Lahore, 2000.

[61] B. Li, "Long-term cyclic oxidation behavior of wrought commercial alloys at high temperatures," tech. rep., Ames Laboratory, IA (US), 2003.

[62] M. P. Boyce, *Gas Turbine Engineering Handbook*. Gulf Professioal Publishing, 2002.

[63] S. Boggia and K. Rüd, "Intercooled recuperated aero engine," *DGLR Paper*, vol. 179, p. 2004, 2004.

[64] W. E. Howald, "Cooling of structural members, particularly for gas turbine engines.," Sept. 8 1970. US Patent 3,527,543.

[65] C. H. S.L. Dixon, *Fluid Mechanics and Thermodynamics of Turbomachinery*. Elsevier, 2010.

[66] X. Montero, M. Galetz, and M. Schtze, "Low-activity aluminide coatings for superalloys using a slurry process free of halide activators and chromates," *Surface and Coatings Technology*, vol. 222, no. 0, pp. 9 – 14, 2013.

[67] R. Boyer, "An overview on the use of titanium in the aerospace industry," *Materials Science and Engineering: A*, vol. 213, no. 1, pp. 103–114, 1996.

[68] M. Nakamura, M. Nobuki, T. Tanabe, T. Kumagai, I. Mutoh, and E. Abe, "Microstructure control and high temperature properties of tial base alloys," *Intermetallics*, vol. 6, no. 7, pp. 637–641, 1998.

[69] S. Zghal, M. Thomas, S. Naka, A. Finel, and A. Couret, "Phase transformations in tial based alloys," *Acta materialia*, vol. 53, no. 9, pp. 2653–2664, 2005.

[70] H. Saari, J. Beddoes, D. Seo, and L. Zhao, "Development of directionally solidified γ-tial structures," *Intermetallics*, vol. 13, no. 9, pp. 937–943, 2005.

[71] R. Royce, *The Jet Engine*. Rolls Royce, 5th Edition.

[72] R. Jones, "Thermal barrier coatings," in *Metallurgical and ceramic protective coatings*, pp. 194–235, Springer, 1996.

[73] N. P. Padture, M. Gell, and E. H. Jordan, "Thermal barrier coatings for gas-turbine engine applications," *Science*, vol. 296, no. 5566, pp. 280–284, 2002.

[74] J. Thornton, "Thermal barrier coatings," in *Materials Forum*, vol. 22, pp. 159–181, 1998.

[75] M. Hetmańczyk, L. Swadźba, and B. Mendala, "Advanced materials and protective coatings in aero-engines application," *Journal of Achievements in Materials and Manufacturing Engineering*, vol. 24, no. 1, pp. 372–381, 2007.

[76] A. G. Evans, D. Mumm, J. Hutchinson, G. Meier, and F. Pettit, "Mechanisms controlling the durability of thermal barrier coatings," *Progress in materials science*, vol. 46, no. 5, pp. 505–553, 2001.

[77] G. General Electric Company, "Method of coating gas turbine components," *European Patent Specification*, vol. 1, no. 1, pp. 1–13, 2011.

[78] C. C. Pier C. Martinengo, "Process for producing protective coatings on metals and metal alloys for use at high temperatures," *United States Patent*, vol. 1, no. 1, pp. 1–3, 1980.

[79] X. Cao, R. Vassen, and D. Stoever, "Ceramic materials for thermal barrier coatings," *Journal of the European Ceramic Society*, vol. 24, no. 1, pp. 1–10, 2004.

[80] Y. Tamarin, *Protective Coatings for Turbine Blades*. ASM International, 2002.

[81] J. L. Pandey and M. K. Banerjee, "High-temperature-resistant (slurry-based) coatings," *Anti - Corrosion Methods and Materials*, vol. 44, no. 6, p. 368, 1997.

[82] N. R. C. Committee on Coatings, National Materials Advisory Board-Division of Engineering, *High-Temperature Oxidation-Resistant Coatings, Coatings for protection from oxidation of superalloys, refractory metals and graphite*. National Academy of Sciencies / National Academy of Engineering, 1970.

[83] A. Agüero, J. del Hoyo, J. García de Blas, M. García, M. Gutiérrez, L. Madueño, and S. Ulargui, "Aluminum slurry coatings to replace cadmium for aeronautic applications," *Surface and Coatings Technology*, vol. 213, pp. 229–238, 2012.

[84] W. Gao, *Developments in high temperature corrosion and protection of materials*. Elsevier, 2008.

[85] Y. Xiong, S. Zhu, and F. Wang, "The oxidation behavior of tialnb intermetallics with coatings at 800 c," *Surface and Coatings Technology*, vol. 197, no. 2, pp. 322–326, 2005.

[86] J. Sherman, B. Chin, P. Huibers, R. Garcia-Valls, and T. A. Hatton, "Solvent replacement for green processing.," *Environmental Health Perspectives*, vol. 106, no. Suppl 1, p. 253, 1998.

[87] A. Kristoffersson, E. Roncari, and C. Galassi, "Comparison of different binders for water-based tape casting of alumina," *Journal of the European Ceramic Society*, vol. 18, no. 14, pp. 2123 – 2131, 1998.

[88] J. M. LeBeau and Y. Boonyongmaneerat, "Comparison study of aqueous binder systems for slurry-based processing," *Materials Science and Engineering: A*, vol. 458, no. 12, pp. 17 – 24, 2007.

[89] J. P. Merutka, "Progress in protective coatings for aircraft gas turbines: A review of nasa-sponsored research," *NASA report TM-79178*, 1981.

[90] R. Streiff, "Protection of materials by advanced high temperature coatings," *Journal de Physique IV*, vol. 3, no. C9, 1993.

[91] P. C Patnaik, "Intermetallic coatings for high temperature applications-a review," *MATERIAL AND MANUFACTURING PROCESS*, vol. 4, no. 1, pp. 133–152, 1989.

[92] G. General Electric Company, "Slurry diffusion aluminide coating composition and process," *European Patent Specification*, vol. 1, no. 1, pp. 1–13, 2012.

[93] M. D. Corporation, "Borides.," 2014. `http://www.materialsdevelopment.com/`.

[94] B. Corporation, "Boriding," 2014. `http://www.bodycote.com/`.

[95] M. Goral, "The microstructure and oxidation resistance of aluminide mecraly-modified coatings obtained by slurry method on rene 80 superalloy," *Journal of Minerals and Materials Characterization and Engineering*, vol. 11, pp. 719–723, 2012.

[96] D. A. Ltd, "Aluminising," 2014. `http://www.diffusion-alloys.com/`.

[97] M. Amirjan and H. Khorsand, "Processing and properties of al-based powder suspension/slurry: A comparison study of aqueous binder systems, stability and film uniformity," *Powder Technology*, vol. 254, no. 0, pp. 12 – 21, 2014.

[98] T. Chartier and A. Bruneau, "Aqueous tape casting of alumina substrates," *Journal of the European Ceramic Society*, vol. 1, no. 12, pp. 243–247, 1993.

[99] C. A. Finch, "Polyvinyl alcohol–developments.," *John Wiley and Sons, Chichester, UK.*, 1992.

[100] J. Bailey, F.E. Koleske, *Poly(Ethylene Oxide)*. Academic Press, New York, 1976.

[101] K. Ueno, S. Nakamura, H. Shimotani, A. Ohtomo, N. Kimura, T. Nojima, H. Aoki, Y. Iwasa, and M. Kawasaki, "Electric-field-induced superconductivity in an insulator," *Nature materials*, vol. 7, no. 11, pp. 855–858, 2008.

[102] D. C. T. Articles, "Deflocculants: A detailed overview," 2014. `http://digitalfire.com/4sight/education/deflocculants_a_detailed_overview_324.html`.

[103] W. F. Dieter Stoye, *Paints, Coatings and Solvents*. Wiley - VCH, 1998, Second Edition.

[104] R. S. Benden and R. S. Parzuchowski, "Gas phase deposition of aluminum using a complex aluminum halide of an alkali metal or an alkaline earth metal as an activator," Jan. 2 1979. US Patent 4,132,816.

[105] D. E. DeSaulniers, F. P. Lamm, M. S. Milaniak, and D. J. Orzel, "Aqueous slurry coating system for aluminide coatings," Nov. 22 1994. US Patent 5,366,765.

[106] P. G. Shewmon, *Diffusion in solids*, vol. 9. McGraw-Hill New York, 1963.

[107] D. Askeland and W. Wright, *Essentials of materials science and engineering*. Cengage Learning, 2013.

[108] W. F. Smith and J. Hashemi, *Foundations of materials science and engineering*. Mcgraw-Hill Publishing, 2006.

[109] Y. Mishin and C. Herzig, "Diffusion in the ti–al system," *Acta Materialia*, vol. 48, no. 3, pp. 589–623, 2000.

[110] L. A. Rocha, E. Ariza, A. M. Costa, F. J. Oliveira, and R. F. Silva, "Electrochemical behavior of ti/al2o3 interfaces produced by diffusion bonding," *Materials Research*, vol. 6, no. 4, pp. 439–444, 2003.

[111] Tech2way.com, "A way to be conceptual," 2014. `http://www.mechsphare.in/2013/04/diffusion-diffusion-is-material.html`.

[112] Z. . S. chemische fabriken, "Dolapix ce 64 dispersing agent / deflocculant," 2014. `http://www.zschimmer-schwarz.com/DOLAPIX_CE_64/simon/zschimmer-schwarz/media/site/downloads/merkblatt/1_K_K_ENG_4494_00_2_100.pdf`.

[113] S. A. M. Gajardo, "Análisis calorimétrico y de difracción de rayos x de aleaciones de base cobre, obtenidad por aleado mecánico.," *Universidad de Chile*, 2008.

[114] E. L. Cussler, *Diffusion: mass transfer in fluid systems*. Cambridge university press, 2009.

[115] A. Palenxona and S. Cirafici, "The nb-y (niobium-yttrium) system," *Journal of phase equilibria*, vol. 12, no. 2, pp. 204–207, 1991.

Additional Mention

The whole research was performed at the facilities of the *Department of Materials Science and Engineering and Chemical Engineering* of Universidad Carlos III de Madrid - Escuela Politécnica Superior.

All the resources used to accomplish this task were provided by this university as well as the support and supervision of its professors.

- **Address:** Avda. de la Universidad, 30, 28911, Leganés, Madrid, Spain.
- **Phone:** +34 91 624 95 00
- **Year of foundation:** 1989.
- **Website:** www.uc3m.es